A High-Resolution Study of the $^{29}Si(p,\gamma)$ Reaction

by

Paul Matthew Wallace

Department of Physics
Duke University

Date: _____
Approved:

_____
Edward G. Bilpuch, Supervisor

_____
Alfred T. Goshaw

_____
Henry S. Greenside

_____
Berndt Müller

_____
Henry R. Weller

Dissertation submitted in partial fulfillment of
the requirements for the degree of
Doctor of Philosophy in the Department of Physics
in the Graduate School of Duke University

1996

ABSTRACT

(Physics – Nuclear)

A High-Resolution Study of the $^{29}Si(p,\gamma)$ Reaction

by

Paul Matthew Wallace

Department of Physics
Duke University

Date: _____
Approved:

_____
Edward G. Bilpuch, Supervisor

_____
Alfred T. Goshaw

_____
Henry S. Greenside

_____
Berndt Müller

_____
Henry R. Weller

An abstract submitted in partial fulfillment of
the requirements for the degree of
Doctor of Philosophy in the Department of Physics
in the Graduate School of Duke University

1996

A HIGH-RESOLUTION STUDY OF THE ^{29}Si(p,γ) REACTION

by

Paul M. Wallace

The γ-decays of 25 resonances in the ^{29}Si(p,γ) reaction have been measured in the energy range $E_p = 1.74 - 2.50$ MeV. This work was performed at the High Resolution Laboratory at Triangle Universities Nuclear Laboratory and represents a major step toward the goal of the determination of the complete level scheme of ^{30}P from the ground state to 8820 keV. Previous and concurrent experiments have measured the ^{29}Si(p,p) cross section as well as γ-ray yields from the ^{29}Si(p,γ), ^{29}Si(p,p$_1\gamma$) and ^{29}Si(p,p$_2\gamma$) reactions in the range $E_p = 1.04 - 3.33$ MeV. Future angular distribution experiments are planned.

Spectral fluctuation properties are believed to give insight into the dynamics of quantum systems. This work was motivated by results from the study of the fluctuation properties of the nuclide ^{26}Al which indicates dynamics that fall between regular and chaotic.

A high-resolution ($\sim$ 220 eV) proton beam is produced by the 4 MeV KN Van de Graaff accelerator housed in the High Resolution Laboratory. This beam is directed onto thin films of ^{29}Si of thickness $1.5 - 3.0\,\mu$g/cm^2. Two high-purity germanium detectors are used to collect detailed γ-ray spectra; one detector is surrounded by a bismuth germanate anti-Compton shield. These spectra have been analyzed and branching ratios for the resonances have been deduced. Once the branching ratios were determined, J^π selection rules and recommended upper limits for reduced transition rates were used to reduce the range of possible quantum number $(J^\pi;T)$ assignments. Of the 25 resonances, sixteen had previous assignments which were confirmed by this work. The allowed ranges were reduced for seven resonances and two resonances had assignments which were changed outright. In addition, a level at $E_x = 6006.1$ keV was discovered; its branching ratios were determined and $J^\pi;T$ assignment restricted.

Acknowledgements

I would like to thank my advisor, Dr. Edward G. Bilpuch, for his support and encouragement during my time as a graduate student. Drs. Gary E. Mitchell and John F. Shriner, Jr. deserve a great round of thanks for their careful attention to the details of this work. The assistance of Dr. Frank Moore has been invaluable during this project, and I also wish to thank him.

Chris Westerfeldt, Paul Carter, and Richard O'Quinn have done a first-rate job maintaining the High Resolution Laboratory; for their service I am very grateful. A very special thanks goes to Chris for the tireless effort and dedication which he brings daily to his work in the HRL, and for the doughnuts.

The myriad of electronics and computer problems which accompany an effort such as this have been deftly handled by Sidney Edwards and Patrick Mulkey. It has been a pleasure working with them.

I have benefited greatly for the day-to-day environment provided by my colleagues: Amzie Adams, Dr. Randy Bybee, Bret Crawford, Matt LaBonte, Lisa Lowie, Dr. Joann Shriner, Sharon Stephenson, and Jerry Vavrina. Their continual support and friendship are of immeasurable value to me. Lance McLean, Chris Grossmann, Lynn Fittje, Joey Hutchins and Suzanne Huerth provided data-taking support; I thank all of them.

I wouldn't be here writing this if not for the faculty of Young Harris College; in particular, the support of Robert Nichols, Hartmut Ramm and Bettie Sellers has proven to be an influence on me to this day. The interest they took in me and my education and the confidence which they instilled in me are invaluable gifts; in my mind they have been my greatest teachers.

At this point I must thank my family: Dad, Mom, Dan, Kristen, Sherry, and Keith. to whom I owe the deepest gratitude. To the Stewart family I also send my love and a big thanks. Finally, words do a disservice to the thanks which my dear wife Beth deserves for her constant love and encouragement. To her especially I am grateful.

Duke University P. M. WALLACE

April 1996

To my father

Dr. James Robert Wallace

Contents

List of Tables

List of Figures

Chapter 1

Introduction

There has been much interest recently in the statistical properties of eigenvalue spectra. In 1984, Bohigas *et al.* [Boh84] conjectured that spectra of systems whose classical analogs are chaotic show fluctuation properties identical to those of the Gaussian orthogonal ensemble (GOE) of random matrix theory (RMT). RMT is a statistical theory of quantum spectra which was developed chiefly during the 1950's and 60's and has since been used extensively in the description of nuclear levels. (See [Por65] and [Bro81] for reviews.) Such a connection between RMT and chaos had not been made before the time of Bohigas' conjecture. Since that time, the conjecture has been supported by much experimental and numerical work [Sel85, Win88, Ble94] and is now generally believed to be true. In addition, it is generally accepted that spectra of systems whose classical analogs are regular (not chaotic) exhibit Poisson statistics; that is, the levels in such spectra are not correlated.

The goal of present work at the High Resolution Laboratory (HRL) at Triangle Universities Nuclear Laboratory (TUNL) is the establishment of a level scheme for ^{30}P. This level scheme should have few missing or spurious levels and few levels with missing or misassigned quantum numbers. Once the spectrum is determined, its fluctuation properties will be measured using the nearest-neighbor spacing distribution and the Dyson-Mehta

Δ_3 statistic. These statistics are very sensitive to flaws (missing or spurious levels and misassigned quantum numbers) in the spectrum: hence the requirement for a high-quality level scheme.

The determination of such a spectrum over a wide energy range is difficult experimentally. In order to establish excitation energies and quantum numbers in the low-energy region, direct reactions are often used. Proton resonance reactions help to locate levels and assign quantum numbers in the region above the proton separation energy S_p. More information may be learned about the resonance region by studying γ-ray decay from proton capture experiments; these studies may also lead to increased knowledge regarding the states in the region just below S_p, the most difficult energy region to probe. In addition, analyses of γ-ray angular distributions from proton capture experiments may help to determine quantum numbers of states above S_p. Angular distribution studies may also lead to increased knowledge of final state quantum numbers. To date, 159 levels have been identified in ^{30}P in the range $E_x = 0 - 8820$ keV.

The present work is a study of the γ-ray decay of 25 resonances in ^{30}P in the energy region 7304 keV $\leq E_x \leq$ 8015 keV. High-resolution γ-ray spectra are collected from each of these resonances and are used to construct decay schemes and determine decay strengths; this information is then used to place limits on possible quantum number assignments for the resonance states. In some cases new information may be learned about lower-lying states to which the resonance directly decays.

Chapter 2 presents the theoretical and experimental background and concludes with remarks concerning the motivation for the present work. The experimental setup used for the study is described in Chapter 3. A discussion of calibrations and data analysis procedures is found in Chapter 4, and results of the study are presented in Chapter 5. Chapter 6 is a summary, and three appendices follow which contain detailed information regarding the data and analysis.

Chapter 2

Background and Motivation

The purpose of this chapter is to provide a context for the present work. Both theoretical and experimental aspects will be discussed, and a short description of the ^{30}P nuclide follows.

2.1 Theoretical Background: Random Matrix Theory

The goal of this experiment is a complete and pure level scheme which will be subjected to various statistical analyses. The theory which provides the tools for these analyses is random matrix theory (RMT) [Bro81, Meh91]. RMT will first be presented by contrasting it to the nuclear shell model. This will be followed by short derivations of some of the relevant results of RMT and a discussion of the connection of RMT with the present problem.

2.1.1 General

The shell model and RMT represent two solutions to the problem of finding a theoretical basis of nuclear structure. These two solutions have different regions of applicability

and are based on widely differing assumptions. The shell model will be presented first, but only for the benefit of placing RMT in its proper context.

During the early years of nuclear research it became clear that nuclei exhibit shell structure much like that of atomic systems: there appeared at certain neutron numbers $N+1$ and proton numbers $Z+1$ large downward jumps in the separation energies S_n and S_p. The numbers N and Z are called *magic numbers* (N or Z = 8, 20, 28, 50, 82, and 126) and represent the closings of major shells. This experimental result led to much theoretical work and ultimately to the nuclear shell model.

In the shell model, the nucleus is pictured as consisting of filled shells containing the maximum number of protons and neutrons allowed by the Pauli principle and unfilled shells containing a number of valence nucleons. The nucleons occupying the filled shells give rise to a potential well $V(r)$ in which the valence nucleons move; these valence nucleons are responsible for the properties of the nucleus. Interactions between the valence nucleons are treated as small perturbations. There are different versions of the shell model which differ by the choice of potential $V(r)$ and the number of valence nucleons. Each version, however, provides a similar means for calculating wavefunctions: the wavefunction ψ_n of the n^{th} nuclear level is computed by the Slater determinant

$$\psi_n(\mathbf{r}_1, \mathbf{r}_2, \ldots, \mathbf{r}_k) = \sqrt{\frac{1}{k!}} \begin{vmatrix} \phi_1(\mathbf{r}_1) & \cdots & \phi_1(\mathbf{r}_k) \\ \vdots & \ddots & \vdots \\ \phi_k(\mathbf{r}_1) & \cdots & \phi_k(\mathbf{r}_k) \end{vmatrix}_n \tag{2.1}$$

where the ϕ_i are the single-particle wavefunctions of the k valence nucleons. The shell model has been found to be reliable in predicting energies and quantum numbers (among other quantities) of low-lying levels [Kra88]. As n increases, however, the number of single-particle states required for a solution for ψ_n increases rapidly, and the calculation soon becomes intractable. The situation is somewhat like that of a gas in a box: given a very

small number of molecules the theory of the system is simple, but as more gas is added the situation gets rapidly out-of-hand from the perspective of a detailed description. Thermodynamics provides a different perspective on the problem: it describes the system not in terms of microscopic states but in terms of variables which are found as averages over the many possible states consistent with given constraints. RMT provides an analogous statistical perspective on the problem of nuclear structure by assuming that detailed calculations of nuclear states are not possible but that certain global properties of the eigenvalue spectrum may be derived. This is done not by creating one Hamiltonian but an (ideally infinite) ensemble of Hamiltonians. Each matrix in the ensemble represents a possible nuclear Hamiltonian. Properties of the nuclear spectrum are derived by computing averages over the entire ensemble; this ensemble is defined by the the symmetries of the physical system. The effect of these symmetries of the form of the Hamiltonian matrices will now be discussed.

2.1.2 Effect of Symmetries on the Form of $\hat{H}$

Although the details of nuclear dynamics are assumed unknown by RMT, nuclear Hamiltonians are rotationally invariant and are also believed to be invariant under time reversal[1]. In general, the Hamiltonian matrices are complex Hermitian; however, these symmetries restrict the elements of the nuclear Hamiltonians to be real. The ensemble of real symmetric matrices is called the *Gaussian orthogonal ensemble*[2]. It will now be shown that rotational and time-reversal invariance give rise to orthogonal matrices. First, a few comments are due regarding time-reversal. The time-reversal operator $\hat{T}$ is antilinear. That is,

$$\hat{T}(c_1|\psi_1\rangle + c_2|\psi_2\rangle) = c_1^*\hat{T}|\psi_1\rangle + c_2^*\hat{T}|\psi_2\rangle. \tag{2.2}$$

[1]To date, no experiments have directly revealed time-reversal invariance in any system, although it is thought to occur in the decay of the neutral kaon. See articles by Henley [Hen89] and Haxton [Hax94].

[2]Other combinations of symmetries give rise to different ensembles; see [Bro81].

Such an operator may be written

$$\hat{T} = \hat{T}_o \hat{C} \tag{2.3}$$

where $\hat{T}_o$ is a linear operator and $\hat{C}$ is the complex conjugate operator: $\hat{C}\psi = \psi^*$. The total angular momentum vector should reverse direction upon inversion of time; that is, we should have $\hat{T}\hat{J}\hat{T}^\dagger = -\hat{J}$. This leads to the expression for the linear operator $\hat{T}_o$ [Rei92]:

$$\hat{T}_o = \mathrm{e}^{-\frac{i}{\hbar}\pi \hat{S}_y} \tag{2.4}$$

where $\hat{S}_y$ is the operator for the y-component of the spin angular momentum. $\hat{T}_o$ is unitary, therefore $\hat{T}$ is antiunitary. Consider the action of $\hat{T}^2$ on states of definite spin:

$$\hat{T}^2|S, S_y\rangle = \mathrm{e}^{-\frac{i}{\hbar}2\pi \hat{S}_y}|S, S_y\rangle = \begin{cases} \quad |\, S, S_y\rangle & \text{for } S = 0, 1, 2, \ldots \\ -\,|\, S, S_y\rangle & \text{for } S = \frac{1}{2}, \frac{3}{2}, \frac{5}{2}, \ldots \end{cases} \tag{2.5}$$

It is seen from this that for systems with integer spin, we have $\hat{T}^2 = 1$, while for systems with half-integer spin, we have $\hat{T}^2 = -1$. This leads to the fact that, when considering the effects of symmetries, systems of integer and half-integer spin must be treated differently. The case for time-reversal invariant systems with integer spin will be treated directly, and the half-integer spin case will be briefly discussed.

For systems of integer spin, the state

$$|\Psi_1\rangle = c|\psi_1\rangle + \hat{T}c|\psi_1\rangle \tag{2.6}$$

is an eigenstate of $\hat{T}$: $\hat{T}|\Psi_1\rangle = |\Psi_1\rangle$. An orthonormal set of such states $|\Psi_n\rangle$ may be constructed [Rei92]. In this basis we have for the matrix element H_{kl} of the Hamiltonian matrix $\hat{H}$,

$$H_{kl} = \langle\Psi_k|\hat{H}|\Psi_l\rangle = (\langle\Psi_k|\hat{T}^\dagger)\,\hat{H}\,(\hat{T}|\Psi_l\rangle). \tag{2.7}$$

For antilinear operators, we have

$$(\langle\psi|\hat{T})\,|\phi\rangle = [\langle\psi|\,(\hat{T}|\phi\rangle)]^*. \tag{2.8}$$

Applying this equation to the rightmost expression in Equation 2.7, we find

$$H_{kl} = [\langle \Psi_k | (\hat{T}^\dagger \hat{H} \hat{T} | \Psi_l \rangle)]^*. \tag{2.9}$$

We are assuming that the Hamiltonian is time-reversal invariant so that $\hat{T}^\dagger \hat{H} \hat{T} = \hat{H}$; thus for matrix elements of such Hamiltonians

$$H_{kl} = [\langle \Psi_k | \hat{H} | \Psi_l \rangle]^* = H^*_{kl}. \tag{2.10}$$

For this to be true the Hamiltonian must be real.

Rotational invariance is not a necessary condition for the reality of matrix elements for systems of integer spin. However, for half-integer spin systems, only when angular momentum is conserved *and* time-reversal invariance holds will the matrix elements of the Hamiltonian be necessarily real. This is due to the fact that for systems with half-integer spin. we are not able to construct an orthonormal basis of the form of Equation 2.6 since the construction of the basis relies on $\hat{T}^2$ being unity. However, if we assume that total angular momentum J is conserved (that is, $[\hat{H}, \hat{J}] = 0$) and if we define

$$\hat{O} = \mathrm{e}^{-\frac{i}{\hbar}\pi \hat{J}_y} \hat{T} \tag{2.11}$$

we see that $\hat{O}^2 = 1$ and we may proceed as before with an argument similar to that shown above. The result is that for systems with half-integer spin *and* for which $[\hat{H}, \hat{J}] = 0$, the matrix operator $\hat{H}$ is real and symmetric.

2.1.3 Joint Probability Distribution Functions for GOE

The preceding discussion describes the overall structure of the Hamiltonians but does not place limits on the matrix elements themselves; we now seek a joint probability distribution function (jpdf) for the matrix elements. Since the dynamics of the system are considered unknown, the matrix elements of the nuclear Hamiltonian $\hat{H}$ should be treated

in the least biased fashion. This may be done by assuming that no one Hamiltonian (that is, no one nuclear potential) is more likely than any other. In addition, the matrix elements are taken to be independent random variables, and the jpdf should be invariant under orthogonal transformations (i.e., the ensemble should be independent of basis). In deriving the jpdf, we may consider the entropy of the ensemble of matrices. In thermodynamics, the entropy may be maximized in order to extract an equilibrium probability density in phase space [Rei80]: in RMT a jpdf $P(\mathcal{H})$ for the matrix elements may be found in a similar way. For an orthogonal matrix, this entropy extremization leads to a Gaussian jpdf. This may be shown most simply by following Porter [Por65]: the entropy may be written

$$S = -\int d\mathcal{H}\, P(\mathcal{H}) \ln P(\mathcal{H}). \tag{2.12}$$

where

$$d\mathcal{H} = 2^{N(N-1)/4} \prod_{i \leq j} dH_{ij} \tag{2.13}$$

and

$$P(\mathcal{H}) = P(H_{11}, H_{22}, \ldots, H_{NN}, H_{12}, H_{13}, \ldots, H_{N-1,N}). \tag{2.14}$$

The integral (2.12) is therefore taken over all $\frac{N}{2}(N+1)$ independent matrix elements H_{ij}. The entropy is extremized subject to two constraints. The first constraint is the normalization of the jpdf:

$$\int d\mathcal{H}\, P(\mathcal{H}) = 1. \tag{2.15}$$

The desire to make the ensemble as structure-free as possible leads to the other constraint. In order to insure that abnormally large matrix elements do not occur, one may require the matrix elements to have a well-defined average. Since the trace of a matrix (and all multiples thereof) is basis-independent, this constraint may be written

$$\int d\mathcal{H}\, P(\mathcal{H}) \mathrm{Tr}(H^2) = c, \tag{2.16}$$

where

$$\mathrm{Tr}(H^2) = \sum_{k=1}^{N}(H_{kk})^2 + 2\sum_{k,l=1;k<l}^{N}(H_{kl})^2, \tag{2.17}$$

and c is a constant. One may then extremize the entropy subject to these constraints so that

$$\delta \int d\mathcal{H}\, P(\mathcal{H})\ln P(\mathcal{H}) = 0. \tag{2.18}$$

Clearly,

$$\delta \int d\mathcal{H}\, P(\mathcal{H}) = \delta \int d\mathcal{H}\, P(\mathcal{H})\mathrm{Tr}(H^2) = 0. \tag{2.19}$$

We may use two Lagrange multipliers λ_1 and λ_2. We find

$$S(\lambda_1, \lambda_2) = -\int d\mathcal{H}\, \left[P(\mathcal{H})\ln P(\mathcal{H}) + \lambda_1 P(\mathcal{H}) + \lambda_2 \mathrm{Tr}(H^2)P(\mathcal{H})\right]. \tag{2.20}$$

This may be extremized by varying $P(\mathcal{H})$ so that $\delta S(\lambda_1, \lambda_2) = 0$. We find

$$\left[\int d\mathcal{H}\, \delta P(\mathcal{H}) \left[\ln P(\mathcal{H}) + 1 + \lambda_1 + \lambda_2 \mathrm{Tr}(H^2)\right]\right] = 0. \tag{2.21}$$

For arbitrary $P(\mathcal{H})$, the term in brackets must equal zero, so we find

$$P(\mathcal{H}) = \mathrm{e}^{-1-\lambda_1-\lambda_2\mathrm{Tr}(H^2)} \tag{2.22}$$

One may solve for λ_1 and λ_2 by substituting this expression into Equations 2.15 and 2.16. Doing so leaves one with the jpdf for the matrix elements which may be written

$$P(\mathcal{H}) = (4\pi v^2)^{-N(N+1)/4}\mathrm{e}^{-\frac{1}{4v^2}\mathrm{Tr}(H^2)}. \tag{2.23}$$

Here, $v^2 = \frac{1}{N}$ [Bro81]. In terms of the matrix elements, this is

$$\begin{aligned} &P(H_{11}, H_{22}, \ldots, H_{NN}, H_{12}, H_{13}, \ldots, H_{N-1,N}) = \\ &(4\pi v^2)^{-N(N+1)/4}\exp\left[-\frac{1}{4v^2}\left(\sum_{k}^{N}(H_{kk})^2 + 2\sum_{k,l=1;k<l}^{N}(H_{kl})^2\right)\right]. \end{aligned} \tag{2.24}$$

The probability density function for diagonal elements is therefore Gaussian with mean zero and variance $2v^2$ and that for the off-diagonal elements is Gaussian with mean zero and variance v^2.

For fluctuation studies, the distribution of eigenvalues is an important quantity. Starting with Equation 2.23 and setting $\mathrm{Tr}(H^2) = \sum_{l=1}^{N} e_l^2$, it may be shown [Rei92] that the jpdf for the eigenvalues is

$$P(e_1, e_2, \ldots, e_N) = k \prod_{r>s=1}^{N} \mid e_r - e_s \mid \exp\left[-\frac{1}{4v^2}\sum_{i=1}^{N} e_i^2\right], \tag{2.25}$$

where k is a normalization constant.

2.1.4 RMT and Quantum Chaos: Fluctuation Measures

In the last ten years RMT has been connected with another (until now quite disparate) branch of physics: chaos. In quantum systems, we cannot use conventional techniques to find signatures of chaos since the Heisenberg uncertainty principle

$$\Delta p \Delta x \geq \frac{\hbar}{2} \tag{2.26}$$

prohibits location of a trajectory with arbitrary precision. We must look elsewhere for signs of chaotic dynamics. One such signature may be found in the fluctuation properties of quantum spectra; in 1984 Bohigas *et al.* [Boh84] conjectured that spectra of quantum analogs of classically chaotic systems follow the statistics of the GOE. This conjecture is now generally accepted [Boh88]. In addition, spectra of quantum analogs of classically regular systems are thought to exhibit Poisson statistics [Boh88]. Spectral fluctuation properties thus may be taken as good indicators of the dynamics of quantum systems.

Fluctuations are deviations from average behavior. For most experimental spectra, the average level spacing D is not constant but is a decreasing function of the energy. These spectra must be "unfolded" by mapping the set of levels into a new set which has constant

average D. Level spacing fluctuations may then be measured relative to this value of D. The mapping procedure is described by Shriner *et al.* [Shr91].

Once a spectrum is unfolded, certain measures (or *statistics*) are used to provide information on fluctuation properties. Two of the most common statistics are the nearest neighbor spacing (NNS) distribution and the Dyson-Mehta Δ_3 statistic[3]. The NNS distribution will be derived by considering an ensemble of 2×2 real symmetric matrices, each providing a single spacing; the result is approximate. Start with the matrix

$$\hat{H} = \begin{pmatrix} H_{11} & H_{12} \\ H_{12} & H_{22} \end{pmatrix}. \tag{2.27}$$

This matrix may be diagonalized by the orthogonal transformation $\tilde{O}HO = H_D$ to obtain the matrix H_D whose diagonal elements are e_1 and e_2, the eigenvalues of H ($e_2 > e_1$). We seek the probability distribution function $P(s)$ which gives the probability for a spacing to have the value s. Start with Equation 2.25 for the matrix H_D:

$$P(e_1, e_2) = k(e_2 - e_1)\mathrm{e}^{-\frac{1}{2v^2}(e_1^2+e_2^2)}. \tag{2.28}$$

Making a change of variables from e_1 and e_2 to the spacing $s = e_2 - e_1$ and the average energy $\bar{e} = (e_1 + e_2)/2$, we find

$$P(s, \bar{e}) = ks\mathrm{e}^{-\frac{1}{8v^2}(-4\bar{e}^2-s^2)}. \tag{2.29}$$

The constant k may be found by requiring that the distribution be normalized:

$$\iint ds\, d\bar{e}\, P(s, \bar{e}) = 1. \tag{2.30}$$

Solving this for k yields

$$k = \frac{1}{v^3\sqrt{32\pi}}. \tag{2.31}$$

[3]Other statistics exist but have not been found to be as reliable as the NNS distribution and Δ_3 for distinguishing between GOE and Poisson spectra. See [Bro81, Byb95].

By integrating $P(s,\bar{e})$ over $\bar{e}$ one arrives at the probability $P(s)$:

$$P(s) = \frac{s}{8v^2}\, e^{-\frac{s^2}{8v^2}}. \tag{2.32}$$

This expression is often written in terms of the dimensionless parameter $x = \frac{s}{D}$ where D is the average spacing. This average spacing may be written

$$D = \int ds\, sP(s) = \sqrt{2\pi}v. \tag{2.33}$$

Therefore we have for the GOE NNS distribution

$$P_G(x) = \frac{\pi x}{2}\, e^{-\frac{1}{4}\pi x^2}. \tag{2.34}$$

While this is not the general result[4] for all N, it agrees with the surmise of Wigner [Wig57] and is often referred to as the *Wigner distribution.* Notice that $\lim_{x\to 0} P_G(x) = 0$; this absence of degeneracies is called *level repulsion* and is a hallmark of the GOE.

We will now derive the probability density function for an uncorrelated distribution of energy levels: this is equivalent to assuming that no symmetries are imposed on the matrices. Assume there is a level at energy e. If D is the average spacing between energy levels, we may say that $\frac{1}{D}ds$ is the probability of finding a level in the interval $e+s \to e+s+ds$. (This probability is not affected by the level at e.) Also note that

$$\int_s^\infty ds'\, P(s') \tag{2.35}$$

is the probability that there is no level in the interval $e \to e+s$. Then the probability that the spacing between the level at e and the next level is between s and $s+ds$ may be written

$$P(s)ds = \frac{1}{D}ds \int_s^\infty ds'\, P(s'), \tag{2.36}$$

so that the spacing distribution may be expressed

$$P(s) = \frac{1}{D}\int_s^\infty ds'\, P(s'). \tag{2.37}$$

[4]The result may be expressed rigorously as an infinite power series. See [Meh91].

Differentiating,

$$\frac{dP}{ds} = -\frac{1}{D}P(s) \tag{2.38}$$

Solving this equation we find

$$P(s) = \frac{1}{D}\mathrm{e}^{-\frac{s}{D}}. \tag{2.39}$$

Setting $x = s/D$, we find the *Poisson distribution*:

$$P_P(x) = \mathrm{e}^{-x}. \tag{2.40}$$

The case of an uncorrelated sequence of energy levels thus results in a distribution which allows degeneracies: in fact, $s = 0$ is the most probable spacing. This is very different from the GOE case, which disallows degeneracies altogether.

It is possible to have results which do not represent either of these extremes but which fall somewhere between them. In the interest of characterizing these results, an empirical interpolation formula has been proposed by Brody [Bro73]:

$$P(x;\omega) = \alpha(\omega+1)x^{\omega}\mathrm{e}^{-\alpha x^{\omega+1}}. \tag{2.41}$$

Here

$$\alpha = \left[\Gamma\left(\frac{\omega+2}{\omega+1}\right)\right]^{\omega+1}, \tag{2.42}$$

where Γ is the gamma function. Note that $\omega = 0$ corresponds to Poisson statistics and $\omega = 1$ corresponds to GOE statistics. Figure 2.1 displays the NNS distribution for varying values of ω. The integral of the distribution is also shown.

Another measure which has found wide use in spectral fluctuation studies is the Dyson-Mehta Δ_3 statistic. While the NNS distribution provides information on the short-range order in spectra, Δ_3 gives insight into the long-range order, or *spectral rigidity*. The definition of Δ_3 for a sequence of L levels between E_{min} and E_{max} is

$$\Delta_3(L) = \min_{A,B}(E_{max} - E_{min})^{-1}\int_{E_{min}}^{E_{max}} dE\,[N(E) - AE - B]^2. \tag{2.43}$$

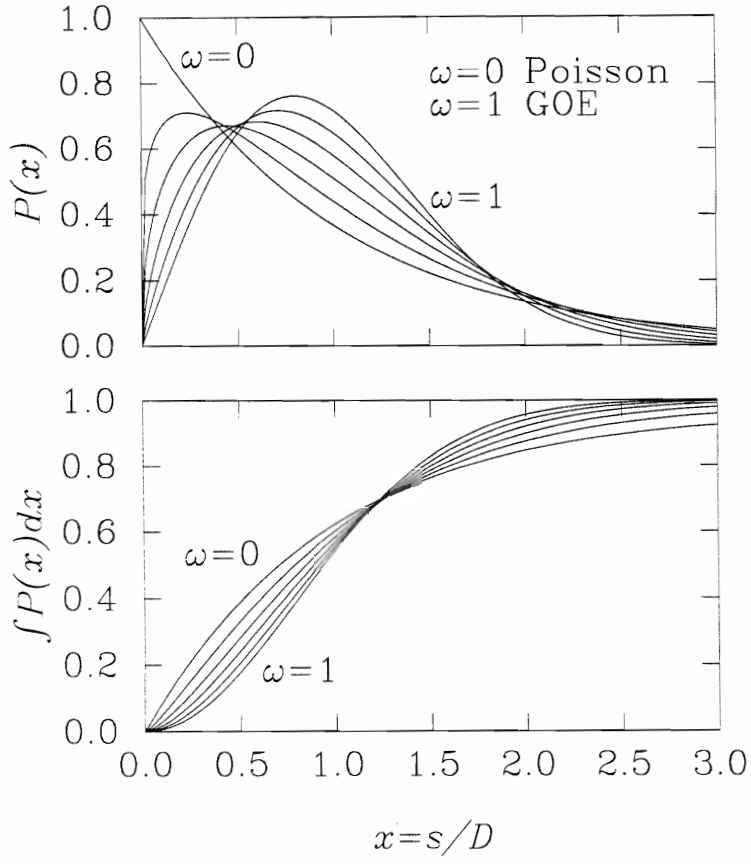

Figure 2.1. Nearest-neighbor spacing distribution and its integral for varying values of ω.

In this equation, the linear parameters A and B are varied until the value of the integral is a minimum. It gives the mean-square deviation of $N(E)$ from a straight line, where

$$N(E) = \int \rho(E) dE \tag{2.44}$$

and is the number of levels with energy less than or equal to E (here $\rho = \frac{1}{D}$ is the level density). Thus the one-dimensional harmonic oscillator has the smallest possible value of Δ_3: the spectrum of this system is perfectly rigid. GOE and Poisson spectra give rise to markedly different behavior of Δ_3, especially at large L. GOE spacings exhibit long-range order; that is, high spectral rigidity and small values of Δ_3. For large L, Δ_3 as derived from

the GOE is roughly logarithmic:

$$\Delta_{3G} \simeq \frac{1}{\pi^2}(\ln L - 0.0687). \tag{2.45}$$

For Poisson spectra, Δ_3 is linear:

$$\Delta_{3P} = \frac{L}{15}. \tag{2.46}$$

There exists an interpolation formula [Sel85] for Δ_3 which is analogous to the Brody distribution for the NNS distribution:

$$\Delta_3(L;\mu) = \Delta_{3G}(\mu L) + \Delta_{3P}([1-\mu]L). \tag{2.47}$$

Here, $\mu = 0$ corresponds to a Poisson spectrum and $\mu = 1$ corresponds to a GOE spectrum. Figure 2.2 shows Δ_3 for varying values of μ.

2.2 Experimental Background and Motivation

Extensive studies have been performed to determine in detail the robustness of the NNS distribution and the Δ_3 statistic [Shr92]. It has been found that level repulsion is rapidly destroyed when states of different symmetry are admixed and that both statistics are extremely sensitive to missing or misassigned quantum numbers. In particular, if the spectrum in question is not *complete* (no missing levels) and *pure* (no misassigned quantum numbers), then the resulting values of ω and μ may be severely biased. For example, adding 10 spurious levels to a pure GOE spectrum of 100 levels leads to a 100% increase in the value of Δ_3; removing 10 levels from the pure GOE spectrum leads to a 200% increase in Δ_3. RMT requires that the NNS distribution and Δ_3 be calculated not for an entire spectrum but on *sequences*: subsets of levels which have an identical set of quantum numbers (for this study, total angular momentum J, parity π, and isospin T). It is desired that single sequences contain as many levels as possible; otherwise errors on ω and μ become large [Shr92]. Therefore, the NNS distribution and Δ_3 are reliable indicators of dynamics only if

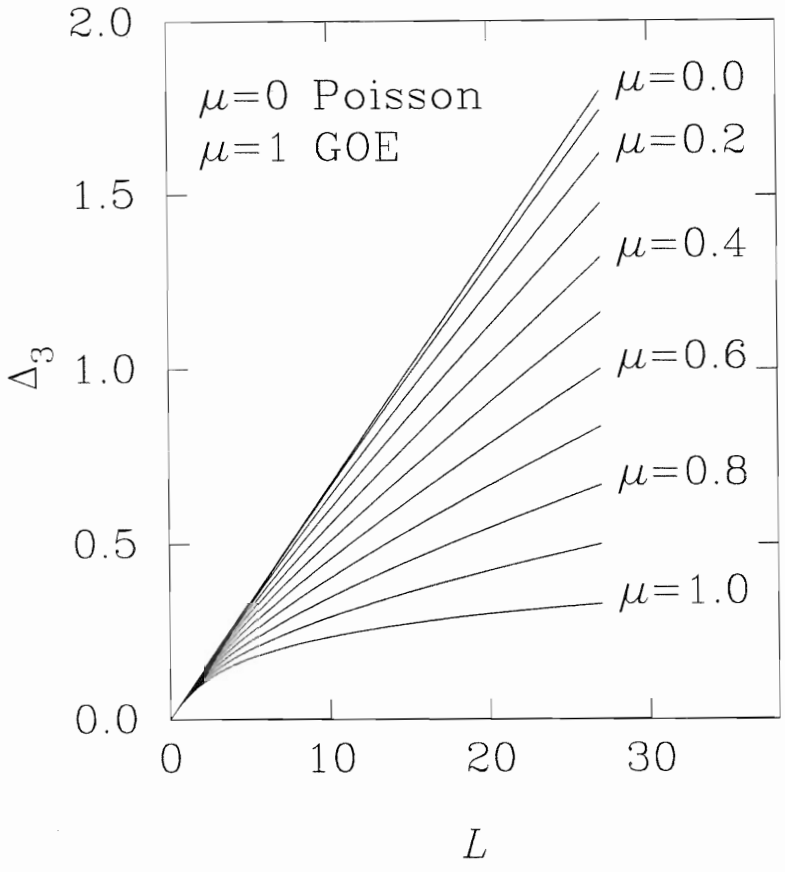

Figure 2.2. The Dyson-Mehta Δ_3 statistic for varying values of μ.

their input data are of very high quality. This sensitivity has great impact on experimental work, as it is extremely difficult to establish high-quality spectra over large energy ranges.

The many numerical and theoretical investigations of spectra have yielded much information regarding chaos on the quantum scale [Sel85, Win88, Ble94]. On the experimental side, atomic, molecular, and nuclear systems have been examined. One of the most widely used system for studies of quantum chaos is the H atom in a uniform magnetic field [Fri89]. This is a very attractive system since its Hamiltonian is well-known. However, an attempt to construct pure and complete sequences for weakly bound states of this

system "is hampered, apart from possible resolution problems, by the fact that transition strengths to levels may become very small and consequently the missing of these levels can considerably counterfeit the level-spacing distribution" [Wun86]. A number of atomic and molecular spectra have been analyzed using the NNS distribution and Δ_3 and have been shown [Ros83, Hal83] to match GOE predictions.

The most extensive experimental data sets to be analyzed with the NNS distribution and Δ_3 are the spectra obtained from nuclear resonance studies [Haq82]. These spectra show evidence of level repulsion. These data are limited to nuclei in highly excited states and a limited mass range, and there is interest in extending this data set to include a broader range of mass and energy. In this vein, a data set of low-lying energy levels from many nuclei spanning the periodic table has been compiled [Shr91] and it has been found that in the ground-state domain the lightest nuclei ($0 < A < 50$) exhibit GOE behavior and the heaviest ($230 < A$) exhibit Poisson behavior; intermediate masses display a smooth transition between these extremes. It is not known if this signals increasing regular dynamics with increasing A or if this is simply the manifestation of a neglected symmetry (such as the rotational quantum number K) which is relevant only in heavy nuclei.

It would be helpful to extend these studies to experimental spectra which span from the ground state into the resonance region. This has been done [Shr90] for the nucleus ^{26}Al: 160 states between the ground state and ~ 8 MeV were identified and analyzed; results were midway between GOE and Poisson but slightly favoring GOE. The data are consistent with being independent of isospin T. If T were a perfect quantum number, then the statistics of a spectrum consisting of two sequences of differing T but the same J and π should move toward Poisson. This is not found to be the case; the spectrum consisting of the admixture of $T = 0$ and $T = 1$ states exhibits behavior which is very close to that of the $T = 0$ sequences alone. (No comparisons to the $T = 1$ sequences were made since these did not contain sufficient numbers of levels to ensure statistical reliability.) This effect is expected

to a small degree since T is not a perfect quantum number. However, it is an approximate symmetry, and the results from ^{26}Al make sense in the light of work by Dyson and Pandey [Dys62, Pan81]. They found that even the small breaking of a symmetry will result in fluctuation patterns that are consistent with the complete absence of that symmetry. This result has been confirmed theoretically for the case of isospin by Guhr and Weidenmüller [Guh90], but no further experimental tests have been performed. Additional high-quality experimental spectra similar to that of ^{26}Al would be valuable for further examination of quantum chaos and its connection with broken symmetries. This is the motivation for the present work.

In searching for additional nuclei for studies similar to that done with ^{26}Al, several factors must be considered. Light nuclei are desired since their average level spacing is larger than that for nuclei with large A; this makes levels easier to resolve. However, nuclei which are too light will not contain enough levels to insure statistical reliability. The energy region just above and below the proton separation energy S_p is very difficult to probe. Nuclei with low S_p are desired, since in these nuclei this energy region will contain a small percentage of the total number of levels. For studies of T mixing, it is necessary that $T = 0$ and $T = 1$ states coexist throughout the entire energy range. The best candidates which match these criteria are the odd-odd light nuclei ^{22}Na, ^{26}Al, ^{30}P, ^{34}Cl, and ^{38}K. Rare gas targets are required for ^{22}Na and ^{38}K; ^{26}Al has already been studied. This leaves ^{34}Cl and ^{30}P, and ^{30}P has the target (^{29}Si) that is easier to prepare and is more stable in beam. Therefore ^{30}P was chosen for study.

2.3 Brief Description of ^{30}P

As a preliminary to the following discussions of the present work, it is appropriate to present general characteristics of ^{30}P ($N = Z = 15$). One unpaired proton and neutron

each resides in the $1d_{\frac{5}{2}}$ shell; the quantum numbers of the ground state are $J = 1$, $\pi = (+)$, and $T = 0$. The mass excess $(M - A)$ is -20.2045 MeV, $S_p = 5601.4$ keV, and $N_p = 11328.2$ keV. The nucleus decays by β^+ emission and K-shell electron capture with $T_{\frac{1}{2}} = 2.497$ m. The β^+ decay dominates, being ~ 800 times more likely that the electron capture process. There are 159 known levels in the range $0 \leq E_x \leq 8820$ keV. Figure 2.3 shows the current level scheme of ^{30}P in this range.

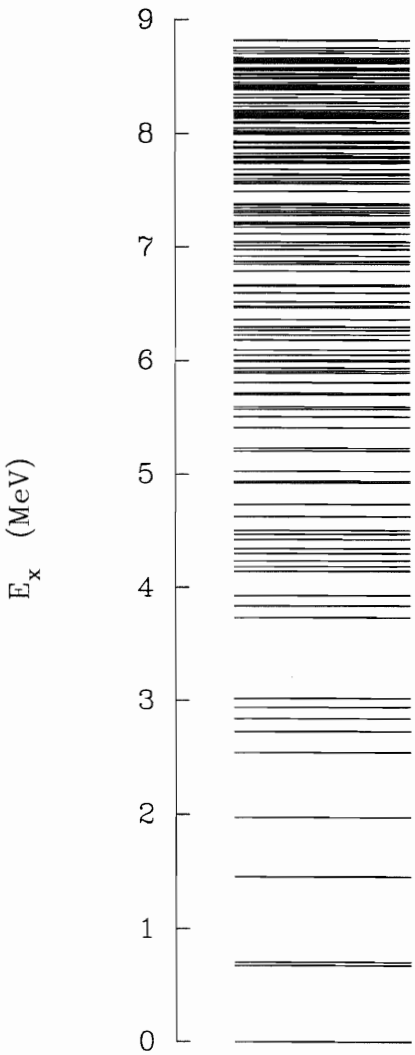

Figure 2.3. The ^{30}P level scheme for $0 \leq E_x \leq 8820$ keV.

Chapter 3

Experimental Setup

3.1 Accelerator and High Resolution System

The data presented in this dissertation were taken at the High Resolution Laboratory (HRL) of the Triangle Universities Nuclear Laboratory (TUNL). The laboratory has been described in detail by Westerfeldt *et al.* [Wes87, Wes88]. The HRL houses a single-ended KN Van de Graaff electrostatic accelerator (schematic shown in Figure 3.1) which has a potential range up to 4.1 MV. To diminish the threat of high-voltage breakdown, the accelerator column is encased in a tank which contains an 80-20 mixture of N_2 and CO_2 gases at high pressure ($\sim$ 300 psi). A low H_2O content (<20 ppm) also helps reduce the possibility of sparking. To generate high dome voltages, a 50 kV power supply provides charge to a screen, which in turn delivers the charge to a rubberized cotton belt powered by a drive motor. The belt carries the charge up the accelerator column and deposits it on the dome via a collector screen, generating a high electric potential at the dome.

In order to maintain a constant voltage, the charge is carried off the dome in three ways: by the beam, through sixty-nine 600MΩ series resistors to ground, and through a corona control circuit. This circuit includes a set of needles which are located inside the

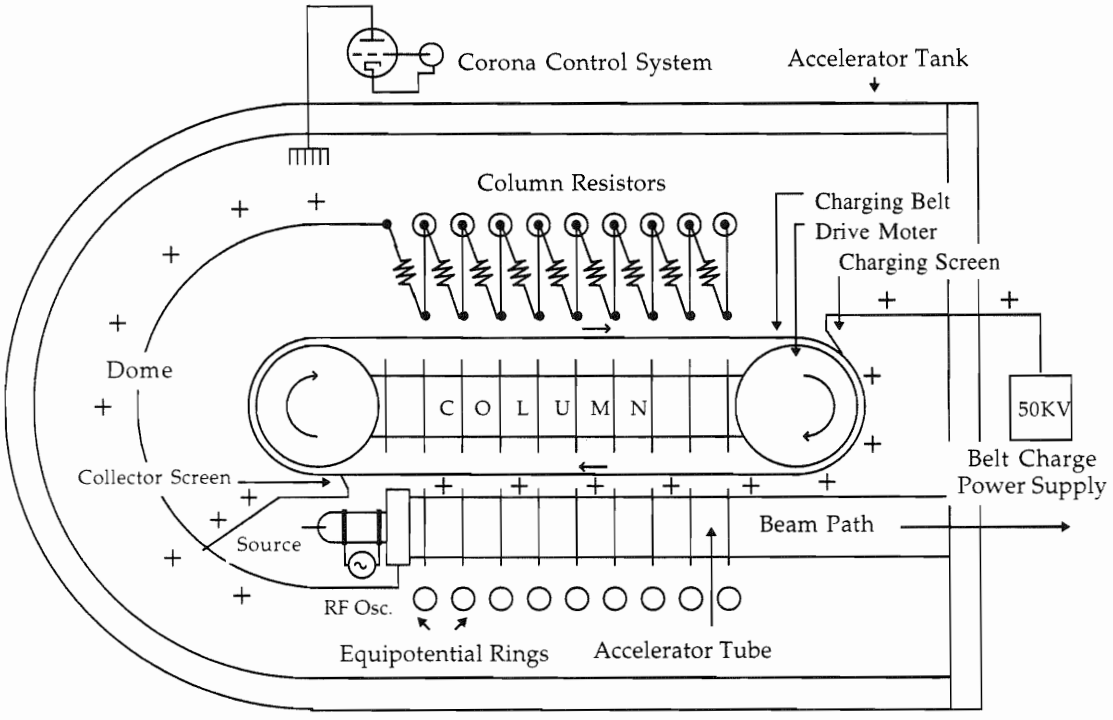

Figure 3.1. Schematic of the HRL single-ended Van de Graaff accelerator.

tank near the dome. The needles are negatively charged and the very strong electric field surrounding the points ionizes the insulating gas. The ionized gas provides a path for charge to flow off the dome and toward the needles; this current can be regulated to control the dome voltage. Between adjacent resistors are stainless steel rings which encircle the column. These rings serve to create equipotential planes and ensure that the accelerated particles (protons for this experiment) experience a smooth electrostatic gradient.

Inside the dome, mounted on the end of the column, is the ion source. H_2 is stored at high pressure (50 psi$< P <$200 psi) inside two small cylinders, each of which is connected to the source bottle through a Pd leak. As the operator increases the current to a Pd leak (the cylinders are used independently), the Pd heats up and becomes porous to H_2. The

pressure gradient forces the H_2 into the source bottle where it is dissociated by a $\sim$ 165 MHz RF field. The plasma created by the RF field consists mainly of electrons and two species of positive hydrogen ion: protons and singly-ionized molecular H (HH^+). A large positive extraction voltage is applied at the rear of the source bottle and a large negative voltage is applied to the focusing electrode at the front, pulling protons and HH^+ ions into the accelerator tube. The ions are then focused and accelerated down the gradient created by the dome and the equipotential rings. At this point the beam typically has a current of $\sim$ 30 μA. The tube is kept at high vacuum ($\sim$ 2 μTorr) by a diffusion pump, mechanical roughing pump, and liquid nitrogen (LN_2) trap.

Once out of the accelerator, the ions are sent through an analyzing magnet which divides the beam into two beams, each consisting of a different ion species. The magnetic field B acts as a momentum analyzer, accelerating particles of mass m, (non-relativistic) velocity v, and charge q along a circular path of radius $r = mv/qB$. The values of q are the same for each species, but their difference in mass and velocity leads to different values of r and thus to different deflection angles. The geometry of the beam lines fix the deflection angles at 25° for the protons and 17° for the HH^+ ions. The protons travel toward the HRL's reaction chambers for use in experiments and the HH^+ ions enter the electrostatic analyzer (ESA). The functions of the ESA will now be described.

Before entering the ESA, the HH^+ beam encounters a pair of vertical slits called corona control slits. When the dome potential is stable and the B-field is properly set, the beam is centered in the beamline and the current on each slit is the same. When the voltage on the dome fluctuates, the horizontal position of the beam changes, since the analyzing B-field does not track fast changes in beam energy. This gives rise to a difference in the slit currents which is proportional to the dome voltage fluctuation (and thus to the change in beam energy). In order to correct for this fluctuation, the slit difference signal is sent to the corona controller which regulates the charge exchange between the dome and the

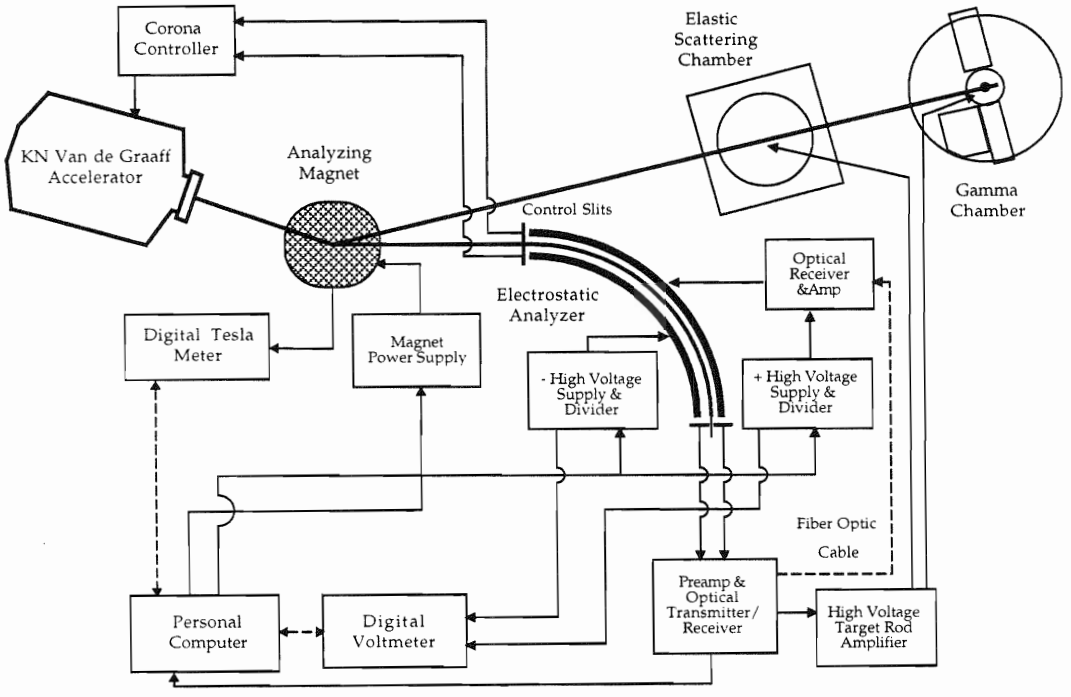

Figure 3.2. Schematic of the HRL control loops.

corona needles to stabilize the beam. This negative feedback system is effective only for low frequency ($\leq$ 20 Hz) dome voltage fluctuations due to the slow drift time of the ions. Figure 3.2 shows a schematic of this and other control loops associated with the ESA.

The ESA itself consists of two parallel stainless steel plates bent into an arc of 90° with mean radius of curvature 1.0 m. The plates are separated by a distance $d = 0.457$ cm and are biased by a pair of programmable high-voltage power supplies. A positive potential ϕ is applied to the outer plate and a negative potential of the same magnitude $-\phi$ is applied to the inner plate. This voltage difference gives rise to an electrostatic field of magnitude

$2\phi/d$ directed toward the inner plate.

The geometry of the ESA is such that the ratio of the proton energy E_p to ϕ is 111.34 eV/V. Each plate is connected to ground by a high-precision resistive divider which is used to convert the plate voltage into a voltage corresponding to E_p. This energy signal is sent to a Digital Multimeter (DMM) which subsequently sends the signal to a Personal Computer (PC) that runs the program LabVIEW. LabVIEW is given an energy set point via a serial line from the VAX. This set point is constantly compared to E_p and LabVIEW drives the plate voltage via two 16-bit Digital-to-Analog Converters (DAC's) such that the difference in the set point and E_p is minimized.

At the entrance to the ESA is a pair of object slits, and at the exit is a pair of image slits. The object slits help to insure that the beam is centered upon entering the ESA, and the image slits, in the manner of the corona control slits, produce a difference signal when the energy of the beam fluctuates. The difference signal from the image slits is converted into a voltage and sent to three places. First, it is sent to the PC in the control room which runs LabVIEW. LabVIEW uses this signal to control the analyzing B-field so that it will track slow changes in the beam energy (for example, while a yield curve is being taken). The difference signal is also sent to the ESA plates via a fiber optic transmitter in a negative feedback system which drives the plate voltage in such a manner that the beam stays centered in the ESA. Lastly, the slit difference signal is amplified by a factor of 111.34 and sent to the target rod in the relevant chamber (in this study, the (p,γ) chamber). The target rod is biased at +3 kV and the slit difference signal is multiplied by 111.34 and sent to the rod to adjust this bias voltage to compensate for rapid (up to 300 Hz) fluctuations in beam energy. For example, if the beam energy fluctuates downward by 500 eV, the target rod voltage drops by 500 V, the amount needed to maintain constant beam energy at the target rod. With this control system, called the beam homogenizer, a beam resolution of $\sim$ 220 eV can be achieved. This resolution is limited by Doppler spreading which results

from thermal motion of the target nuclei, and has been improved upon by using cooled gas targets

3.2 Detector System

In order to obtain a complete and pure level scheme, it is important not only that the accelerator be capable of resolving states in regions of high level density, but also that the γ-rays be detected with high resolution and that even very weak γ-rays be seen. The γ-ray chamber in the HRL has recently [Dra94] been reconfigured for the acquisition of such high-resolution γ-ray spectra with Compton-suppressed background. The data in the present study were taken using this chamber and represent the first set of experiments for which the γ-chamber has been used in this configuration.

After leaving the analyzing magnet, the proton beam is steered and focused by a number of magnets as it travels the length of the beamline. As it enters the γ-chamber, the beam current is typically 7 μA. The beam then strikes the target (described below), and the resulting emitted particles and γ-rays are detected. Five detectors were used: two 60% efficient High-Purity Germanium (HPGe) detectors used for detecting γ-rays with high resolution, a Bismuth Germanate ($Bi_4Ge_3O_{12}$, abbreviated BGO) detector used as an anti-coincidence shield for one of the HPGe detectors, a sodium iodide (NaI(Tl)) γ-ray detector, and a silicon surface barrier (SSB) charged particle detector. The NaI and SSB detectors were primarily used to generate ^{29}Si(p,p), ^{29}Si(p,γ), and ^{29}Si(p,p$_1\gamma$) yield curves for the identification of resonances. For information on principles of operation for these detectors, see Knoll [Kno79].

Both the Compton-suppressed HPGe (CSGe) detector with its BGO shield and the unsuppressed HPGe (USGe) detector sit on carriages which can be repositioned for data taking at different angles [LaB95]. The ranges are $25° - 160°$ and $55° - 125°$ for the USGe

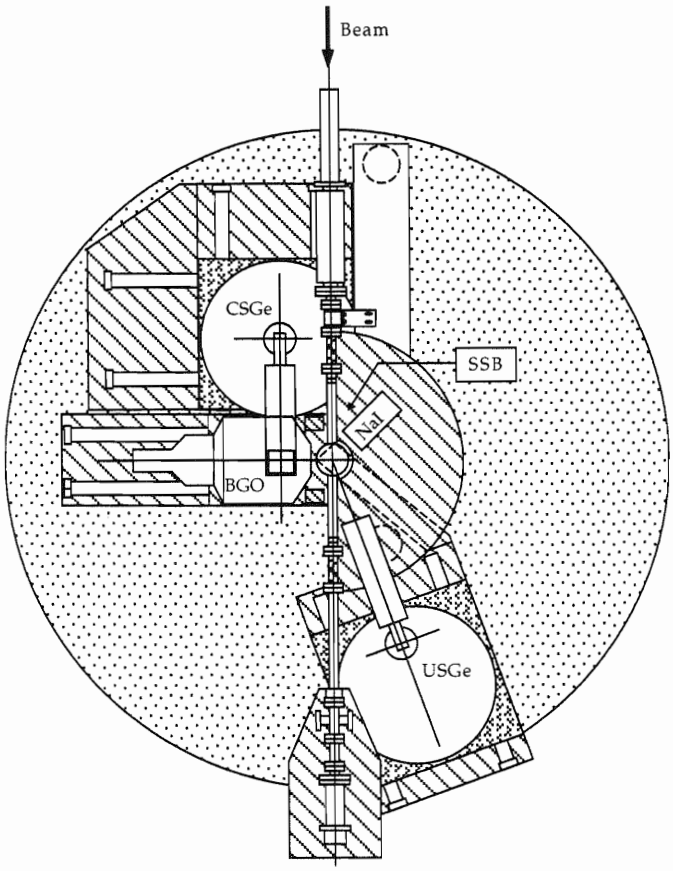

Figure 3.3. Overhead view of the γ-ray chamber.

and CSGe, respectively. The NaI detector is positioned at 140° and the SSB is fixed at 165°. An overhead view of the system is shown in Figure 3.3.

Compton scattering events are those in which a γ-ray enters the detector and scatters off atomic electrons and out of the detector, having deposited only a fraction of its incident energy inside the detector. These events increase the background and therefore are undesirable. To reduce the occurrence of these events, the BGO detector is used to detect the Compton-scattered photons that escape one of the HPGe's. The CSGe detector is

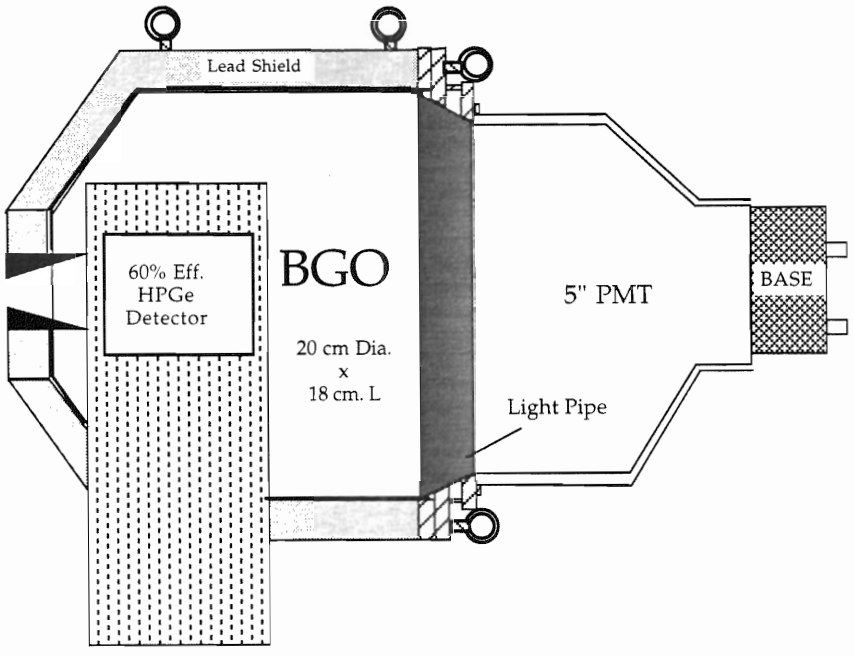

Figure 3.4. Cross-sectional view of the Compton-suppression system.

surrounded by the BGO (see Figure 3.4). Any signal from the CSGe which is in time coincidence with a signal from the BGO is assumed to be representative of a Compton-scattering event and is electronically vetoed. In establishing a high-quality level scheme it is important to observe even weak transitions between nuclear states, and the absence of the Compton background allows many of these transitions to rise above the noise. In addition, the escape peaks associated with pair production are greatly diminished. Figure 3.5 displays portions of two spectra taken concurrently in order to show the effect of the Compton suppression.

HPGe semiconductor detectors have very high resolution ($\sim$ 1.9 keV for the 1332 keV ^{60}Co γ-ray) and so are ideal for the present study. BGO is a highly efficient γ-ray detector due to its high density (7.3 g/cm^3) and the high atomic number of Bi ($Z = 83$) and so will detect the vast majority of γ-rays which escape the CSGe. Although its efficiency

is high, BGO has very poor resolution (about 10-20%) and is not used as a primary detector in high-resolution experiments.

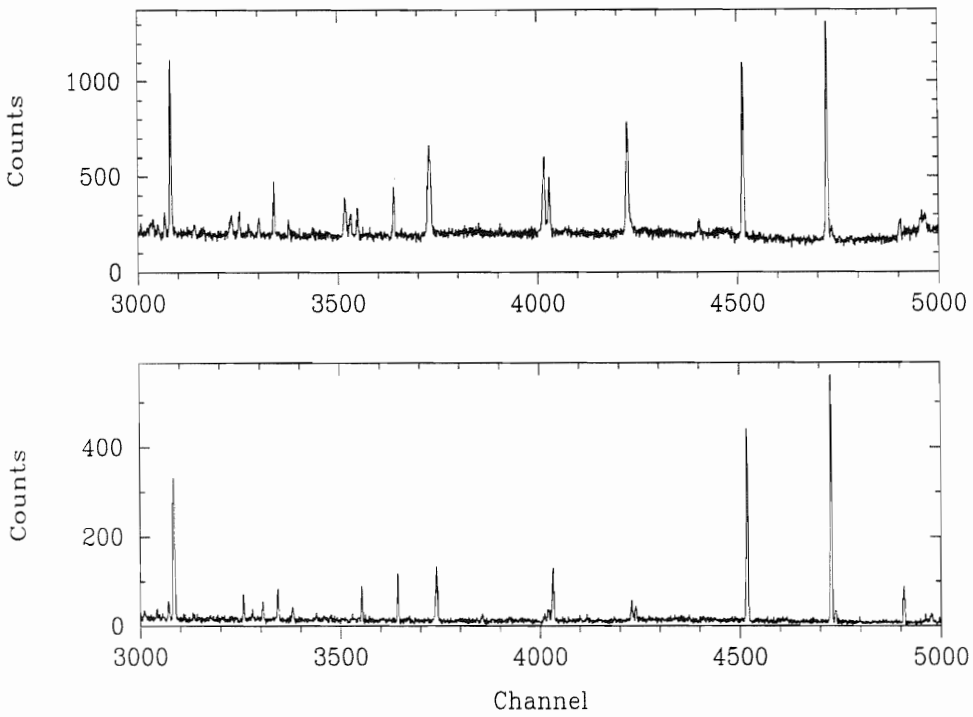

Figure 3.5. Portions of the unsuppressed spectrum (top) and suppressed spectrum (bottom) from ^{29}Si(p,γ) at E_p = 2.081MeV. The energy range is $E_\gamma \sim 3.0 - 5.0$ MeV. The effect of the Compton suppression is evident in the reduced background and diminished escape peaks at channels $\sim$ 4020 and 4230.

3.3 Data Acquisition

3.3.1 General

For an event in a given detector, the output of the preamplifier is a voltage pulse with height proportional to the deposited energy. During the experiment, this output is sent to various electronics modules in the control room which further process the signals

and send them through a Multiprogrammable Branch Driver (MBD) to a VAXStation 3200 computer for storage.

The experiments consist of a series of runs whose lengths are determined by the beam current on target (typically $\sim 7\,\mu$A) and by the value of a preset scaler. This scaler is given a preset value, which is the amount of charge which will pass through the target during the run. Since for these experiments this number is $\sim 4 \times 10^4\,\mu$C, individual runs last ~ 2.2 hours. The charge is collected in a Faraday cup behind the γ-chamber and sent to a current integrator which digitizes the signal and sends it to the preset scaler. When the amount of integrated charge equals the preset value, the crate inhibit is raised and data acquisition is halted. There are also two hex-input scalers which count the number of times during a run that certain events occur in the processing of detector signals. A clock is input into one of the hex scalers, and thus the elapsed time during a run is monitored.

The crate inhibit unit is designed to halt data acquisition when one or more specific conditions arise. Four of its six inputs were used in these experiments. The first input is from a manual data on/off switch operated by the experimenter. The second is a signal from the PC running LabVIEW. When E_p deviates from the energy set point by more than 30 eV, the PC sends a signal to the second input which raises the inhibit. During a run the target rods must be biased by +3 kV; if they are not, the signal at the third input will inhibit data collection. The fourth input comes from the preset scaler which tells the inhibit unit that the desired amount of current has passed through the target.

3.3.2 HPGe/BGO Electronics

The analysis of a signal from the HPGe detectors involves the determination of timing information as well as energy information. Each HPGe detector preamplifier has an energy output and a timing output which are routed to two different sets of electronics modules. The BGO detector is used for timing only.

The determination of the energy of a signal from an HPGe detector is relatively simple. The energy signal is first sent to a Tennelec TC245 amplifier. The TC245 has two special features which were used in the collection of the data: pileup rejection (PUR) and ballistic deficit correction (BDC). The PUR circuitry vetoes events of energy E_1 and E_2 which occur close enough in time that they could be interpreted as a single event of energy $E_1 + E_2$, thereby reducing the number of bad signals and suppressing the background. Differences in charge carrier drift times give rise to *ballistic deficit*, which leads to degraded resolution. Since high resolution spectra are very important for this study, this resolution loss is highly undesirable and is corrected for by the BDC circuitry. The TC245 amplifies and shapes signals for acceptance into a quad-input ADC which resides in the CAMAC crate. This ADC digitizes this gated signal, which is forwarded through the MBD to the VAX for storage. The gates are generated by the timing electronics which are discussed below.

The timing electronics serve to determine coincidences between the CSGe and BGO detectors and between the two HPGe detectors. The timing signals from the HPGe and BGO preamplifiers are each sent to an Timing Filter Amplifier (TFA). These amplifiers output fast (ns range) negative signals which are sent to a 4-channel Tennelec TC454 Constant Fraction Discriminator (CFD). Channels 1 and 2 are used by the HPGe signals, and signals from the BGO are sent through a third TFA into channel 3. The role of the CFD is to provide a precisely-defined logic pulse for the subsequent timing analysis as well as ADC gate signals for the USGe. All events which occur simultaneously in the CSGe and BGO are assumed to be Compton scattering or pair production events; thus the CFD output pulses corresponding to these detectors are sent to a logic unit which outputs a pulse every time a signal arrives from the CSGe *without* a coinciding signal from the BGO. The result is the vetoing of many of the signals which originate from Compton scattering or pair production events. The output from the logic unit is used for three tasks: gating the CSGe energy

signal at the ADC, counting the number of CSGe events at the scaler device, and stopping a Time-to-Amplitude Converter (TAC). The purpose of the TAC is to identify coincident events in the CSGe and USGe. The TAC has two inputs: a start and a stop. The start signal comes from the CFD output from the USGe detector. The stop signal is delayed 31.5 ns before entering the TAC so that true coincident events will be separated in time by this amount. The output of the TAC is a signal whose height is proportional to the time between these two input pulses. The output of the TAC is the input for channel 3 of the CAMAC ADC. This channel was not used in the present experiments, but will be useful in the future for $\gamma - \gamma$ coincidence measurements. A diagram of the HPGe/BGO electronics setup is shown in Figure 3.6.

3.3.3 NaI and SSB Electronics

The signals from the NaI and SSB detectors were treated in a simpler manner than those from the HPGe and BGO detectors since no timing analysis is required for events originating in these detectors. In addition, the signals are processed identically, with one exception: C(p,p) events registered by the SSB detector are gated out of the charged-particle spectrum, while no such procedure is needed for the NaI γ-ray spectrum. (The C comes from the foils used to make the targets; for information about targets, see Section 3.4.) An output signal from the NaI or SSB preamplifier is sent first to an amplifier which shapes the pulse and outputs both a unipolar signal and a bipolar signal. The unipolar signal is sent directly to a second quad-input CAMAC ADC in gated input mode. The gate is generated by the bipolar signal which is sent to two places: a Timing Single Channel Analyzer (TSCA) and through a delay to a Single Channel Analyzer (SCA). The TSCA associated with the SSB detector has a gate which is set around undesired signals which arise from elastic scattering off the C on the targets; no such gate is set with the NaI TSCA. Whenever the SSB TSCA encounters a pulse originating from a C(p,p) event, it outputs

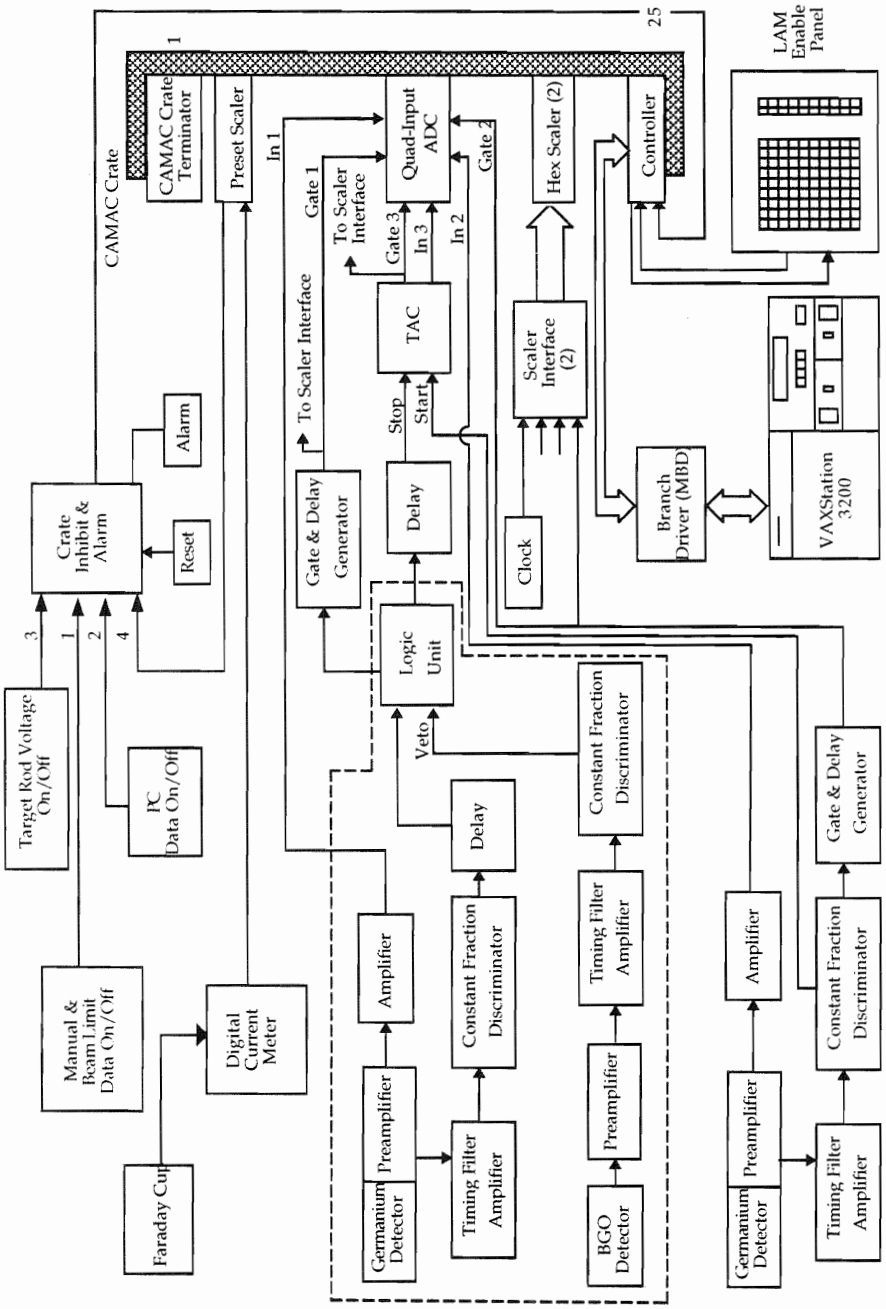

Figure 3.6. Data acquisition electronics for HPGe and BGO detectors.

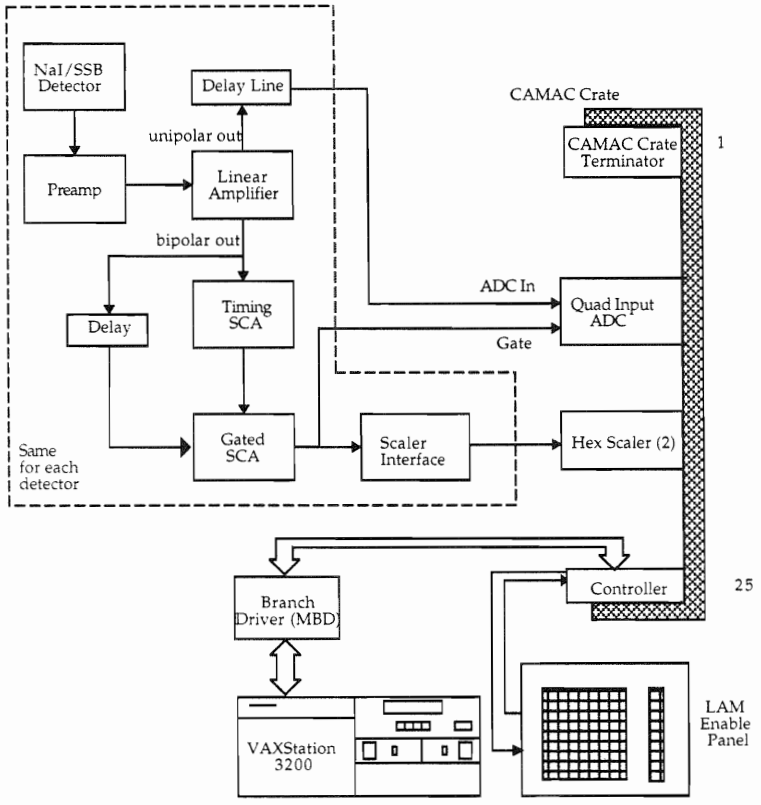

Figure 3.7. Data acquisition electronics for NaI and SSB detectors.

a pulse which is input to the same SCA to which the delayed bipolar signal is sent. A low-level discriminator on both SCA's is used to eliminate low-voltage electronic noise. The SSB SCA then outputs a logic pulse every time an event occurs which does not arise from either of these cases; these pulses are used as input gates at the ADC. The NaI SCA outputs a gate signal only when an event occurs which does not arise from noise. This system is shown schematically in Figure 3.7.

3.4 Targets

3.4.1 ^{29}Si Targets

The targets used for taking the ^{30}P data consist of thin films of ^{29}Si evaporated onto 5.0 μg/cm^2 carbon foils. The isotope was obtained from Oak Ridge National Laboratory in the form of SiO_2 enriched to about 95% ^{29}Si. The target thicknesses were kept very small (1.5 and 3.0 μg/cm^2) in order to see resonances with small total widths (down to <10 eV) and to resolve adjacent resonances with very small spacings (down to < 1 keV). For E_p = 2.1 MeV (the average E_p for this work), a 1.5 μg/cm^2 Si target corresponds to an energy loss of $\sim$ 170 eV and a 3.0 μg/cm^2 target to $\sim$ 340 eV. The target thickness used for a particular resonance was decided upon by comparing its width and adjacent spacings to these numbers.

The carbon foils were obtained from the Arizona Carbon Foil Company on glass slides. Distilled H_2O is used to float the foils off the slides and onto stainless steel target rings. The target rings are then placed on a rack in a bell jar which is kept at a base pressure of < 1 μTorr by a system consisting of a diffusion pump, mechanical roughing pump, and LN_2 trap. This rack is positioned in the jar so that the foils are above a 0.005″ Ta closed boat (part no. SI7B-.005TA from the R. D. Mathis Company) which is filled with Ta powder and isotope in the ratio 7-8:1. Between the boat and the rack are two metal slides: the lower slide has an aperture of diameter 1.9 cm and the upper slide is a shutter which may be opened during evaporation (see Figure 3.8). The slide with the aperture serves to channel the evaporated material toward the foils and away from the bell jar. The distance between the foils and the boat is $\sim$ 15 cm. While the shutter is closed, a current of 85 A is run through the boat in order to raise it to a temperature of $\sim$ 1100° C. At this temperature the moisture contained in the Ta boat evaporates, but the Si/Ta mixture in the boat is unaffected. This "outgassing" procedure ensures that no excess H_2O builds

up on the targets during Si evaporation. During outgassing, which generally lasts no more than 30 s, the vacuum jumps to a value of $\sim 100\,\mu$Torr and rapidly improves to nearly base pressure. After the current is turned down and the vacuum returns to base pressure, the evaporation is begun. The current is turned up to 115 A, bringing the boat to a temperature of $\sim 1450°$. At this time the shutter is opened. The Ta powder is a reducing agent for the SiO_2, and this temperature is high enough to melt the SiO_2 and allow the reduction to take place. It is believed that the evaporated material is in the forms Si and SiO. The time required for evaporation depends on desired target thickness and the amount of Si/Ta in the boat. It has been found that two evaporations on average are possible from 20 mg Si.

In addition to the foils, a quartz crystal is exposed to the boat. At the start of evaporation the crystal oscillates at an initial frequency f_i which decreases to a final value f_f as material evaporates and collects on the quartz. A Thickness Monitor then uses the value $f_i - f_f$ along with several user-input parameters (among them the density of Si) to determine the thickness of the evaporated material on the targets in kÅ. However, this number is indicative not of the amount of Si alone, but also of O, small amounts of Ta, and traces of such elements as F and Na. Therefore, only a relative measure of the thickness is available. By comparing elastic scattering from natural Si ($^{28}SiO_2$) targets to Coulomb (non-resonant) scattering, it was determined that 0.07 kÅ on the monitor corresponds to a thickness $T \simeq 1.5\,\mu$g/cm^2 and 0.13 kÅ to $T \simeq 3.0\,\mu$g/cm^2.

3.4.2 ^{27}Al Targets

The preparation of ^{27}Al targets is similar to that of the ^{29}Si targets. The foils used are identical, as is the evaporation chamber and setup. Prior to the ^{27}Al evaporation, a small amount of Victawet is placed in a 0.005″ Ta open boat and evaporated at a current of 10 A for about 3 minutes. This material coats the inner surface of the bell jar and aids in later cleaning. Ultrapure Al (100% ^{27}Al) is then obtained in wire form (diameter=0.04″)

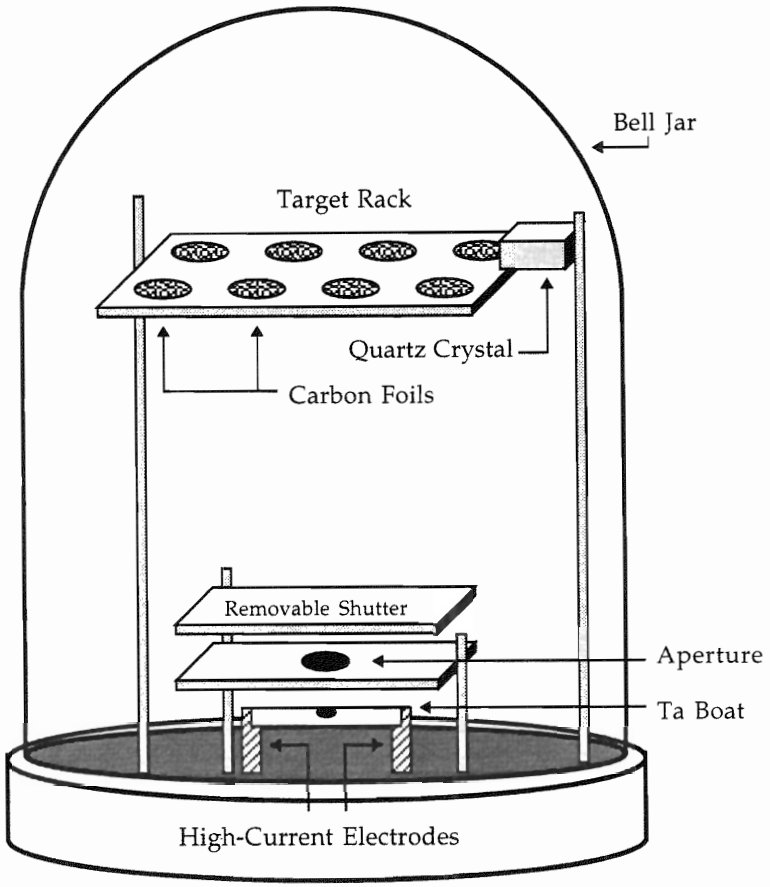

Figure 3.8. Setup for preparing targets.

and three 0.25″ pieces are clipped and placed in second 0.005″ Ta open boat. The current through the boat is slowly increased to 50 A, at which point the Al melts and begins to evaporate onto the foils. For targets about 10 μg/cm^2 thick, the evaporation should be stopped when the monitor reads 0.350 kÅ. The evaporation process lasts between 4 and 5 minutes, after which the bell jar and the components within are coated with a visible layer of Al.

Chapter 4

Data Collection and Analysis

The primary data in this study consist of sets of high-resolution 8192 channel γ-ray spectra. one set for each of the 25 resonances studied. In general, each set contains four spectra: two on-resonance spectra and two off-resonance spectra. The meaning of these data. as well as their collection and analysis, will be discussed in the present chapter.

4.1 Data Collection

Before an experiment, the experimenter allocates sections of the VAX's memory for storage of data and other relevant information (scalers, etc.) using the software package XSYS [Sod87]. These sections are called *data areas* and four of them are used to collect and display spectra in this experiment: data areas 1-4. Data area 1 contains a 512 channel charged particle spectrum from the SSB detector, data area 2 contains a 512 channel γ-ray spectrum from the NaI detector, and data areas 3 and 4 contain 8192 channel spectra from the suppressed and unsuppressed HPGe detectors, respectively. All of these spectra contain gates which are set around different energy regions and are used to generate yield curves. Data area 1 is used to create a ^{29}Si(p,p) yield curve and data areas 2-4 are used to create

yield curves for the ^{29}Si(p,γ) and ^{29}Si(p,p$_1\gamma$) reactions. For this study, these yield curves are used only for the location of previously identified resonances and are not the subject of any offline analysis. The identification was performed by comparing yield curves to those previously obtained at the HRL [Fra91b, Vav96].

Once a resonance is located, the beam energy is adjusted to correspond to the energy of the resonance E_r being studied. The HPGe spectra are then collected for an extended period of time. Typically, about 2.5×10^5 μC are allowed to pass through the target for a given resonance; the actual number varies and depends on the ^{29}Si(p,γ) cross section at E_r. In the interest of isolating the γ-rays which are emitted from ^{30}P, this amount of data is taken both on and off resonance. The off-resonance data are collected at the energy closest to E_r at which the yield curve has fallen to background levels. Therefore, the off-resonance spectra include γ-rays from target impurities and background, but very few γ-rays from ^{30}P. The comparison of on-resonance and off-resonance spectra thus aids in identifying the γ-rays from the ^{29}Si(p,γ) reaction. The on-resonance and off-resonance spectra are taken by breaking up the experiment into runs of $\sim 4 \times 10^4$ μC and alternating between on and off-resonance energies. With beam currents on target of about 7 μA, data collection for a single resonance typically lasts about 24 hours.

The angular distribution of γ-rays for an isolated resonance may be expressed [Eva55] as

$$W(\theta) = \sum_{n=0}^{L} A_{2n} P_{2n}(\cos\theta). \tag{4.1}$$

During an experiment the suppressed detector is placed at 55°, since this is a zero of $P_2(\cos\theta)$, the leading non-isotropic term in the expansion. The reduced background of the suppressed spectrum allows for accurate fits of weak transitions and thus decreased intensity errors. The measured energies in the suppressed spectrum, however, are Doppler shifted by about +0.15% at 55° and are not reliable indicators of the true γ-ray energy. In order that energies be accurately determined, the unsuppressed detector remains at 90° throughout

the experiments; at this angle the Doppler shift is minimal. Although the background is higher in the unsuppressed HPGe, this has very little effect on the peak centroids. In light of these considerations, the suppressed spectra are used to determine γ-ray intensities and the unsuppressed spectra are used to determine γ-ray energies.

4.2 Calibrations

For this work it is very important that the energies and intensities of decays in ^{30}P have small errors; this requires high-quality calibrations. For energy calibrations we want to know the function $E_\gamma(x)$ for the range $0 < E_\gamma < 8$ MeV, where x is the channel number. In order to accurately determine this function one must be able to generate γ-rays (called *source* γ-rays) throughout this region which have well-known energies. Efficiency calibrations are necessary since the efficiency of HPGe detectors is not independent of energy [Kno79]: we seek the relative efficiency $\epsilon(x)$. More requirements exist for the determination of efficiency calibrations, since one must know both the energy of the source γ-rays and relative intensities I_γ. Since no one readily available nuclide provides γ-rays with well-known energies and intensities which cover the entire energy range, two different nuclides are used to provide the source γ-rays. Thirteen γ-rays [LS78] from a 10 μCi commercial ^{152}Eu source were used in the low-energy range $0 < E_\gamma < 1523$ keV. Similarly, 17 γ-rays [End90b] from the strong ^{27}Al(p,γ) resonance at $E_p = 0.99186$ MeV were used in the high-energy range $1523 < E_\gamma < 7933$ keV. These high-energy γ-rays come from the nuclide ^{28}Si. The ^{152}Eu and ^{28}Si source spectra are taken before an experiment and are used for energy and efficiency calibrations for all data taken during the run.

The source γ-rays are fit with the program GELIFT [Rad89] which is a least-squares peak-fitting FORTRAN package. GELIFT returns a file with extension .STO. The .STO file contains six numbers for every γ-ray: the centroid expressed as an energy

Table 4.1. ^{152}Eu source γ-rays[a]

E_γ (keV)	E_γ Error (keV)	I_γ (Relative)	I_γ Error (Relative)
244.692	0.002	3590	60
295.939	0.008	211	5
344.276	0.004	12750	90
367.789	0.005	405	8
411.115	0.005	1070	10
488.661	0.039	195	2
688.678	0.006	400	8
778.903	0.006	6190	80
867.388	0.008	1990	40
964.131	0.009	6920	90
1212.950	0.012	670	8
1299.124	0.012	780	10
1408.011	0.014	10000	30

[a]From [LS78]

E_γ (energy) and its error, the centroid expressed as a channel x (channel number) and its error, and the background-subtracted area under the peak (proportional to I_γ) and its error. The .STO files are used to create input files for the programs which generate the calibrations. The calibration procedures are described in the following sections. Table 4.1 (4.2) shows the energies and relative efficiencies of the low-energy (high-energy) source γ-rays and Figure 4.1(4.2) shows the suppressed low-energy (high-energy) source data.

4.2.1 Energy Calibrations

The energy calibration for a given ^{30}P spectrum is the combination of the individual low- and high-energy calibrations. From the tables it is seen that the highest energy γ-ray from ^{152}Eu (1408 keV) is lower than the lowest energy γ-ray from ^{28}Si (1523 keV). This

Table 4.2. ^{28}Si source γ-rays[a]

E_γ (keV)	E_γ Error (keV)	I_γ (Relative)	I_γ Error (Relative)
1522.81	0.02	2787	94
1658.34	0.02	610	16
1779.03	0.02	94766	4
1873.26	0.02	288	9
2838.83	0.03	5598	4
3061.82	0.03	1110	40
3124.14	0.03	790	30
4497.17	0.05	4563	26
4607.86	0.05	3960	120
4742.30	0.05	8500	300
4799.31	0.05	287	11
5662.52	0.06	700	20
6019.98	0.06	5634	94
6265.11	0.06	2150	70
6878.79	0.07	498	8
7923.45	0.08	4090	120
7933.45	0.08	3309	60

[a]From [End90b]

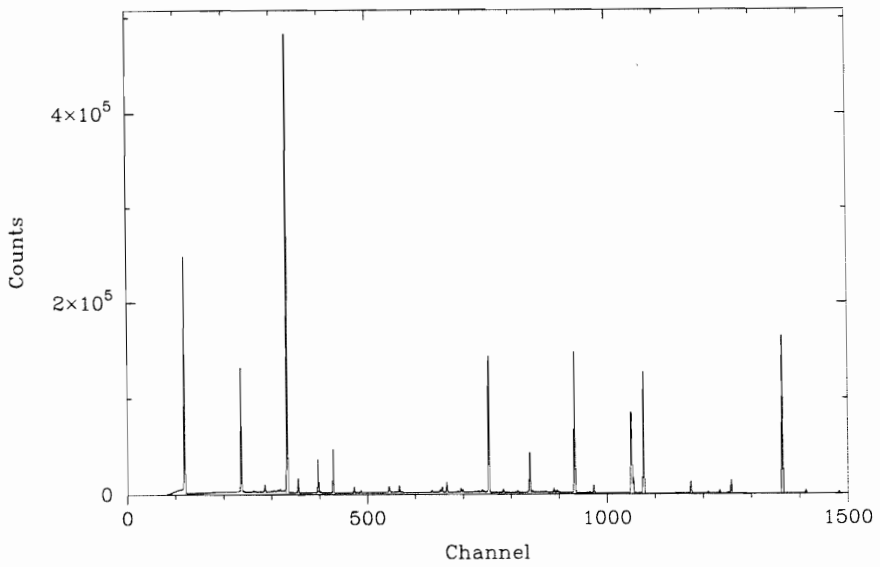

Figure 4.1. Suppressed ^{152}Eu source data. The energy range is $\sim 0 - 1600$ keV.

creates a problem in that one cannot reliably assign a value of E_γ to the channels between these energies. This gap is bridged by using the 1523 keV γ-ray from ^{28}Si for both low- and high-energy calibrations: this γ-ray is simply added to the ^{152}Eu list. Thus for calibration analysis there are not 13 but 14 source γ-rays which span the low-energy region.

Once the source data are collected and fit with GELIFT the positions x_i of the source γ-rays must be associated with their known energy values E_i. These known values are kept in a user-created file with the extension .SOU. The program SOURCE matches the energies from the .SOU file with their corresponding channels in the .STO file. The SOURCE output file contains these matched energies and channels and has extension .SIN. We thus have a set of points on the energy-channel plane and these points are fit to a polynomial

$$E_\gamma(x) = \sum_{n=0}^{N} c_n x^n \tag{4.2}$$

for varying values of N ($N = 1 - 5$) by the program ENCAL [Rad89]. The coefficients c_n are the calibration parameters and are adjusted for the best fit. For each value of N,

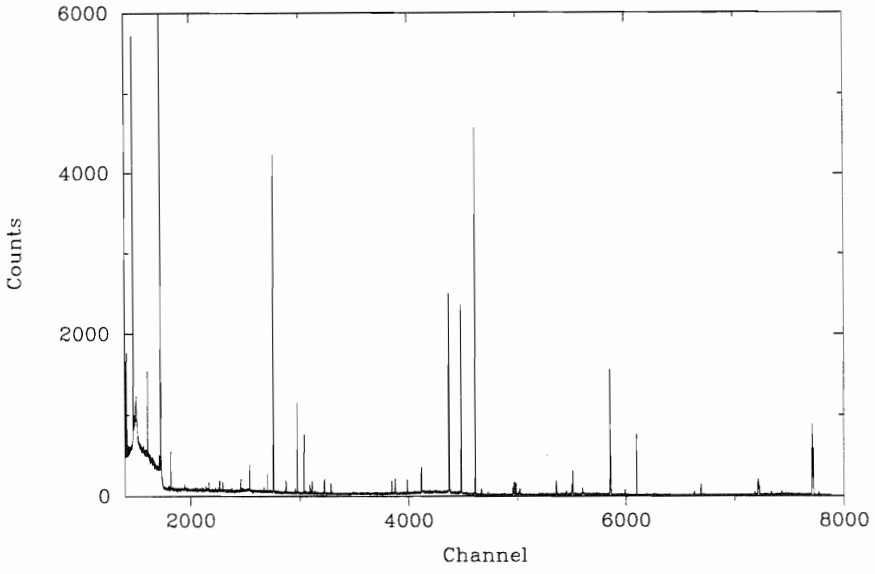

Figure 4.2. Suppressed ^{28}Si source data. The energy range is $\sim$ 1400 – 8000 keV. The strong peak at channel $\sim$ 1800 is the 1779 keV ^{27}Al(p,p$_1\gamma$) γ-ray.

ENCAL computes the rms quantity

$$\langle \Delta^2 \rangle^{1/2} = \left\{ \sum_{i=1}^{k} (E_i - E_\gamma(x_i))^2 \right\}^{1/2}, \tag{4.3}$$

where E_i is the energy of the i^{th} source γ-ray from the .SOU file ($k = 14$ for the low-energy calibration, and $k = 17$ for the high-energy calibration). The quantity $\langle \Delta^2 \rangle^{1/2}$ provides a measure of the goodness of fit for each value of N. For all fits, the linear ($n = 1$) term in Equation 4.2 dominates. However, it is found that $\langle \Delta^2 \rangle^{1/2}$ is most often a minimum for $N = 4$ or 5. The small higher order coefficients serve to adjust the fit to nonlinearities in the data acquisition system. The parameters c_n are stored in a file with extension .CAL and are read into GELIFT for analysis of the HPGe spectra. Shown in Figure 4.3 (4.4) is the low-energy (high-energy) calibration and its associated value of $\langle \Delta^2 \rangle^{1/2}$ for the data taken in May of 1995.

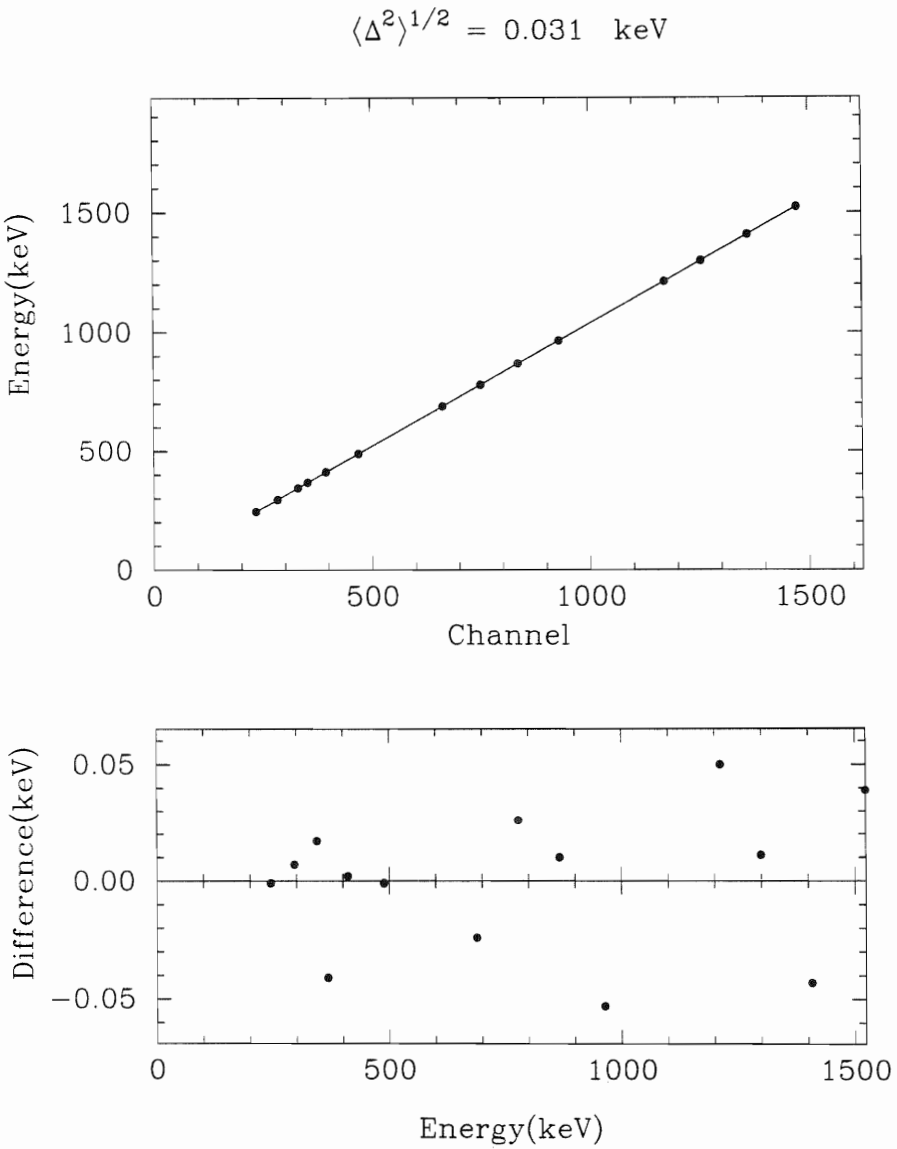

Figure 4.3. Low-energy calibration. The top figure shows $E_\gamma(x)$ for N=5 and the bottom figure shows (data – fit). The rms quantity $\langle\Delta^2\rangle^{1/2}$ is also given.

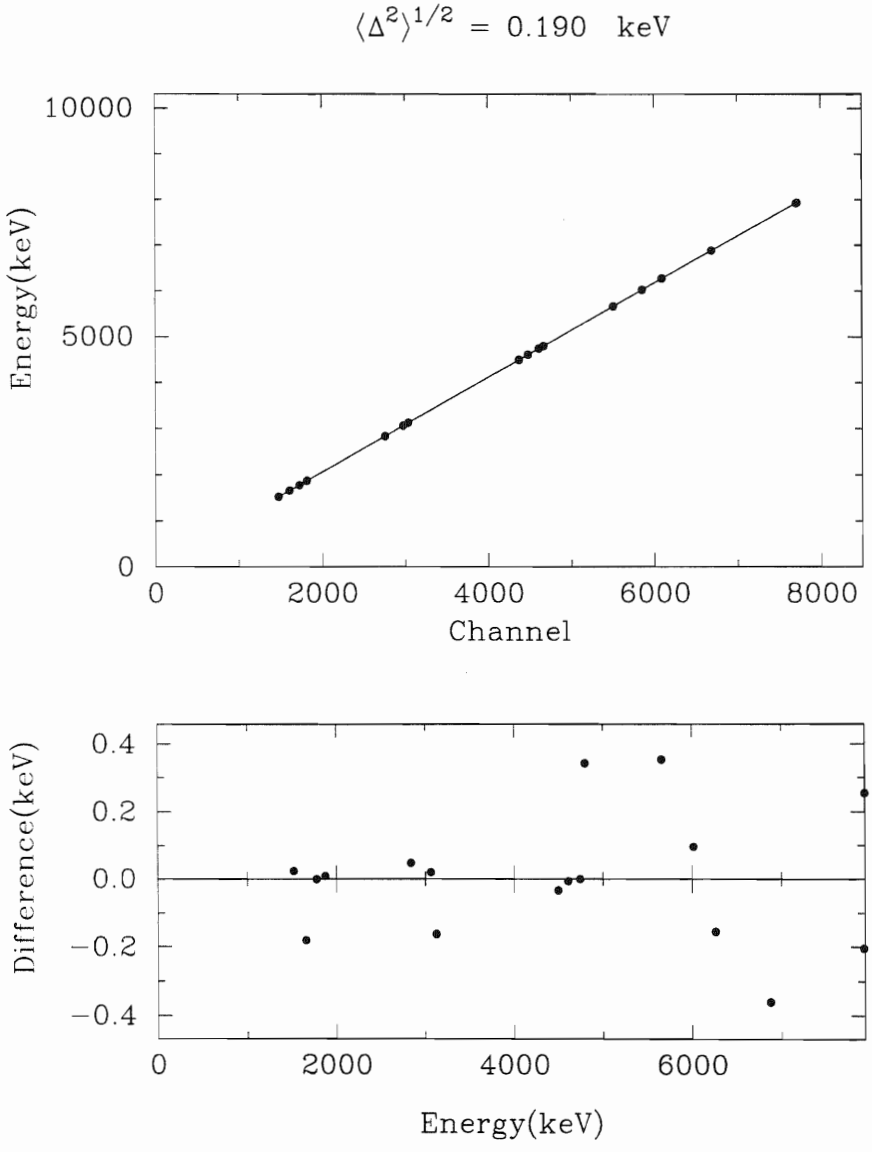

Figure 4.4. High-energy calibration. The top figure shows $E_\gamma(x)$ for N=5 and the bottom figure shows (data – fit). The rms quantity $\langle\Delta^2\rangle^{1/2}$ is also given.

4.2.2 Efficiency Calibrations

The program EFFIT [Rad89] uses the .SIN file to determine relative efficiencies at the positions of the source γ-rays. The relative efficiency of the detector at energy E_i is $\epsilon(E_i) = I_e(E_i)/I_s(E_i)$, where the $I_e(E_i)$ are the raw intensities (the number of counts in the peak) and the $I_s(E_i)$ are is the source intensities given in the .SIN file. The points $\epsilon(E_i)$ are read from both the low- and high-energy .SIN files and the user performs a visual match of the two regions by adjusting a normalization parameter. The entire set of points is then fit by EFFIT to minimize $\langle\Delta^2\rangle^{1/2}$. The functional form used in the fit is

$$\epsilon(E_\gamma) = \exp\left[(A + By + Cy^2)^{-G} + (D + Ez + Fz^2)^{-G}\right]^{-1/G}, \tag{4.4}$$

where $y = E_\gamma/\ln 100$ and $z = E_\gamma/\ln 1000$ [Rad89]. The parameters $(A, B, \ldots, G)$ from the fit are stored in a file with extension .EFF which is used in subsequent analysis of HPGe spectra. The fit from the May, 1995 experimental run and the corresponding value of $\langle\Delta^2\rangle^{1/2}$ is shown in Figure 4.5, where it is expressed as a percent.

4.3 Data Analysis and Quantum Number Assignments

Once the calibrations are complete, the HPGe spectra are fit with GELIFT. The .STO file which is output by GELIFT is used to create the input file for the program GRAY. This program assists the user in assigning quantum numbers by exploiting known information on selection rules and transition probabilities for nuclear radiative transitions. Before a detailed account of the analysis procedure is given, these selection rules and transition probabilities will be summarized.

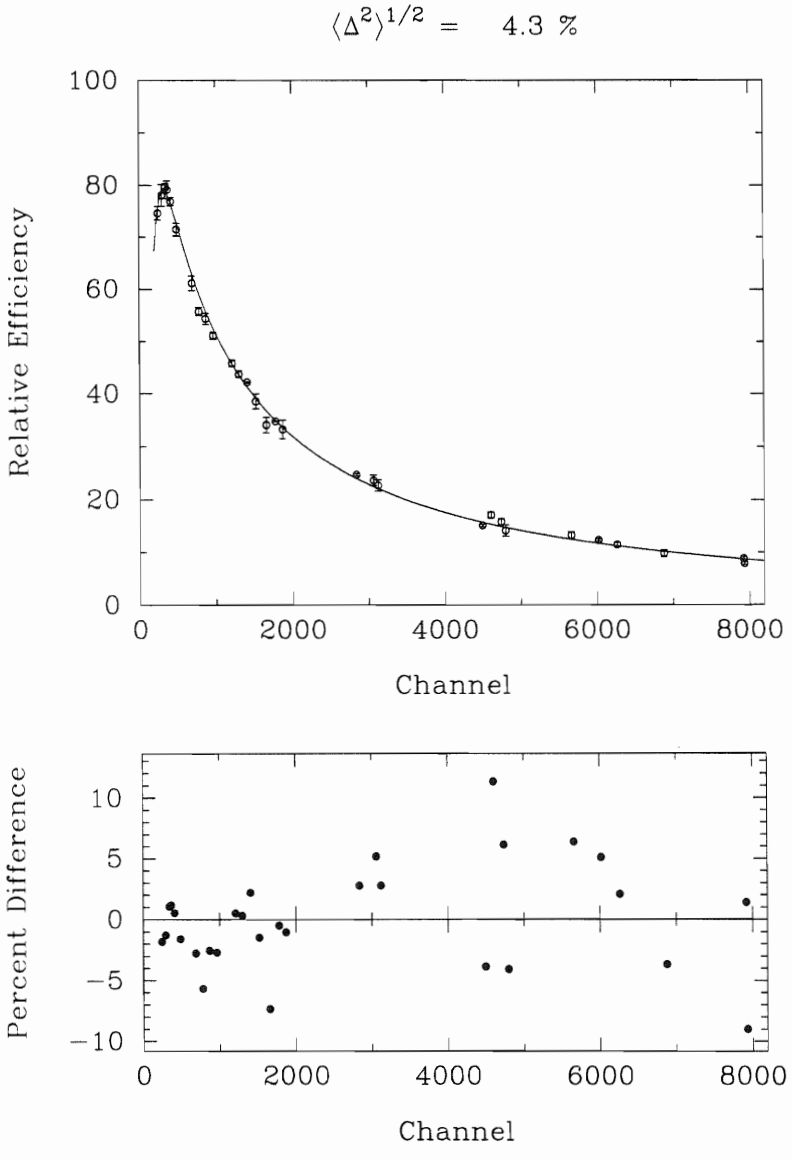

Figure 4.5. Efficiency calibration. The top figure shows the relative detector efficiency and the bottom figure shows (data – fit) for each source γ-ray. The rms quantity $\langle\Delta^2\rangle^{1/2}$ is also given.

4.3.1 Nuclear Radiative Transitions

Selection Rules

A photon of multipolarity Lcarries an angular momentum of magnitude $L\hbar$ with a z-component $m\hbar$. If this photon has been emitted from a nucleus as it undergoes a transition between initial state ψ_i and final state ψ_f with total angular momenta $\vec{J}_i$ and $\vec{J}_f$, respectively, then its energy will be $E_\gamma = E_i - E_f$. By the conservation of angular momentum we have

$$\vec{J}_i = \vec{J}_f + \vec{L}. \tag{4.5}$$

Multipole radiation may be emitted in such a transition only if

$$|J_i - J_f| \leq L \leq J_i + J_f \text{ and } m_i - m_f = m. \tag{4.6}$$

All values of L and m which satisfy these rules may be present in the emitted radiation, with one exception: the case $J_i = J_f$. In this instance, these equations allows radiation with $L = 0$, a physically unrealizable situation. The value $L = 0$ corresponds to the monopole term in the multipole expansion, which in the electric case is simply the total charge of the nucleus, Ze. This quantity is static and therefore does not radiate. The magnetic case is simple: to our knowledge, magnetic monopoles do not exist. The lowest possible multipole is therefore $L = 1$, the dipole. In the special case $J_i = J_f = 0$ we may have decay by internal conversion or double γ decay. One last comment is due regarding angular momentum selection rules. In the case where $J_i = 0$ *or* $J_f = 0$, we have *pure* multipole transitions. The radiation is then composed of type EJ or MJ where J is the nonzero member of the J_i, J_f pair; in other cases we have the possibility of mixed multipole transitions.

The electromagnetic interaction conserves parity as well as total angular momentum, and associated with this symmetry are further selection rules. Electric and magnetic fields

must have opposite parities for a given multipolarity since the Poynting vector $\vec{S} \propto \vec{E} \times \vec{B}$ changes direction under spatial reflection. Indeed, we have $\pi(EL) = (-1)^L$ and $\pi(ML) = (-1)^{L+1}$. To see what effect this has on radiation emitted from a particular transition, consider the probability T_{fi} for electromagnetic transitions between the states ψ_i and ψ_f; T_{fi} is proportional to the matrix element Q_{fi} of a general (electric or magnetic) multipole operator $\hat{Q}$ [Rin80] between these states:

$$T_{fi} \propto Q_{fi} = \int \psi_i(x) \hat{Q} \psi_f(x) d^3x. \tag{4.7}$$

There are two cases which lead to the vanishing of this matrix element:

$$\begin{aligned} &\text{I. } \pi_i = \pi_f,\ \pi_{\hat{Q}} = (-) \\ &\text{II. } \pi_i = -\pi_f, \pi_{\hat{Q}} = (+). \end{aligned} \tag{4.8}$$

This leads to the conclusion that radiation from a given transition may not contain EL and $E(L+1)$. Similarly, ML and $M(L+1)$ may not coexist. When more than a single multipolarity exists, the electric and magnetic contributions have alternating values of L. The parity selection rules are summarized by stating that if $\pi_f = \pi_i$, the radiation will contain even electric and odd magnetic multipoles, and if $\pi_f \neq \pi_i$, the radiation will contain odd electric and even magnetic multipoles. See Blatt and Weisskopf [Bla91] for more information on J^π selection rules.

A general state vector may be written $|\psi\rangle = \sum_{T'} \alpha_{T'} |\psi_{T'}\rangle$ where the sum is over all possible isospin values. Since the strong nuclear force is charge-independent, there often exists a coefficient α_T for which $|\alpha_T|^2 \simeq 1$. The corresponding value T may then be assigned to the state and for many purposes isospin may be considered to be a good symmetry. The general isospin selection rules are $\Delta T = 0, \pm 1$ in general, and $\Delta T = \pm 1$ for $E1$ transitions in $Z = N$ nuclei [Wil60]. The second rule is approximate (due to the charge dependence of the Coulomb force) but is relevant to the present study since ^{30}P is a self-conjugate ($Z = N$) nucleus. In addition to being classified by the values of $J_i^{\pi_i}$ and $J_f^{\pi_f}$, transitions may be

described as being *isoscalar* (IS) if $\Delta T = 0$ or *isovector* (IV) if $\Delta T = \pm 1$. For example, if the the initial state has $J^\pi; T = 1^-; 1$ and the final state has $J^\pi = 0^+; 0$ then the transition is classified as $E1$ isovector ($E1$IV).

Transition Probabilities

Selection rules only tell us which transitions are *possible*; they cannot provide information concerning the relative *probabilities* of the allowed transitions. The *transition probability* T of a certain transition is defined as the inverse of its partial lifetime τ and may be expressed as [Bla91]

$$T(QL) \equiv \frac{1}{\tau} = \frac{\Gamma_\gamma}{\hbar} = \frac{8\pi(L+1)}{\hbar L[(2L+1)!!]^2} \left(\frac{E_\gamma}{\hbar c}\right)^{2L+1} B(QL). \tag{4.9}$$

Here $Q = E(M)$ for electric (magnetic) radiation, L is the multipolarity of the radiation, Γ_γ is the partial γ width for the relevant transition, and

$$B(QL) = \frac{1}{2J_i + 1} |\langle \psi_f \| \hat{Q} \| \psi_i \rangle|^2 \tag{4.10}$$

is called the *reduced transition probability*. Here J_i is the spin of the nucleus in state ψ_i, $\hat{Q}$ is again the general multipole operator [Rin80], and $\langle \psi_f \| \hat{Q} \| \psi_i \rangle$ is its reduced matrix element. Values for $T(QL)$ and $B(QL)$ may be found experimentally through determination of the widths $\Gamma_\gamma = \frac{\hbar}{\tau} = \hbar T$. Assuming a single-proton transition in a rectangular shell-model potential, Weisskopf [Bla91] derived estimates B_W for the reduced transition probabilities:

$$B_W(EL) = \frac{(1.2)^{2L}}{4\pi} \left(\frac{3}{L+3}\right)^2 A^{2L/3}\, \mathrm{e}^2 \mathrm{fm}^{2L} \tag{4.11}$$

for electric multipole radiation, and

$$B_W(ML) = \frac{10}{\pi}(1.2)^{2L} \left(\frac{3}{L+3}\right)^2 A^{(2L-2)/3}\, \mu_\mathrm{N}^2 \mathrm{fm}^{2L-2} \tag{4.12}$$

for magnetic multipole radiation. Here $A = Z + N$ is the nucleon number and μ_N is the nuclear magneton. These "Weisskopf estimates" serve to define units for reduced transition

probabilities; if for a certain transition $B(QL) = n\, B_W(QL)$, this transition is said to have a reduced transition probability of n *Weisskopf units* (W.u.). Up to the octopole ($L = 3$) transitions, the Weisskopf estimates for the reduced transition probabilities are:

$$\begin{aligned} B_W(E1) &= 0.06446A^{2/3}\ \mathrm{e^2fm^2} \\ B_W(E2) &= 0.05940A^{4/3}\ \mathrm{e^2fm^4} \\ B_W(E3) &= 0.05940A^{2}\ \mathrm{e^2fm^6} \\ B_W(M1) &= 1.790\ \mu_{\mathrm{N}}^2 \\ B_W(M2) &= 1.650A^{2/3}\ \mu_{\mathrm{N}}^2\mathrm{fm^2} \\ B_W(M3) &= 1.650A^{4/3}\ \mu_{\mathrm{N}}^2\mathrm{fm^4}. \end{aligned} \tag{4.13}$$

Weisskopf estimates for the transition probabilities T_W are found from Equation 4.9, and thereby estimates for widths may also be found from $\Gamma_W = \hbar T_W$.

Much may be learned about the probabilities of certain decay types from Equations 4.9, 4.11, and 4.12. It may be seen that EL radiation is likely to be $\sim 10^5$ times stronger than $E(L+1)$ radiation, and similarly for ML and $M(L+1)$ [Bla91, Sie87]. Also, ML transitions are $\sim 10^2$ times less likely than EL transitions. Since parity is conserved, EL competes with $M(L+1)$ and ML with $E(L+1)$. In the first case EL dominates $M(L+1)$ so that when the leading multipole is electric the radiation may be assumed to be nearly pure EL. In the second case the $E(L+1)$ competes very well with the ML and the radiation may be *mixed*. The quantities

$$\delta_{E2/M1} \equiv \sqrt{\frac{\Gamma_{E2}}{\Gamma_{M1}}} \tag{4.14}$$

and

$$\delta_{E3/M2} \equiv \sqrt{\frac{\Gamma_{E3}}{\Gamma_{M2}}} \tag{4.15}$$

are called *mixing ratios* and are presented here with the phase convention of Rose and Brink [Ros67]. The first (second) one describes the relative amounts of $E2$ and $M1$ ($E3$ and $M2$)

Table 4.3. Recommended upper limits for $B(QL)$ for nuclei with $21 \leq A \leq 44$.

Transition type	RUL (W.u.)
$E1$IS	0.002
$E1$IV	0.1
$E2$IS	100
$E2$IV	5
$E3$IS	50
$M1$IS	0.05
$M1$IV	5
$M2$IS	0.2
$M2$IV	5

radiation when the leading multipole is $M1$ ($M2$). $M3$ and all multipoles with $L \geq 4$ are considered too weak to be seen in the present work.

From the examination of a large number of decays in light nuclei ($A = 21 - 44$). Endt [End93] has suggested *recommended upper limits* (RUL's) on the value of $B(QL)$ for the various decay types. They are defined by assuming that the logarithms of the B's are normally distributed for a given decay type and requiring that the probability for $B(QL)$ to exceed its RUL be less than or equal to 0.001. As will be discussed below, these quantities are used to eliminate possible $J^\pi; T$ assignments for the resonance states. Table 4.3 summarizes the RUL's for the decay types considered by Endt.

4.3.2 Data Analysis

Once the calibrations are complete, the analysis of the HPGe γ-ray spectra may proceed. First, the .CAL files containing the energy calibration parameters are read using GELIFT. All peaks in the suppressed spectrum, unsuppressed spectrum, and off-resonance

suppressed spectrum[1] are fit. The values E_γ, σ_{E_γ}, I_γ, and σ_{I_γ} for each peak are written to a .STO file during the fitting procedure.

The .STO files are used to identify the source nuclei of the γ-rays. A given γ-ray source is labeled as ^{30}P, contaminant, or unassigned. Contaminants are any identifiable source other than ^{30}P and include natural background radiation and target impurities. In general, the suppressed spectrum contains more γ-rays than the unsuppressed due to the lowered background; therefore the suppressed .STO file contains the "master list" of γ-rays which are to be identified. At this point the other .STO files are simply useful tools for the identification process.

Once as many peaks as possible are identified, the program COMBINE is run. The first job for COMBINE is creating an input file for the program GRAY which assists in the assignment of quantum numbers. This input file has the name P30XXXX.DAT, where XXXX is the value of E_p for the resonance at hand. GRAY requires that P30XXXX.DAT contain the following information for each γ-ray in the suppressed spectrum: 1) whether or not the γ-ray is assigned, and if it is, then 2) its source, and 3) the energies of the initial and final states of the transition. COMBINE prompts the user for all of this information and also matches the energies from the USGe detector with their corresponding intensities from the CSGe detector. It also corrects the γ-ray intensities by reading the .EFF file and dividing the number of counts in each channel x by the value of $\epsilon(x)$. In addition, COMBINE prompts the user for values of the statistical energy and efficiency errors due to the fits. The energy errors are arrived at by examining the value of $\langle\Delta^2\rangle^{1/2}$ from the calibration curves and have been set at $\sigma_{E_\gamma} = 0.2$ (0.4) keV for the low-energy (high-energy) regions. For efficiencies, σ_ϵ is the value of $\langle\Delta^2\rangle^{1/2}$ from the efficiency fit rounded up to the nearest whole number percentage. The information contained in P30XXXX.DAT is then input into GRAY, which uses this information along with various user-created data files to

[1] Unless otherwise specified, all spectra mentioned should be assumed to be on-resonance.

assist with the creation of ^{30}P decay schemes and the determination of $J^{\pi};T$ assignments.

GRAY performs many jobs, including further identification of unassigned γ-rays, determination of the excitation energy E_x and branching ratios for the state of interest, and analysis of possible $J^{\pi};T$ assignments. The first task is comparing the energies of the γ-rays marked as unassigned in P30XXXX.DAT to the energies of all known decays in ^{30}P. If the energy of any unassigned γ-ray falls within 3 keV of any known decay in ^{30}P, this is considered a possible match by GRAY and it is logged in an output file called P30.LOG. For every possible match, P30.LOG contains the following information: initial and final energies of the possible decay, γ-rays which are known to feed the level at E_i and γ-rays which are known to decay from the level at E_f. The user then examines P30.LOG and, based on this information, confirms or rejects the possibilities. At this point it is hoped that all ^{30}P γ-rays which appear in the spectra have been found. While there is no way of knowing for certain if this is the case, GRAY has a means of checking for major errors. It may be asked to output a file which compares the total intensities into $\sum_i I_i^{in}$ and out of $\sum_j I_j^{out}$ each level populated in the decay. If all γ-rays have been identified, then these two numbers should agree. In addition, this file compares intensities of individual γ-rays to those expected from previously known branching ratios. By inspecting this file, the user may spot spurious γ-rays and/or places where γ-rays have been omitted.

GRAY is also used to determine E_x and branching ratios for the resonance. E_x is found as a weighted average over all unique paths to ground. As stated above, all γ-rays which fall in the range $0 - 1523$ keV are given an error of 0.2 keV and all γ-rays which fall in the range $1523 - 8000$ keV are given an error of 0.4 keV. These values are then used to calculate the error on E_x using standard statistical methods. If there are n γ-rays with $E_i = E_x$ (called *primary* γ-rays), the branching ratio for the k^{th} primary γ-ray is computed by

$$\mathrm{BR}_k = I_k \left(\sum_{i=1}^{n} I_i \right)^{-1} . \tag{4.16}$$

where I_i is the intensity of the i^{th} primary γ-ray. The statistical error σ_s on this branching ratio is computed using standard statistical analysis. The total error on the branching ratio is then calculated by adding this error and the error from the efficiency fit σ_ϵ in quadrature: $\sigma_{BR} = (\sigma_{I_\gamma}^2 + \sigma_\epsilon^2)^{1/2}$.

Once E_x and branching ratios are known, GRAY assists the user in narrowing down the possible $J^\pi;T$ assignments for the resonance state in question. It does this by employing the selection rules and the RUL's for the reduced transition probabilities. Generally speaking, the quantum numbers of the states to which the resonance state decays are known. All multipoles up to $E3$ and $M2$ are considered in the analysis. First, a range of possible assignments is found using the rules for J and π. Once this is done, the RUL's for the $B(QL)$ are used to further eliminate possibilities. For every assignment allowed by the J^π analysis, values of $B(QL)$ are calculated for each primary γ-ray. If the $B(QL)$ exceeds its associated RUL by a factor of 2 or more for any of the primaries, the $J^\pi;T$ assignment for the resonance state is eliminated. In this way one may hope to arrive at a unique $J^\pi;T$. In practice, however, this is not usually the case; one is often left with a range of possibilities. This analysis procedure for the 7921.8 keV resonance is followed in detail in Appendix A.

Chapter 5

Results

The present chapter provides a brief discussion about each resonance[1] studied in this work. In most cases a summary of results from previous measurements is included along with a brief discussion concerning the analysis using J^π selection rules and RUL's. Some analyses resulted in the changing of a previous assignment or the discovery of a new level; these cases are discussed in more detail. The results are summarized in Table 5.2 at the end of the chapter. More detailed information regarding the analysis and results appears in the appendices: Appendix A details the data, analysis, and results for the 7921.8 keV resonance; branching ratios are listed in Appendix B; comparisons of $B(QL)$'s to their associated RUL's for each resonance are given in Appendix C.

Analog state matching to levels in ^{30}Si provided several of the previous isospin assignments for ^{30}P states; however, correct J^π assignments for the analog state and nearby states are prerequisites for reliable matching. Since many J^π assignments in ^{30}P remain unknown, assignments of analog states have not been made in this study; these assignments are being deferred until additional J^π assignments have been made.

In this chapter and in the appendices, quantum number assignments will be labeled

[1]The 7921.8 keV resonance is not included since detailed information regarding this level is found in Appendix A.

by $J^\pi;T$. For example, the quantum numbers of a negative parity state with definite total angular momentum $J = 3$ and definite isospin $T = 1$ will be written $3^-;1$. Parentheses surrounding an isospin value indicate that it is the most likely assignment; a listing of $2^+;(0)$ means that $T = 1$ is not ruled out but is improbable. Parentheses surrounding a set of numbers indicates that all assignments consistent with those numbers are possible. For example, $J^\pi;T = (2,3^-)$ means that $2^+;0$, $2^+;1$, $2^-;0$, $2^-;1$, $3^-;0$, and $3^-;1$ are all possible. Also, $(2.3,4)^+$ means that $J = 2,3,\text{or}4$, parity is positive and the isospin is unknown.

5.1 $E_x = 7304.9$ keV

The previous assignment for this level is $2^-;0$ [Fra91b], and the present work gives a possible range of $1^+,2$, and $3^+;1$. It is clear from the work of Nelson [Nel83] that the state has negative parity; this leaves 2^-. The $T = 0$ assignment [Har69] is based on branching ratios which differ from those measured in the present study. Therefore, the isospin for this state is unknown and the final assignment is 2^-.

5.2 $E_x = 7306.3$ keV

The previous assignment for this level is $2^-;0$ [Rei85, Fra91b]. The current analysis allows assignments of $2^-;0$ and $2^-;1$. However, the $2^-;1$ assignment seems unlikely. The transition to 6094.6 keV, a $3^-;1$ state, is possibly a mixed M1/E2 transition. If this transition is purely E2 or M1, both values of $\delta_{E2/M1}$ cause B(M1) or B(E2) to exceed twice its RUL. However, for a range $0.72 < \delta_{E2/M1} < 0.84$, both B's exceed their RUL's by less than a factor of two. Therefore, while less likely than $T = 0$, an assignment of $T = 1$ is not strictly forbidden. The final assignment is thus $2^-;(0)$. The value of δ may be found by performing an angular distribution study of the 7306.3 $\rightarrow$ 6094.6 keV transition, and the

isospin value might be determined.

5.3 $E_x = 7322$ keV

This state is very weak in the capture channel, and has a total width of $\sim$ 16.5 keV [Nel83]. Although it was not observed in the ^{29}Si(p,γ) yield curve [Vav96], it does have a small γ-ray yield; primary γ-rays were measured in the present work. The analysis using J and π selection rules gives a possible range of $0, 1, 2, 3$, and 4^-. Since no values of the strength S or the gamma width Γ_γ are known, no values of B could be calculated[2]. Therefore no RUL analysis was performed on this level and no further information could be learned about its quantum numbers from these measurements. The previous assignment for this level is 1^-; (1) [Fra91b]. The J^π value is well-established experimentally [Har69, Poi70, Nel83]. The previous $T = 1$ assignment is suggested by analog state matching [Fra91a]. Our assignment is 1^-, T unknown. The energy error is placed at ± 3 keV due to the large width of the resonance.

5.4 $E_x = 7383.4$ keV

Before the present work the possible range for quantum numbers for this level was $0^+, 1, 2, 3, 4^+$ [Fra91b]. This large range was due to the fact that only one primary γ-ray transition was known: 7383.4 $\rightarrow$ 2937.9 [Rei85]. This study uncovered five additional primary decays which helped to narrow the possible range to $J = 2$ or 3, π and T unknown.

[2]If the value of S is known, the RUL analysis is possible. The equation $S = (2J+1)\Gamma_p\Gamma_\gamma/(\Gamma_p + \Gamma_\gamma)$ may be used to find a lower limit on Γ_γ. This limit is $\Gamma_\gamma = S/(2J+1)$ and may be used to perform the RUL analysis.

5.5 $E_x = 7492.7$ keV

Initially this state had an assignment of $1^+;0$ [Poi70, Rei85, End90a]. Analysis using J and π selection rules gives a possible range of 1, 2, and 3^-. RUL analysis narrows this to $1^+;0$, $1^+;1$, $1^-;0$, and $2^+;1$. Nelson's data [Nel83] clearly gives positive parity, and his assignment of $\ell = 0$ forbids the $J = 2$ assignment. Therefore, we are left with 1^+, T unknown. Reinecke claims that $T = 1$ is ruled out by M1IS transitions which exceed their RUL's. Assuming pure M1, this is true for transitions to the $T = 1$ states at 2937.9, 4182.6, and 4502.3 keV. However, the possibility of these transitions being mixed E1/M2 allows the resonance state to have $T = 1$. An angular distribution study of these transitions may be helpful in determining T.

5.6 $E_x = 7560.5$ keV

5.6.1 Resonance State

Since no previous γ-ray decay information was known for this level, all of the fifteen primary γ-rays measured in this study have not been previously reported. This resonance was found to decay to a previously unknown level at 6006.1 keV; information for this level is given in the following subsection. Elastic scattering studies [Nel83] have provided an assignment of $3(1)^+$ for the 7560.5 keV level[3]. This state is seen to decay to positive-parity states with $J = 1 - 5$, so J^π analysis gives a possible range of 2^-, 3, and 4^-. Calculating RUL's. one finds that the only possible J^π is 3^+, in accordance with the previous assignment.

[3]This assignment indicates that $J = 3$ is the most likely angular momentum value but that $J = 1$ is not absolutely ruled out.

5.6.2 $E_x = 6006.1$ keV

This is a previously unobserved level. The transition from the 7560.5 keV state to the 6006.1 keV state is quite strong, allowing several γ-rays with $E_i = 6006.1$ keV to be observed and identified. These γ-rays are summarized in Table 5.1 and the decay scheme for this level is shown in Figure 5.1.

Table 5.1. Branching ratios for E_x=6006.1 keV

E_f (keV)	BR (%)
1454.67	29±2
1973.62	34±2
2539.03	11±2
2723.96	15±1
2839.9	11±1

The γ-rays from the 6006.1 keV state limit J^π to be $0^-, 1, 2, 3, 4, 5^-$. From the possible assignments for 7560.5 ($3^+;0$ and $3^+;1$), this range is further narrowed to $1^+, 2, 3,$ and 4. There is a remote possibility that this state is actually the level at 5993 ± 4 keV [Uzu74, Dyk76], which has a J^π range of $(0, 1, 2)^-$. Only in the case of $J^\pi = 2^-$ could the two states be the same.

5.7 $E_x = 7562.5$ keV

The original assignment for this state is $2^+;1$ [Ram81, Rei85]. The present J^π and RUL analyses also allowed only this possibility.

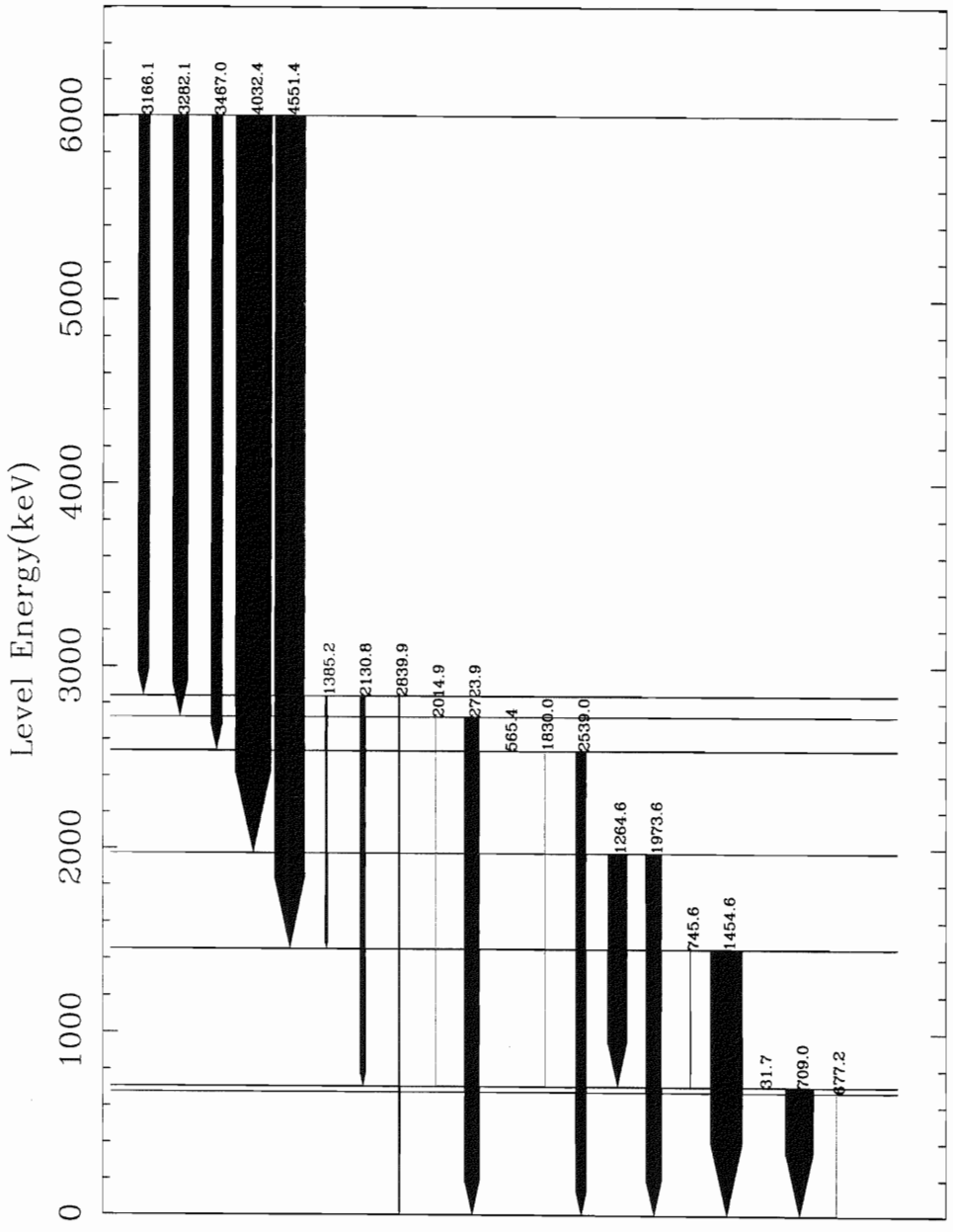

Figure 5.1. Decay scheme for $E_x = 6006.1$ keV state. The width of the arrows indicates the strength of the transition.

5.8 $E_x = 7304.9$ keV

The previous assignment for this level is $2^-;0$ [End90a]. The J and π selection rules gave $1^+, 2, 3, 4^-$ as possibilities and the RUL analysis restricted the possible range to $(2^-, 3); 0$. Since $J^\pi = 2^-$ is well-established from (p,p) studies, the assignment of $2^-;0$ is retained.

5.9 $E_x = 7605.0$ keV

The previous J^π assignment of 3^+ for this resonance is reported from angular distributions of direct reactions [Ram81], (p,p) studies [Nel83], and RUL analysis [Rei85][4]. However, this assignment is inconsistent with the J^π range of $(1,2)^+$ given by this work. The inconsistency is the result of a primary transition (not observed previously) to the first excited state at 677.3 keV which has $J^\pi; T = 0^+; 1$. If the assignment for the resonance state is truly 3^+ then this transition must be an M3, which is highly unlikely. Endt [End93] does list an M3 RUL of 10 W.u. based on five transitions, four of which are transitions from the first excited state to ground. The value of B(M3) for this transition was calculated to be 2450 W.u., far above the RUL. For the present time, the assignment will be $(1,2)^+$.

5.10 $E_x = 7636.0$ keV

The J^π analysis gives this state a range of $2, 3, 4^-$ and RUL analysis narrows this range to $J = 3$, π and T unknown. The previous assignment is $3^+;1$ [Fra91b]. The origin of the $T = 1$ assignment is unknown. If it is due to Reinecke's RUL analysis, this work does not support that conclusion; if it is due to analog state matching, it is not considered in this study. Therefore T is left unassigned. The parity assignment is also in question. The

[4] In [Rei85], only transitions up to M1 and E2 were considered for RUL analysis.

assignment $\pi = (+)$ is based on Reinecke's RUL analysis of the resonance to ground state transition. Due to a difference in branching ratios, the present study allows $\pi = (+)$ or $(-)$. Our assignment is thus $J = 3$, π and T unknown.

5.11 $E_x = 7644.3$ keV

This state had a previous assignment of $3^+;1$ [End90a]. The present analysis of this resonance using J and π selection rules restricts the assignments to 2, 3, and 4^-. RUL analysis reduced this set of assignments to $J = 3$, π and T unknown. From inspection of Nelson's data [Nel83] it is clear that this state has positive parity, so the assignment is restricted to 3^+. The $T = 1$ assignment is dropped since it is based only on analog state matching [Rei85]. Our assignment is 3^+.

5.12 $E_x = 7786.4$ keV

Previously, no branching ratios had been measured for this resonance. Six primary γ-rays were found, and the J^π values of the final states restrict the assignments for the 7786.4 keV state to $0^-, 1, 2, 3, 4, 5^+$. The RUL analysis further narrowed this range to $1^+, 2, 3, 4^-, 4^+;1$. Nelson [Nel83] lists $J = (2, 3, 4)$ based on an assignment of $\ell = 3$ and $\pi = (-)$ from the (p,p) yield curve at 90°. These assignments are consistent with the range found in this work, so the range $(2, 3, 4)^-$ is retained, and T remains unknown.

5.13 $E_x = 7802.6$ keV

There is no γ-ray yield seen from this resonance. All ^{30}P γ-rays seen in the data are due to the resonance at 7891 keV which has a total width of 70 keV. The previous assignment of $(2, 3, 4)^-$ from (p,p) work [Nel83] is retained.

5.14 $E_x = 7826.3$ keV

The previous assignment is due to Nelson [Nel83] and is $(2,3)^-$. The J^π analysis gave a possible J^π range of $0, 1, 2, 3, 4^-$ and the RUL analysis further restricted this range to $1^+; 0, 1^-; 0, 2$, and 3^+. The intersection of these two allowed sets is 2^-, and this assignment is made.

5.15 $E_x = 7873.7$ keV

No previous γ-decay information was known for this resonance; eight new primary γ-rays are assigned in this work. These primaries serve to restrict the possible assignments of this level to 1^+, 2, 3, 4, and 5^-. This range is the result of the J^π analysis; since no values of S or Γ_γ are known for this level, no RUL analysis was performed. The previous assignment is 4^-, T unknown [Nel83, Fra91b] and this J^π is retained.

5.16 $E_x = 7883.8$ keV

No previous spectroscopic information was given for this level. The J^π analysis gives $2^-, 3. 4$, and 5^- and the RUL analysis further narrows this field to $(3,4)^+$, T unknown. This range is kept as the current assignment.

5.17 $E_x = 7891$ keV

This level has a total width of 70 keV [Nel83] and interferes with several nearby resonances. No primary γ-rays had previously been observed from this resonance; four are measured in the present work. These primaries limit the J^π range to $0, 1, 2, 3, 4^-$. The resonance is clear in elastic scattering, and previous (p,p) work [Poi70, Nel83] has resulted in a J^π assignment of 2^-. A probable isospin value of 1 is based only on analog state

matching [End90a] and is not considered in this work. Therefore the final assignment is 2^-. The energy error is set at ± 3 keV due to the large width of the resonance.

5.18 $E_x = 7920.9$ keV

The previous J^π assignment for this level is 2^+ [Kos76, Nel83, Fra91b]. An isospin assignment of $T = 1$ from analog state matching is given by Endt [End90a] and is not considered here. The J^π analysis gives a possible range of $1, 2, 3, 4^-$ and the RUL analysis reduces this set to $2, 3^+$, T unknown. Since the previous assignment is a subset of the range given by this study, the final assignment is 2^+.

5.19 $E_x = 7922.1$ keV

No previous spectroscopic information was given for this resonance. Analysis using J and π selection rules gave a possible range of $2^-, 3, 4, 5^-$. Since no values of S or Γ_γ are known, RUL analysis could not be carried out, and this range may not be narrowed further.

5.20 $E_x = 7931.5$ keV

There is no γ-ray yield seen from this resonance. All ^{30}P γ-rays seen in the data are from the resonance at 7891 keV which has a total width of 70 keV. Previous elastic scattering work [Poi70, Nel83] has resulted in a $J^\pi = 0^+$ for this state, and this assignment is kept.

5.21 $E_x = 7996.7$ keV

Previous researchers gave this state an assignment of 0^+ [Poi70, Nel83]. However, the J^π analysis restricts the assignments for this level to $1, 2, 3^-$. The $J = 0$ assignment is

ruled out by a primary transition to the 677.3 keV state for which $J^\pi = 0^+$. The level at 8001.4 keV is wide enough ($\Gamma = 4.8$ keV) to interfere with the 7996.7 keV resonance and also has a primary transition to 677.3 keV. However, the intensity of the transition in the 7996.7 keV data is ~ 1.5 times stronger than it would be if it were due entirely to the 8001.4 keV resonance. The RUL analysis reduces the range to $1, 2^+$, and $2^-; 0$, and since Nelson assigned $\ell = 0$ one can have only $J = 1^+$. This results in an assignment of 1^+, T unknown.

5.22 $E_x = 8001.2$ keV

The previous assignment for this level is 1^- [Poi70, Nel83, Fra91b]. The six primaries observed in this study lead to a range of $1, 2, 3^-$ from J^π analysis and to a final range of $1, 2^+$ from the subsequent RUL analysis. The previous assignment of 1^- is retained.

5.23 $E_x = 8007.4$ keV

Nelson [Nel83] has assigned $\ell = 2$ and positive parity to this state, leaving a possible J^π range of $(1, 2, 3)^+$. The J^π analysis of the present work led to $J^\pi = 1, 2, 3^-$ and the RUL analysis restricted this set to $(1, 2)^+$ and $2^-; 0$. The intersection of these sets is $(1, 2)^+$ and this is the final assignment.

5.24 $E_x = 8014.3$ keV

This resonance has an original assignment of 2^+ [Nel83, Fra91b]. The $J^\pi; T$ assignments allowed by this work are $(1, 2, 3)^+$ and $(0^+, 3^-); 1$. Since the previous assignment is a subset of the range allowed in the present study, 2^+ is retained.

Table 5.2. Summary of results

E_x (keV)	Previous Work	Present Work	Final Assignment
7304.9 ± 0.1	$2^-;0$	$1^+, 2, [3^+;1]^a$	2^-
7306.3 ± 0.1	$2^-;0$	$2^-;(0)$	$2^-;(0)$
$7322. \pm 3.$	$1^-;(1)$	$0, 1, 2, 3, 4^-$	1^-
7383.4 ± 0.2	$0^+, 1, 2, 3, 4^+$	$2, 3$	$2, 3$
7492.7 ± 0.2	$1^+;0$	$1^+, [1^-;0]^a, [2^+;1]^a$	1^+
7560.5 ± 0.1	$3(1)^+$	3^+	3^+
7562.5 ± 0.1	$2^+;1$	$2^+;1$	$2^+;1$
7579.9 ± 0.1	$2^-;0$	$(2^-, 3);0$	$2^-;0$
7605.0 ± 0.1	$3^+;(0)$	$(1, 2)^+$	$(1, 2)^+$
7636.0 ± 0.1	$3^+;1$	$3^+, [3^-;1]^a$	3
7644.3 ± 0.1	$3^+;1$	3	3^+
7786.4 ± 0.2	$(2, 3, 4)^-$	$1^+, 2, 3, [4^+;1]^a$	$(2, 3, 4)^-$
7802.6 ± 0.3	$(2, 3, 4)^-$	—	$(2, 3, 4)^-$
7826.3 ± 0.2	$(2, 3)^-$	$2^-;0$	$2^-;0$
7873.7 ± 0.2	4^-	$1^+, 2, 3, 4, 5^-$	4^-
7883.8 ± 0.2	—	$(3, 4)^+$	$(3, 4)^+$
$7891. \pm 3.$	$2^-;(1)$	$0, 1, 2, 3, 4^-$	2^-
7920.9 ± 0.1	2^+	$2, 3^+$	2^+
7921.8 ± 0.2	—	$3^+;0$	$3^+;0$
7922.1 ± 0.2	—	$2^-, 3, 4, 5^-$	$2^-, 3, 4, 5^-$
7931.5 ± 0.3	0^+	—	0^+
7996.7 ± 0.2	0^+	$1, 2^+, [2^-;0]^a$	1^+
8001.2 ± 0.1	1^-	$1, 2^+$	1^-
8007.4 ± 0.2	$(1, 2, 3)^+$	$(1, 2)^+, [2^-;0]^a$	$(1, 2)^+$
8014.3 ± 0.2	2^+	$(1, 2, 3)^+, (0^+, 3^-);1$	2^+

[a] Brackets are used merely to clarify notation.

Chapter 6

Summary

It is generally accepted that information regarding the dynamics of quantum systems may be found in their energy eigenvalue spectra. In particular, non-chaotic motion is manifest in spectra which have uncorrelated levels and chaotic motion is manifest in spectra whose level distributions conform to the GOE of random matrix theory. The goal of current work at the TUNL HRL is to obtain a level scheme for ^{30}P which is as complete and pure as possible; this is done by studying the ^{29}Si(p,γ) reaction. Once completed, this level scheme will be the subject of statistical analyses (NNS distribution, Dyson-Mehta Δ_3 statistic) which will help to reveal the dynamics of this nuclide. This work will complement previous experimental results which indicate that the fluctuations of ^{26}Al lie between the GOE and Poisson extremes.

To perform this study, closely-lying resonances had to be resolved, and the γ-ray spectra had to be as detailed as possible. Therefore, both a high-resolution proton beam and a high-resolution detector system were used. The KN Van de Graaff electrostatic accelerator at the TUNL HRL is capable of producing proton beams up to 4 MeV with resolution of $\sim$ 220 eV. This accelerator was used in conjunction with a Compton-suppressed HPGe γ-ray detector system. These detectors have very high resolution and the Compton suppressor

served to reduce the background of the γ-ray spectra, allowing weak peaks to be seen.

In order to accurately determine energies and intensities of the peaks in the γ-ray spectra, high-quality energy and efficiency calibrations were needed. These calibrations were based on 13 γ-rays from a commercial ^{152}Eu source and 17 γ-rays from the ^{27}Al(p,γ) reaction at $E_p = 0.99186$ MeV.

Spectra for 25 resonances in the range 7304 keV $\leq E_x \leq$ 8014 keV were collected. The data were then fit and analyzed in order to establish E_x and branching ratios for each resonance. This information was used in conjunction with J^π selection rules and RUL's to eliminate possible $J^\pi;T$ assignments. Once this was done we were left with a set of assignments which were allowed by this work; this set was compared to previous work on the resonance in question. Sixteen resonances had previous assignments which were confirmed by this work; these assignments were left unchanged[1]. Seven resonances had previous ranges which were narrowed, and two resonances had assignments were changed outright. In addition, the level at 6006.1 keV was observed for the first time. For this resonance, branching ratios were calculated and several possible $J^\pi;T$ assignments were eliminated. Of the 26 decays which were observed in this study, 18 have unambiguous J, 22 have unambiguous π, and 4 have unambiguous T. Seventeen have known J^π combinations and 4 have known $J^\pi;T$ combinations. Previously, no $J^\pi;T$ information was known for four of the resonances: of these, two have been given a set of allowed J^π assignments, one has an unambiguous J^π assignment, and one has an unambiguous $J^\pi;T$ assignment.

These measurements represent a major step toward the goal of the establishment of a pure and complete level scheme for ^{30}P. Where the present work does not correct or improve upon previous measurements, it confirms them. In addition, by making clear which resonances require further study, these results provide a direction for future angular distribution experiments.

[1]Seven of these had previous isospin assignments based only on analog state matching and these assignments were dropped until further work is done. See Chapter 5 for explanation.

Appendix A

Data Analysis for E_x=7921.8 keV

This appendix presents discussions of the data, analysis, and results for the resonance at 7921.8 keV. The data were taken in January 1995. The majority of the appendix is in the form of figures and tables; in order to preserve readability these are presented after the text.

A.1 Data

The γ-ray spectra for the 7921.8 keV resonance are shown in Figures A.1, A.2, A.3, and A.4. The on-resonance data were taken at E_p = 2.4077 MeV, and the off-resonance data were taken at 2.4186 MeV, 10.9 keV higher. The off-resonance energy corresponds to the centroid of a very wide (Γ = 28 keV) resonance which later was found to have no observable γ-ray yield. The data are presented using logarithmic ordinates in order to make weak peaks easier to see.

Many peaks were identified as originating from nuclides other than ^{30}P. Target impurities provide several of these peaks. Traces of ^{19}F and ^{23}Na exist on the carbon foils used to make the targets, and evidence of these elements is observed in all the spectra. ^{19}F

is most clearly seen in the suppressed data, Figures A.1 and A.3. The broad peaks found between channels 6000 and 7000 in these spectra correspond to γ-rays from the ^{19}F(p,$\alpha_1\gamma$), ^{19}F(p,$\alpha_2\gamma$), ^{19}F(p,$\alpha_3\gamma$), and ^{19}F(p,$\alpha_4\gamma$) reactions. The γ-rays thus are from ^{16}O, and the peaks are Doppler-broadened due to the high recoil velocity of the ^{16}O nuclei. The γ-rays at 109.9 and 197.1 keV are produced by the ^{19}F(p,p$_1\gamma$) and ^{19}F(p,p$_2\gamma$) reactions. The other major contaminant on the targets is ^{23}Na. Evidence for this contaminant is seen near channel 1600. where the γ-rays from ^{23}Na(p,$\alpha_1\gamma$) appear as a Doppler-broadened peak. The peak at 440.0 keV arises from the ^{23}Na(p,p$_1\gamma$) reaction.

Other extraneous γ-rays are seen in the data. The rings which hold the targets are made of stainless steel. and γ-rays from the reactions ^{52}Cr(p,γ) and ^{56}Fe(p,γ) are seen in the spectra. It is believed that, despite having beam currents of < 20 nA on the rings, these reactions occurred at a rate sufficient to create observable γ-ray peaks. These γ-rays are from the decay of the nuclides ^{53}Mn and ^{57}Co and represent the majority of contaminant peaks.

Natural background radiation also contributes γ-rays to the spectra. Prior to the start of the experiment. background spectra were taken over a period of 12 hours. The suppressed background spectrum from the January 1995 experimental run is shown in Figure A.5.

A.2 Analysis

States in the resonance region sometimes interfere with each other. Significant interference occurs when the spacing between two resonances is comparable to the width(s) of one or both of the states. The γ-ray spectra of one or both of the resonances will contain peaks from both resonances, and often peaks in the spectrum of interest are augmented by contributions from the interfering state. In the present case, the 70-keV wide state at 7891

keV interferes with the 7921.8 keV resonance (see Figure A.6). This must be taken into account in the analysis.

The resonance at 7891 keV has four primary γ-rays, the two strongest of which (to the ground state and to 709.0 keV) appear in the spectra of the 7921.8 keV resonance. The transition to the ground state is seen in the on-resonance data as a peak with energy 7921.4 keV, but this peak is due entirely to the 7891 keV resonance. Both resonances contribute to the peak at 7212.9 keV; thus they each have a primary transition to 709.0 keV. The method by which this information was obtained will now be discussed.

On-resonance data was taken at 7921.8 keV and off-resonance data was taken about 10 keV higher at 7931.5 keV. As previously stated, no γ-ray yield was observed from the 7931.5 keV resonance; the few ^{30}P γ-rays found in its spectra are from the 7891 keV resonance[1]. Among these γ-rays are the two found in the 7921.8 keV spectra. The quantity

$$\frac{\sigma_E}{\sigma_r} = \frac{k_r^2\Gamma^2/4}{k_E^2[(E-E_r)^2+\Gamma^2/4]} \tag{A.1}$$

is the ratio of the Breit-Wigner cross sections [Kra88] for the interfering resonance evaluated at the resonance energy E_r and the energy E of the resonance being analyzed (k is the wave number). This calculation reveals that at $E = 7921.8$ keV the cross section of the 7891 keV resonance is 57% of its maximum. A similar calculation at $E = E_{off} = 7931.5$ keV gives 44%. Therefore, if a peak at 7921.8 keV is due entirely to the 7891 keV resonance, it should have ~ 1.3 times the number of counts found in the same peak at 7931.5 keV. This is indeed the case for the resonance to ground state transition: this peak contains 1285 ± 46 counts in the 7921.8 keV data and 907 ± 39 counts in the 7931.5 keV data. Similar calculations were performed for the peak representing the primary transition to 709.0 keV. This peak contains 203 ± 20 counts in the 7921.8 keV data and 77 ± 12 counts in the 7931.5 keV data. Therefore, ~ 100 or half the counts in the 7921.8 keV peak are due to the interfering resonance. The intensities for these γ-rays were adjusted in the file P30_2407.DAT according to these

[1]This was determined by comparing branching ratios.

results. In addition, the intensity of transition from 709.0 keV to ground was reduced appropriately and errors on all affected γ-rays were propagated.

All peaks found in these spectra were fit with GELIFT and written to .STO files. A total of 104 peaks were fit in the suppressed on-resonance spectrum. Of these, 73 were identified and 31 were left unidentified. The program COMBINE was then run to match the energies from the unsuppressed spectrum with the intensities from the suppressed spectrum. The output file of COMBINE is P30_2407.DAT; the contents of this file are shown in Table A.1.

The contents of the file P30_2407.DAT were then entered into the GRAY database. Ten primaries were found, five of which were previously reported [Cam93]. The intensity check described in Chapter 4 was then performed. This check is not intended to be rigorous; it is an estimate. The comparison of the total feeding and decay intensities for each level populated is shown in Table A.2, and the comparison of observed and expected intensities for individual γ-rays is shown in Table A.3. Since it is seen from these tables that there are no large inconsistencies in the decay, we are fairly certain that no major branches have been left out. Once all the primary transitions were found, the excitation energy and branching ratios for the resonance were calculated. E_x was determined to be 7921.8 ± 0.2 keV. The primaries and their branching ratios are presented in Table A.3. The final decay scheme is presented in Figure A.7.

A.3 Results

At this point the data were analyzed using the J and π selection rules. No previous spectroscopic information was known for this level. All states to which this resonance decays have positive parity and their J values range from 1 to 5. Considering decay types up to E3 and M2, the possible J^π range is 2^-, 3, and 4^-. There values correspond to eight possible

$J^\pi;T$ assignments, two for each J^π combination. Each of these eight possibilities was analyzed using GRAY. The values of B were calculated for each possible $J^\pi;T$ and compared to their associated RUL. All assignments but $3^+;0$ were eliminated by this method. The RUL analysis is presented in Table A.5.

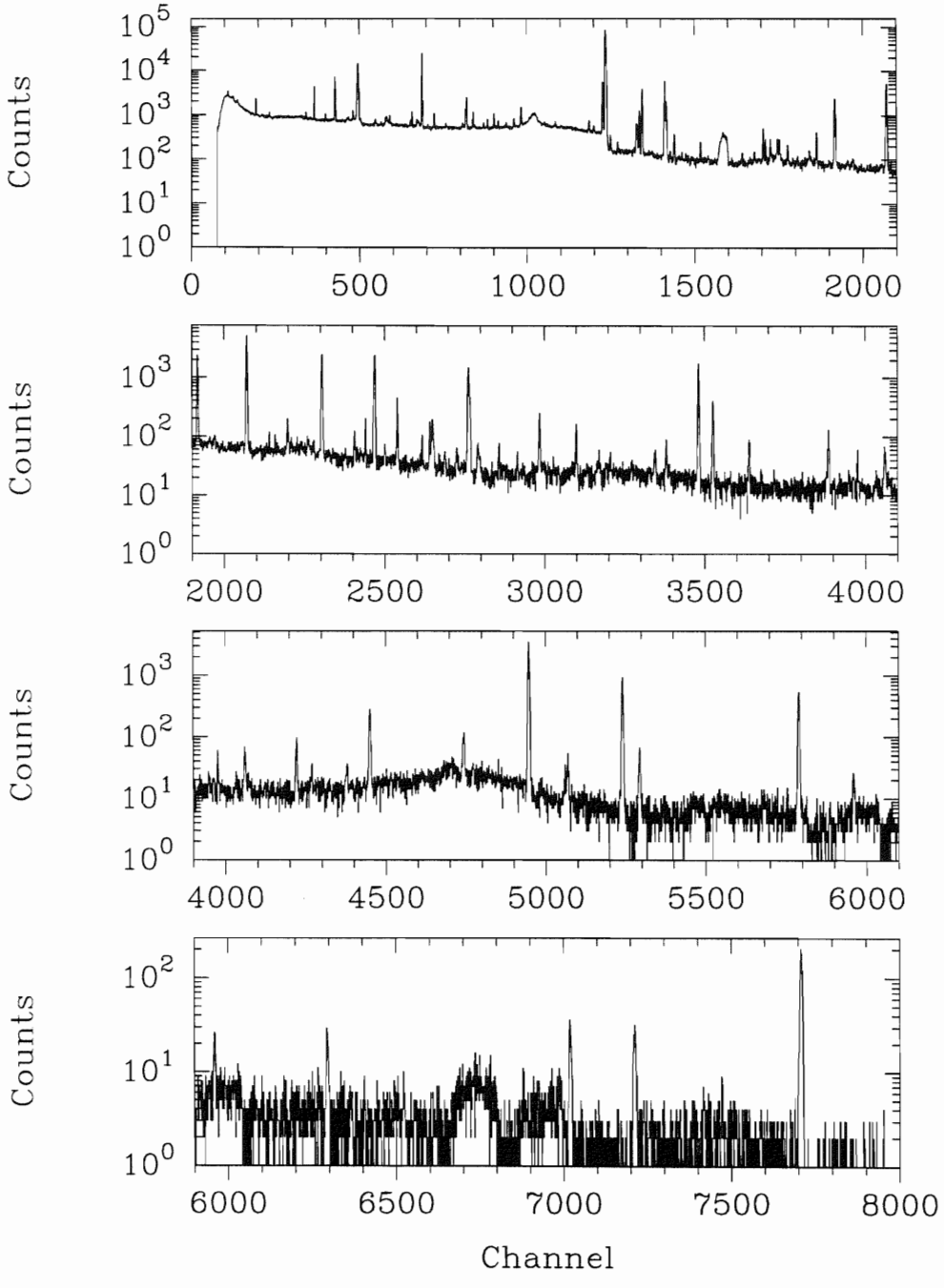

Figure A.1. Suppressed on-resonance spectrum for $E_x = 7921.8$ keV

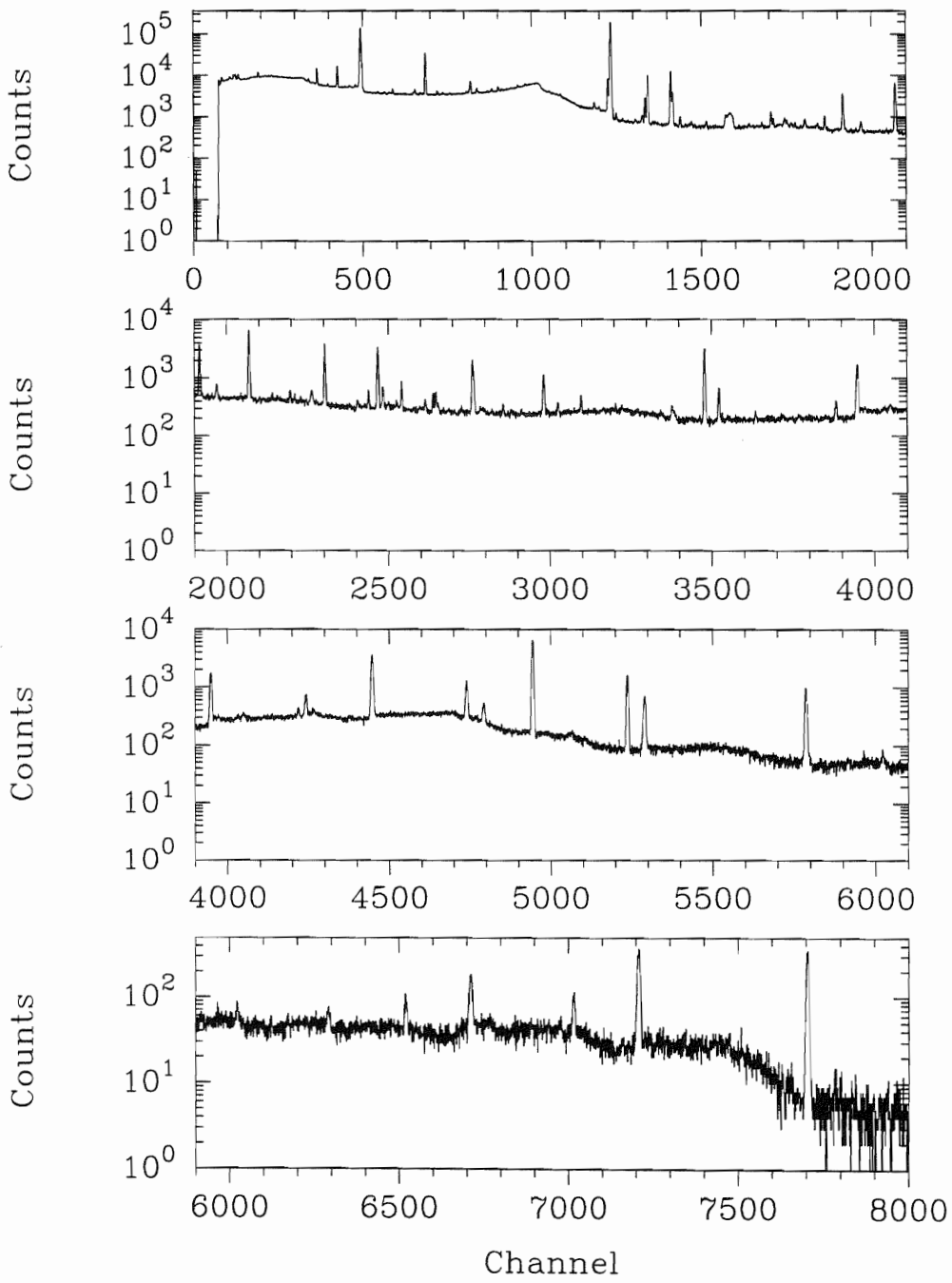

Figure A.2. Unsuppressed on-resonance spectrum for $E_x = 7921.8$ keV

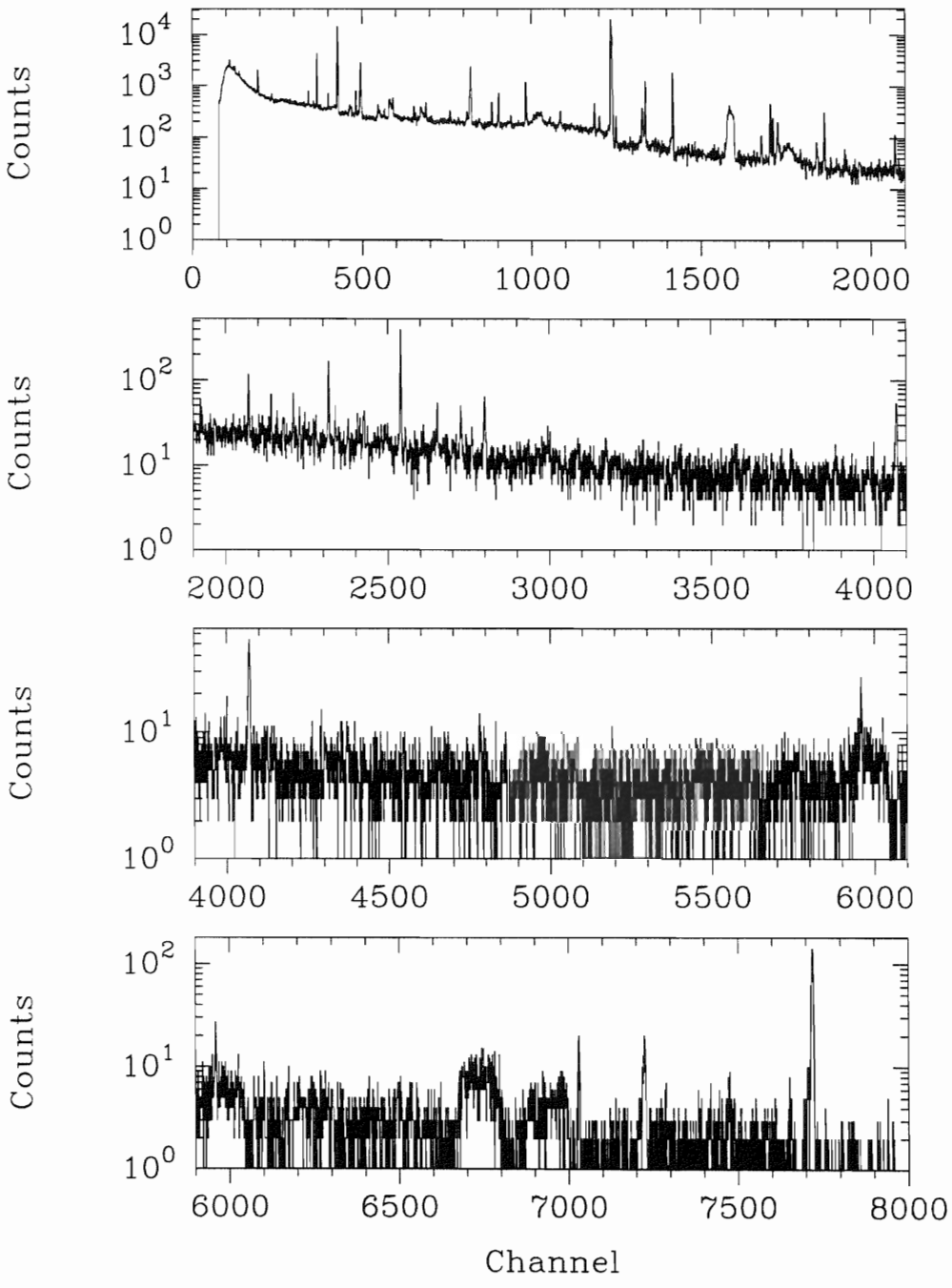

Figure A.3. Suppressed off-resonance spectrum for $E_x = 7921.8$ keV

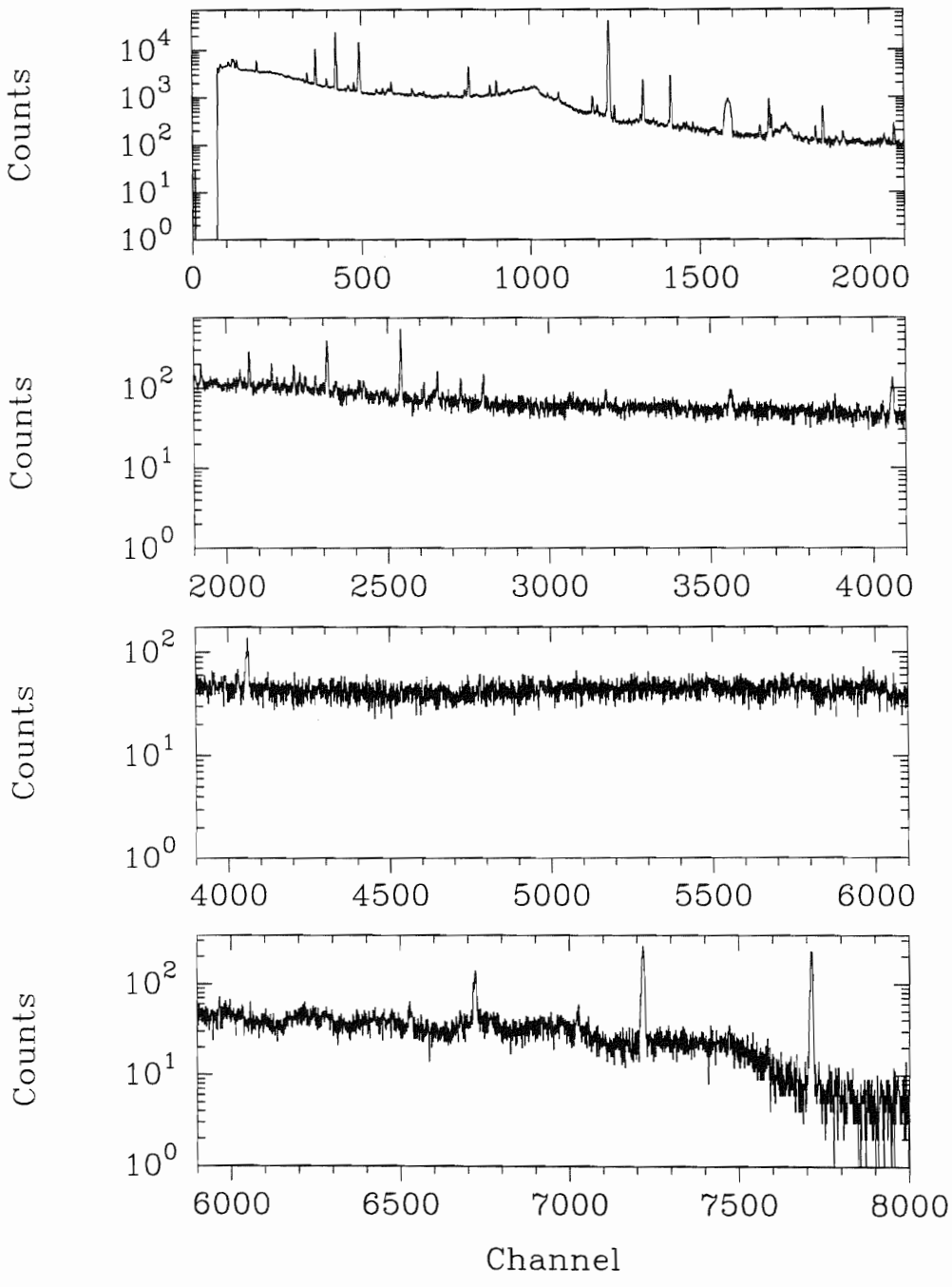

Figure A.4. Unsuppressed off-resonance spectrum for $E_x = 7921.8$ keV

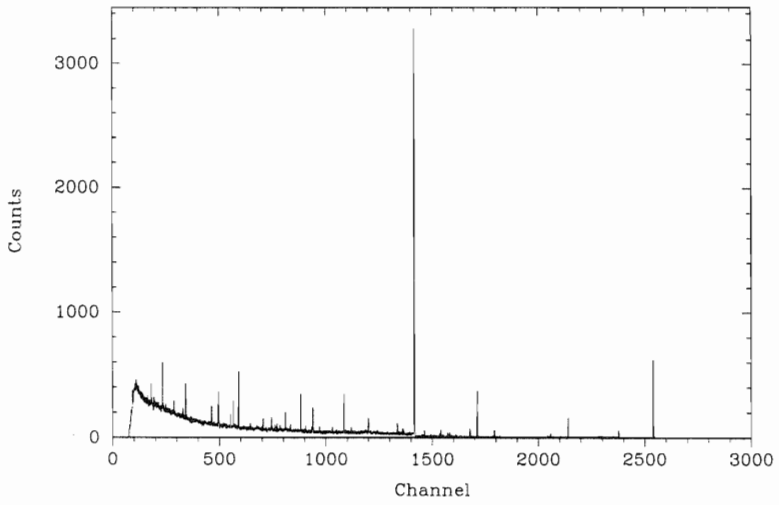

Figure A.5. Suppressed room background spectrum. The large peak at channel $\sim$ 1430 is from the β-decay of ^{40}K and the peak at channel $\sim$ 2540 is from the β-decay of ^{208}Bi.

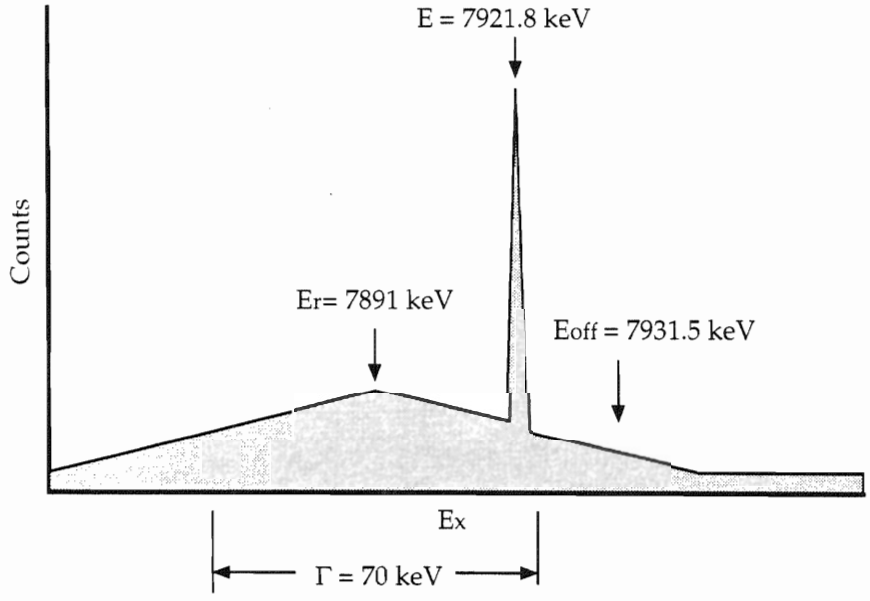

Figure A.6. Sketch of interfering resonances. The 70-keV wide resonance at 7891 keV interferes with the 7921.8 keV resonance.

Table A.1. γ-rays observed in the decay of the 7921.8 keV state

E_γ (keV)	σ_{E_γ} (keV)	I_γ (Relative)	σ_{I_γ} (Relative)	E_i (keV)	E_f (keV)	Source Nuclide
109.6	0.20	12369	2071	109.9	0.0	^{19}F
197.0	0.20	220	20	197.1	0.0	^{19}F
237.8	0.20	16	6	238.6	0.0	^{212}Pb
270.8[a]	0.20	56	22			
351.7	0.20	14	4	351.9	0.0	^{214}Pb
377.3	0.20	159	7	377.9	0.0	^{52}Cr
410.8[b]	0.20	21	4			
439.7	0.20	386	9	440.0	0.0	^{23}Na
496.3[a]	0.20	29	4			
510.7	0.20	1242	17	3708.5	3197.7	^{208}Tl
565.3	0.20	18	5	2539.0	1973.6	^{30}P
599.5[a,b]	0.20	57	7			
608.7	0.20	19	4	609.3	0.0	^{214}Bi
676.3	0.20	32	4	677.3	0.0	^{30}P
708.7	0.20	1399	18	709.0	0.0	^{30}P
745.3	0.20	38	5	1454.7	709.0	^{30}P
844.1	0.20	92	8	843.8	0.0	^{27}Al
846.0	0.20	110	9	846.8	0.0	^{56}Fe
865.9	0.20	52	5			
870.4	0.20	9	4	6919.	6049.	^{19}F
899.4[a]	0.20	13	4			
911.5	0.20	21	5	968.8	57.8	^{228}Ac
931.4[a,b]	0.20	39	5			
943.9[a]	0.20	15	4			
991.4	0.20	24	5	3928.9	2937.8	^{30}P
1013.4	0.20	92	7	1014.4	0.0	^{27}Al
1087.4	0.20	14	5	2311.3	1223.7	^{56}Fe
1120.1	0.20	21	7	1729.2	609.3	^{214}Bi
1137.5[a]	0.20	22	7			

Table A.1. γ-rays observed in the decay of the 7921.8 keV state (continued)

E_γ (keV)	σ_{E_γ} (keV)	I_γ (Relative)	σ_{I_γ} (Relative)	E_i (keV)	E_f (keV)	Source Nuclide
1223.4	0.20	34	6	1224.0	0.0	^{56}Fe
1238.1	0.20	26	6	1847.4	609.3	^{214}Bi
1264.3	0.20	557	14	1973.6	709.0	^{30}P
1273.0	0.20	13475	61	1273.3	0.0	^{29}Si
1289.2	0.20	17	3	1289.7	0.0	^{52}Cr
1311.4[a]	0.20	13	3			
1368.2	0.20	31	7	1368.7	0.0	^{23}Na
1370.9[a,b]	0.20	31	7			
1377.2	0.20	95	6	1377.6	0.0	^{56}Fe
1385.0	0.20	393	12	2839.9	1454.7	^{30}P
1454.4	0.20	681	15	1454.7	0.0	^{30}P
1460.6	0.20	168	8	1460.8	0.0	^{40}Ar
1483.4	0.20	33	4	2937.8	1454.7	^{30}P
1562.7	0.40	15	3			
1693.2	0.40	9	3			
1731.2	0.40	14	4	1797.6	57.8	^{214}Bi
1757.6	0.40	55	5	1757.6	0.0	^{56}Fe
1764.4	0.40	21	4	1764.5	0.0	^{214}Bi
1779.1	0.40	27	4	1778.8	0.0	^{28}Si
1798.4	0.40	31	5	4736.4	2937.9	^{30}P
1805.3	0.40	32	5	4343.6	2539.0	^{30}P
1830.2	0.40	20	4	2539.0	709.0	^{30}P
1882.5[a]	0.40	6	3			
1897.1	0.40	11	4	1897.4	0.0	^{56}Fe
1919.7	0.40	40	5	1919.6	0.0	^{56}Fe
1973.6	0.40	397	13	1973.6	0.0	^{30}P
1989.2[a]	0.40	5	3			
2027.5	0.40	9	3	2407.0	378.0	^{52}Cr
2084.4	0.40	4	2	3705.4	1621.1	^{56}Fe

Table A.1. γ-rays observed in the decay of the 7921.8 keV state (continued)

E_γ (keV)	σ_{E_γ} (keV)	I_γ^a (Relative)	σ_{I_γ} (Relative)	E_i (keV)	E_f (keV)	Source Nuclide
2130.9	0.40	963	20	2839.8	709.0	^{30}P
2195.8	0.40	5	2	2573.3	378.0	^{52}Cr
2203.1	0.40	8	3	2204.1	0.0	^{214}Bi
2260.9	0.40	26	5	2937.9	677.3	^{30}P
2370.7	0.40	567	16	4343.5	1973.6	^{30}P
2476.6	0.40	10	3	2478.2	0.0	^{56}Fe
2509.8	0.40	29	4			
2539.4	0.40	590	17	2539.0	0.0	^{30}P
2614.9	0.40	55	6	2614.6	0.0	^{208}Tl
2689.5	0.40	18	4			
2719.2	0.40	27	5	3096.9	377.9	^{52}Cr
2723.8	0.40	51	6			
2766.4[a]	0.40	10	3			
2839.9	0.40	433	17	2839.9	0.0	^{30}P
2844.4	0.40	85	9	4298.1	1454.7	^{30}P
2873.5	0.40	18	4			
2937.7	0.40	19	4	2937.9	0.0	^{30}P
3000.9[a]	0.40	8	3			
3046.0[a]	0.40	8	3			
3066.8[c]	0.40	60	7	7921.8	4343.5	^{30}P
3185.0	0.40	39	5	7921.8	4736.4	^{30}P
3257.4[a]	0.40	6	3			
3263.8[a]	0.40	9	3			
3298.4[a]	0.40	10	4			
3443.1[a]	0.40	11	3			
3474.3	0.40	17	4	4182.6	709.0	^{30}P
3577.6	0.40	520	18	7921.8	4343.5	^{30}P
3622.9	0.40	119	9	7921.8	4298.1	^{30}P
3738.4	0.40	23	4	7921.8	4182.6	^{30}P

Table A.1. γ-rays observed in the decay of the 7921.8 keV state (continued)

E_γ (keV)	σ_{E_γ} (keV)	I_γ (Relative)	σ_{I_γ} (Relative)	E_i (keV)	E_f (keV)	Source Nuclide
3992.3	0.40	46	6	7921.8	3928.9	^{30}P
3992.7	0.40	7	3	3993.0	0.0	^{56}Fe
4090.9[a]	0.40	12	4			
4177.2[a]	0.40	19	5			
4336.4	0.40	40	6			
4504.6[a]	0.40	16	5			
4571.0[c]	0.40	127	11	7921.8	2839.8	^{30}P
4871.9[c]	0.40	53	9	7921.8	2539.0	^{30}P
5082.2	0.40	1731	40	7921.8	2839.8	^{30}P
5209.0	0.40	21	6			
5382.9	0.40	535	23	7921.8	2539.0	^{30}P
5437.4[c]	0.40	32	6	7921.8	1973.6	^{30}P
5948.5	0.40	368	20	7921.8	1973.6	^{30}P
6468.6	0.40	18	5	7921.8	1454.7	^{30}P
7212.9	0.40	18	7	7921.8	709.0	^{30}P
7410.7[c]	0.40	43	8	7921.8	0.0	^{30}P
7921.4	0.40	257	20			

[a] Value of E_γ taken from suppressed spectrum.

[b] Peak seen in off-resonance data.

[c] Single escape peak.

Table A.2. Feeding/decay balance for E_x=7921.8 keV

E_x (keV)	Intensity In (Relative)	Intensity Out (Relative)
0.0	26.34 ± 0.27	—
677.3	0.193 ± 0.037	0.237 ± 0.030
709.0	11.92 ± 0.19	10.38 ± 0.13
1454.7	3.93 ± 0.12	5.33 ± 0.12
1973.6	6.94 ± 0.19	7.08 ± 0.14
2539.0	4.21 ± 0.17	4.53 ± 0.13
2839.9	12.85 ± 0.30	13.28 ± 0.22
2937.9	0.408 ± 0.052	0.579 ± 0.056
3928.9	0.341 ± 0.045	0.178 ± 0.037
4182.6	0.171 ± 0.030	0.126 ± 0.030
4298.1	0.883 ± 0.067	0.631 ± 0.067
4343.6	3.86 ± 0.13	4.45 ± 0.13
4736.4	0.289 ± 0.037	0.230 ± 0.037
7921.8	—	25.31 ± 0.41

Table A.3. γ-ray intensities for E_x=7921.8 keV

E_γ (keV)	E_i (keV)	E_f (keV)	Observed I_γ^a (Relative)	Expected I_γ^b (Relative)
31.7	709.3	677.3	0.00	0.06
565.4	2539.0	1973.6	0.00	0.07
677.3	677.3	0.0	0.94	0.65
709.0	709.0	0.0	41.20	43.19
745.6	1454.7	709.0	1.12	0.85
964.3	2937.9	1973.6	0.00	0.01
991.0	3928.9	2937.9	0.71	1.01
1264.6	1973.6	709.0	16.39	13.84
1385.2	2839.9	1454.7	11.58	14.79
1454.7	1454.7	0.0	20.04	18.50
1483.2	2937.9	1454.7	0.97	0.77
1643.6	4182.7	2539.0	0.00	0.03
1717.0	4736.4	3019.4	0.00	0.02
1759.1	4298.1	2539.0	0.00	0.67
1798.5	4736.4	2937.9	0.91	0.75
1804.6	4343.6	2539.0	0.94	0.75
1830.0	2539.0	709.0	0.59	0.52
1973.6	1973.6	0.0	11.69	11.32
2130.9	2839.9	709.0	28.38	27.03
2209.0	4182.7	1973.6	0.00	0.03
2228.9	2937.9	709.0	0.00	0.10
2260.6	2937.9	677.3	0.77	0.56
2342.1	3019.4	677.3	0.00	0.02
2370.0	4343.6	1973.6	16.71	14.25
2474.2	3928.9	1454.7	0.00	0.29
2539.0	2539.0	0.0	17.38	16.85
2728.0	4182.7	1454.7	0.00	0.02
2839.9	2839.9	0.0	12.74	9.18
2843.4	4298.1	1454.7	2.50	2.84

Table A.3. γ-ray intensities for E_x=7921.8 keV (continued)

E_γ (keV)	E_i (keV)	E_f (keV)	Observed I_γ^a (Relative)	Expected I_γ^b (Relative)
2937.9	2937.9	0.0	0.56	0.32
3185.4	7921.8	4736.4	1.15	1.10
3281.7	4736.4	1454.7	0.00	0.14
3473.6	4182.7	709.0	0.50	0.53
3505.4	4182.7	677.3	0.00	0.01
3578.2	7921.8	4343.6	15.32	15.00
3623.7	7921.8	4298.1	3.50	3.50
3739.1	7921.8	4182.7	0.68	0.70
3992.9	7921.8	3928.9	1.35	1.30
4027.4	4736.4	709.0	0.00	0.08
4182.7	4182.7	0.0	0.00	0.08
4736.4	4736.4	0.0	0.00	0.11
5081.9	7921.8	2839.9	51.00	51.00
5382.7	7921.8	2539.0	15.76	16.00
5948.2	7921.8	1973.6	10.84	10.80
6467.1	7921.8	1454.7	0.53	0.50
7212.7	7921.8	709.0	0.33	0.30

[a] Calculated from information in P30_2407.DAT.

[b] Calculated from branching ratios for resonance state and previously known branching ratios for all other states populated in the decay.

Table A.4. Branching ratios for E_x=7921.8 keV

	Present Work	Previous Work[a]
E_f (keV)	BR (%)	BR (%)
709.02	0.3±0.1	—
1454.67	0.5±0.1	—
1973.62	10.8±0.9	11
2539.03	16±1	20
2839.9	51±3	51
3928.9	1.3±0.2	—
4182.65	0.7±0.1	—
4298.1	3.5±0.3	3
4343.6	15±1	15
4736.4	1.1±0.2	—

[a]From [Cam93]

Table A.5. B's vs. RUL's for E_x=7921.8 keV

$J^\pi;T$ Assignment	E_f (keV)	$J^\pi;T$ (Final)	Transition Type	B (W.u.)	RUL (W.u.)
$2^-;0$	4298	$4^+;0$	M2/E3 IS	140/75600	0.2/50
	4343	$5^+;0$	E3 IS	354000	50
$2^-;1$	4298	$4^+;0$	M2/E3 IV	140/75600	5/‡
	4343	$5^+;0$	E3 IV	354000	‡
$3^+;1$	4343	$5^+;0$	E2 IV	15	5
$3^-;0$	4343	$5^+;0$	M2/E3 IS	458/253000	0.2/50
$3^-;1$	4343	$5^+;0$	M2/E3 IV	458/253000	5/‡
$4^-;0$	4182	$2^+;1$	M2/E3 IV	13/6740	5/‡
$4^-;1$	4182	$2^+;1$	M2/E3 IS	13/6740	0.2/‡

‡ No RUL given.

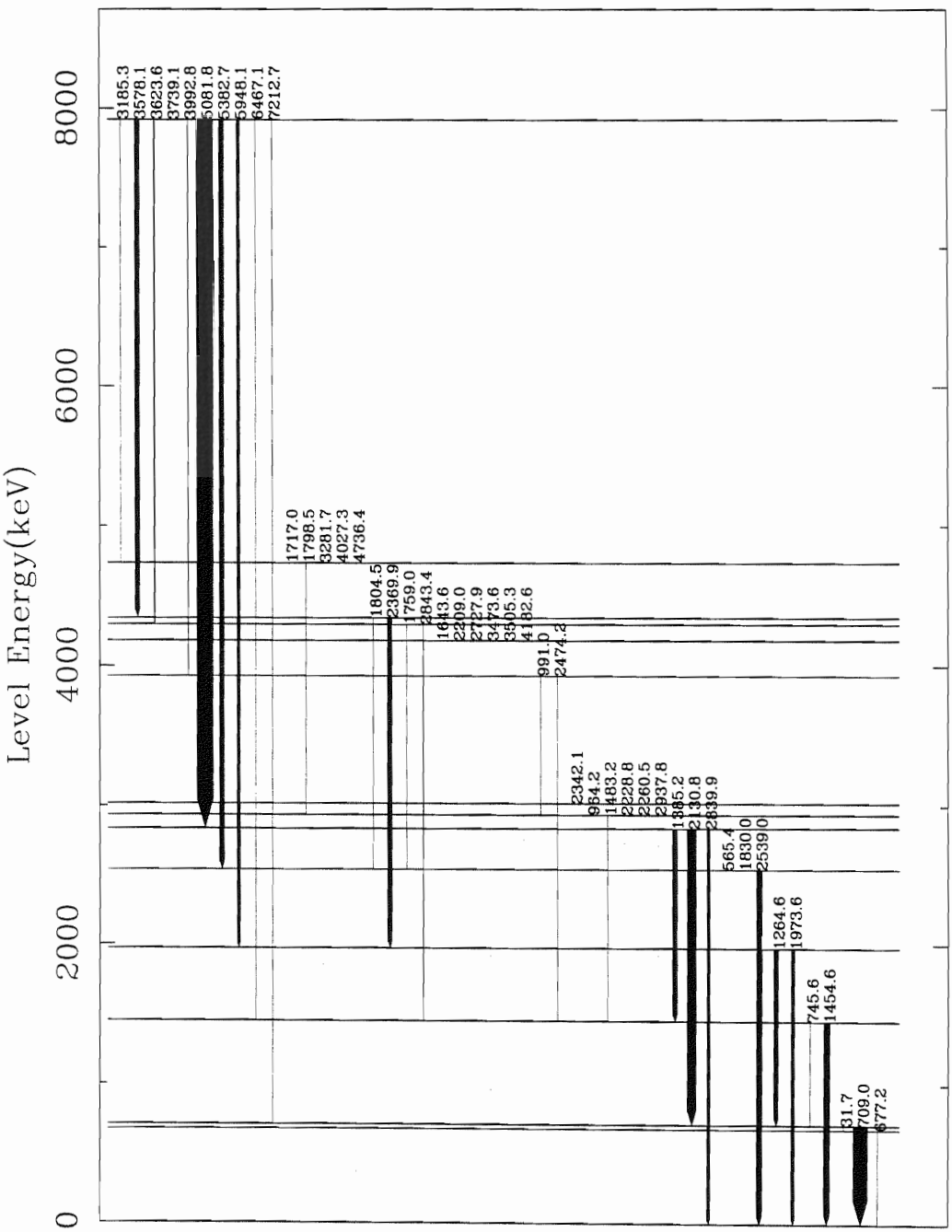

Figure A.7. Decay Scheme for $E_x = 7921.8$ keV. The width of the arrows indicates the strength of the transition.

Appendix B

Branching Ratios

All but two of the states studied have observable γ-ray yields. The branching ratios for these levels are presented in this appendix. In cases where branching ratios were reported by previous researchers, those results are listed along with the branching ratios from the present work. For the majority of cases there is good agreement, although often the present study adds a number of weak transitions. However, there are some resonances where the difference in results is striking[1]. In all of these cases nearby states interfered with the resonance; these resonances were treated in a manner similar to that described in Appendix A for the 7921.8 keV state.

[1]See tables for resonances at 7826.3, 7922.1, and 8001.2 keV.

Table B.1. Branching ratios for E_x=6006.1 keV

E_f (keV)	BR (%)
1454.67	29±2
1973.62	34±2
2539.03	11±2
2723.96	15±1
2839.9	11±1

Table B.2. Branching ratios for E_x=7304.9 keV

	Present Work	Previous Work[a]
E_f (keV)	BR (%)	BR (%)
0.0	1.7±0.2	2.4
709.02	18±1	21
1454.67	0.9±0.1	—
1973.62	20.0±1	23
2539.03	0.9±0.1	0.9
2723.96	0.3±0.1	—
2839.9	3.5±0.2	2.6
2937.87	18.4±0.9	16
3733.9	6.8±0.4	6.7
4143.67	1.3±0.1	—
4182.65	6.0±0.4	5.4
4502.32	22.0±1	22

[a]From [Rei85]

Table B.3. Branching ratios for E_x=7306.3 keV

	Present Work	Previous Work[a]
E_f (keV)	BR (%)	BR (%)
709.02	0.6±0.1	—
1454.67	12.5±0.7	18
1973.62	20.0±1	18
2723.96	3.5±0.3	2.0
2839.9	4.7±0.3	4.4
2937.87	40±2	46
3835.9	4.7±0.5	4.1
4143.67	0.8±0.1	—
4182.65	4.8±0.3	—
4232.2	1.1±0.1	—
4422.4	0.7±0.1	1.1
4736.4	0.8±0.1	—
6094.6	4.0±0.2	—
6269.6	1.5±0.2	—

[a]From [Rei85]

Table B.4. Branching ratios for E_x=7322 keV

E_f (keV)	BR (%)
0.0	33±3
1454.67	11±2
2937.87	30±2
4143.67	2.6±6
4182.65	1.5±0.5
4502.32	22±2

Table B.5. Branching ratios for E_x=7383.4 keV

E_f (keV)	Present Work BR (%)	Previous Work[a] BR (%)
0.0	2.0±0.3	—
1454.67	1.6±0.3	—
2723.96	1.9±0.3	—
2937.87	83±4	100
5508.6	3.3±0.2	—
5933.64	8.5±0.5	—

[a]From [Rei85]

Table B.6. Branching ratios for E_x=7492.7 keV

E_f (keV)	Present Work BR (%)	Previous Work[a] BR (%)
0.0	1.5±0.3	2.2
677.29	13±1	15
1454.67	1.3±0.3	—
2723.96	1.2±0.2	1.4
2937.87	48±2	46
4143.67	0.6±0.2	—
4182.65	22±1	23
4468.33	4.8±0.4	4.7
4502.32	7.7±0.5	7.6

[a]From [Rei85]

Table B.7. Branching ratios for E_x=7560.5 keV

E_f (keV)	BR (%)
0.0	0.7±0.1
709.02	1.5±0.2
2539.03	1.4±0.2
2723.96	1.1±0.1
2937.87	11.2±0.7
3733.9	8.6±0.5
4143.67	0.54±0.09
4182.65	23±1
4232.2	0.44±0.08
4298.1	1.1±0.1
4343.6	0.6±0.1
4422.4	0.7±0.1
5508.6	6.9±0.4
5576.90	23±1
5933.64	11.9±0.7
6006.07	7.6±0.4

Table B.8. Branching ratios for E_x=7562.5 keV

	Present Work	Previous Work[a]
E_f (keV)	BR (%)	BR (%)
0.0	11.2±0.7	13
677.29	1.6±0.2	2.4
709.02	3.5±0.3	4.6
1454.67	17±1	18
2539.03	3.4±0.2	2.9
2723.96	1.2±0.1	1.1
2937.87	1.9±0.2	1.9
3019.39	1.9±0.2	1.5
3835.9	8.8±0.5	7.3
3928.9	1.2±0.1	1.3
4182.65	0.37±0.06	0.6
4422.4	1.03±0.09	0.9
4736.4	6.9±0.4	6.1
4937.9	4.9±0.3	4.6
5206.4	3.1±0.2	2.9
5506.1	20±1.	20
5701.7	11.7±0.6	11
6299.3	0.4±0.1	—

[a]From [Rei85]

Table B.9. Branching ratios for E_x=7579.9 keV

	Present Work	Previous Work[a]
E_f (keV)	BR (%)	BR (%)
0.0	1.3±0.2	2.8
709.0	—	0.9
1454.67	3.6±0.6	5.5
1973.62	4.2±0.4	4.2
2539.03	3.3±0.3	3.0
2723.96	22±1	21
2937.87	18±1	17
3835.9	2.8±0.2	2.0
3928.9	1.9±0.2	2.0
4143.67	1.5±0.3	1.7
4182.65	0.9±0.1	—
4232.2	1.1±0.1	0.9
4626.55	0.4±0.1	0.6
5576.90	2.1±0.2	1.4
5933.64	1.3±0.2	—
6094.6	36±2	37

[a]From [Rei85]

Table B.10. Branching ratios for E_x=7605.0 keV

	Present Work	Previous Work[a]
E_f (keV)	BR (%)	BR (%)
0.0	2.6±0.2	2.3
677.29	0.25±0.07	—
709.02	1.2±0.1	1.6
1454.67	0.44±0.08	—
2539.03	1.15±0.09	1.5
2723.96	0.94±0.08	0.9
2937.87	87±4	90
3019.39	0.26±0.05	—
4182.65	3.4±0.2	3.2
4502.32	0.50±0.05	0.5
5508.6	1.9±0.1	—

[a]From [Rei85]

Table B.11. Branching ratios for E_x=7636.0 keV

	Present Work	Previous Work[a]
E_f (keV)	BR (%)	BR (%)
0.0	1.6±0.2	2.6
1454.67	0.7±0.1	—
1973.62	1.7±0.1	1.9
2539.03	37±2	37
2723.96	8.3±0.5	9.0
2839.9	5.4±0.3	5.6
2937.87	5.0±0.3	5.2
3835.9	11.8±0.6	12
3928.9	0.99±0.09	0.4
4182.65	4.9±0.3	4.9
4232.2	3.3±0.2	2.8
4298.1	1.7±0.1	1.4
4422.4	5.2±0.3	5.2
4736.4	11.9±0.6	12
5206.4	0.58±0.06	—
6299.3	0.39±0.05	—

[a]From [Rei85]

Table B.12. Branching ratios for E_x=7644.3 keV

	Present Work	Previous Work[a]
E_f (keV)	BR (%)	BR (%)
0.0	—	0.8
709.02	0.24±0.6	0.4
1973.62	2.7±0.2	2.8
2539.03	32±2.	33
2723.96	10.4±0.6	12
2839.9	6.3±0.3	6.3
2937.87	10.3±0.5	9.4
3019.39	—	0.2
3835.9	12.2±0.6	11
4143.67	0.31±0.03	—
4182.65	4.3±0.2	4.9
4232.2	1.7±0.1	1.6
4298.1	0.96±0.07	0.9
4422.4	5.3±0.3	5.3
4626.55	0.40±0.04	0.4
4736.4	11.2±0.6	11
5206.4	0.81±0.06	—
6299.3	0.36±0.03	—

[a]From [Rei85]

Table B.13. Branching ratios for E_x=7786.4 keV

E_f (keV)	BR (%)
1973.62	29±2
2539.03	30±2
2839.9	22±2
3928.9	6.5±0.8
4143.67	2.4±0.6
6006.07	10±1

Table B.14. Branching ratios for E_x=7826.3 keV

	Present Work	Previous Work[a]
E_f (keV)	BR (%)	BR (%)
0.0	—	67
709.02	—	21
1454.67	25±2	7
2937.87	17±2	5
3019.39	1.8±0.7	—
4143.67	2.0±0.5	—
4182.65	54±4	—

[a]From [Cam93]

Table B.15. Branching ratios for E_x=7873.7 keV

E_f (keV)	BR (%)
1454.67	5±1
1973.62	11±2
2539.03	13±2
4232.2	33±3
4736.4	5.9±0.8
4926.4	9±1
5508.6	11±1
5933.64	13±1

Table B.16. Branching ratios for E_x=7883.7 keV

	Present Work	Previous Work[a]
E_f (keV)	BR (%)	BR (%)
1454.67	7.0±0.8	—
1973.62	6.2±0.8	15
2539.03	17±1	17
2723.96	1.8±0.4	—
2839.9	33±2	39
3835.9	3.6±0.5	—
3928.9	2.1±0.4	—
4298.1	4.9±0.5	5
4343.6	23±2	24
4422.4	1.4±0.3	—

[a]From [Cam93]

Table B.17. Branching ratios for E_x=7891 keV

E_f (keV)	BR (%)
0.0	87±6
709.02	9.2±0.9
3019.39	2.4±0.4
4143.67	1.7±0.3

Table B.18. Branching ratios for E_x=7920.9 keV

	Present Work	Previous Work[a]
E_f (keV)	BR (%)	BR (%)
709.02	11.2±0.9	16
1454.67	6.4±0.5	9
1973.62	20±1	22
2539.03	28±2	15
2723.96	3.0±0.3	—
2937.87	2.7±0.3	—
3835.9	5.6±0.4	7
3928.9	6.1±0.5	13
4143.67	1.8±0.2	—
4626.55	5.1±0.4	9
4736.4	6.2±0.4	9
5206.4	2.9±0.2	—
5508.6	0.5±0.1	—

[a]From [Cam93]

Table B.19. Branching ratios for E_x=7921.8 keV

	Present Work	Previous Work[a]
E_f (keV)	BR (%)	BR (%)
709.02	0.3±0.1	—
1454.67	0.5±0.1	—
1973.62	10.8±0.9	11
2539.03	16±1.	20
2839.9	51±3.	51
3928.9	1.3±0.2	—
4182.65	0.7±0.1	—
4298.1	3.5±0.3	3
4343.6	15±1.	15
4736.4	1.1±0.2	—

[a]From [Cam93]

Table B.20. Branching ratios for E_x=7922.1 keV

	Present Work	Previous Work[a]
E_f (keV)	BR (%)	BR (%)
0.0	—	32
709.02	—	7
1454.67	5±1	—
1973.62	14±2	12
2539.03	21±2	16
2839.9	40±4	20
3835.9	—	2
3928.9	9±1	3
4343.6	11±1	5
4626.55	—	1
4736.4	—	2

[a]From [Cam93]

Table B.21. Branching ratios for E_x=7996.7 keV

	Present Work	Previous Work[a]
E_f (keV)	BR (%)	BR (%)
0.0	78±4.	75
677.29	1.5±0.4	3
3019.39	9.3±0.6	11
3733.9	5.6±0.5	8
4937.9	2.9±0.3	—
5506.1	2.9±0.3	—
5508.6	—	3

[a]From [Cam93]

Table B.22. Branching ratios for E_x=8001.2 keV

	Present Work	Previous Work[a]
E_f (keV)	BR (%)	BR (%)
0.0	—	57
677.29	72±6	32
709.02	9±1	—
1454.67	9±1	—
2937.87	11±1	7
3019.39	—	4

[a]From [Cam93]

Table B.23. Branching ratios for E_x=8007.4 keV

	Present Work	Previous Work[a]
E_f (keV)	BR (%)	BR (%)
0.0	5.9±0.4	9
677.29	0.49±0.08	2
709.02	0.7±0.1	1
1454.67	2.1±0.2	3
1973.62	0.7±0.1	—
2723.96	0.50±0.09	—
2937.87	65±4	64
3019.39	0.23±0.08	—
3733.9	0.67±0.09	—
3928.9	1.2±0.1	—
4182.65	20±1	21
5576.90	0.68±0.08	—
5933.64	1.5±0.1	—

[a]From [Cam93]

Table B.24. Branching ratios for E_x=8014.3 keV

	Present Work	Previous Work[a]
E_f (keV)	BR (%)	BR (%)
0.0	14±2	20
709.02	14±2	15
1454.67	13±2	—
4182.65	29±3	32
5508.6	30±3	33

[a]From [Cam93]

Appendix C

RUL Analysis

This appendix contains a table for each of the resonances which were analyzed using Endt's RUL's. The assignments listed are those allowed by J^π analysis but forbidden by RUL analysis: that is, for these assignments, $B \geq 2 \times \text{RUL}$. Three symbols are used in the following tables:

1. §: Denotes assignments for which more than two transitions have values of B which exceed twice their associated RUL. No more than two transitions per assignment are listed.

2. †: Denotes values of B which exceed 10^7 W.u.

3. ‡: Denotes RUL's for transition types E3IV and M3IS[1]. RUL's for these types have not been defined since so few of these transitions have been observed. For the present work, if $B \geq 10^3$ for a possible E3IV or M3IS transition, that transition is taken to not be allowed.

[1]M3 transitions, while not considered in the J^π analysis, do show up as possibilities in Table C.3. This is due to the unknown J^π of the 5933.6 keV resonance.

Table C.1. B's vs. RUL's for E_x=7304.9 keV

$J^\pi;T$ Assignment	E_f (keV)	$J^\pi;T$ (Final)	Transition Type	B (W.u.)	RUL (W.u.)
$0^-;0^\S$	1454	$2^+;0$	M2 IS	7.4	0.2
	1973	$3^+;0$	E3 IS	65000	50
$0^-;1^\S$	4182	$2^+;1$	M2 IS	1140	0.2
	4502	$1^+;1$	E1 IS	0.013	0.002
$1^-;0^\S$	2539	$3^+;0$	M2/E3 IS	6.9/2140	0.2/50
	2839	$3^+;0$	M2/E3 IS	37/13100	0.2/50
$1^-;1^\S$	1973	$3^+;0$	M2/E3 IV	87/21700	5/‡
	4502	$1^+;1$	E1 IS	0.0043	0.002
$3^+;0$	4502	$1^+;1$	E2 IV	33	5
$3^-;0^\S$	709	$1^+;0$	M2/E3 IS	12/1185	0.2/50
	3733	$1^+;0$	M2/E3 IS	94/52200	0.2/50
$3^-;1^\S$	3733	$1^+;0$	M2/E3 IV	94/52200	5/‡
	4502	$1^+;1$	M2/E3 IS	1020/922000	0.2/50
$4^-;0^\S$	709	$1^+;0$	E3 IS	1470	50
	3733	$1^+;0$	E3 IS	40600	50
$4^-;1^\S$	4182	$2^+;1$	M2/E3 IS	127/92000	0.2/50
	4502	$1^+;1$	E3 IS	717000	50

Table C.2. B's vs. RUL's for E_x=7306.3 keV

$J^\pi;T$ Assignment	E_f (keV)	$J^\pi;T$ (Final)	Transition Type	B (W.u.)	RUL (W.u.)
$1^+;0$	6094	$3^-;1$	M2/E3 IV	25200/†	5/‡
$1^+;1$	6094	$3^-;1$	M2/E3 IS	25200/†	0.2/50
$2^+;0$	4232	$4^-;0$	M2/E3 IS	39/29600	0.2/50
$2^+;1$	4232	$4^-;0$	M2/E3 IV	39/29600	5/‡
	6094	$3^-;1$	E1 IS	0.0050	0.002
$2^-;1$	6094	$3^-;1$	M1/E2 IS	0.15/480	0.05/100
$3^+;0$	6269	$1^+;0$	E2 IS	280	100
		$1^+;1$	E2 IV	280	5
$3^+;1$	6269	$1^+;1$	E2 IS	280	100
		$1^+;0$	E2 IV	280	5
$3^-;0$	6269	$1^+;1$	M2/E3 IV	8820/†	5/‡
		$1^+;0$	M2/E3 IS	8820/†	0.2/50
$3^-;1$	6094	$3^-;1$	M1/E2 IS	0.11/343	0.05/100
	6269	$1^+;1$	M2/E3 IS	8820/†	0.2/50
		$1^+;0$	M2/E3 IV	8820/†	5/‡
$4^-;0^{\S}$	1454	$2^+;0$	M2/E3 IS	10/2060	0.2/50
	2723	$2^+;0$	M2/E3 IS	9.5/3190	0.2/50
$4^-;1^{\S}$	2937	$2^+;1$	M2/E3 IS	138/51000	0.2/50
	4182	$2^+;1$	M2/E3 IS	88/64100	0.2/50

Table C.3. B's vs. RUL's for E_x=7383.4 keV

$J^\pi;T$ Assignment	E_f (keV)	$J^\pi;T$ (Final)	Transition Type	B (W.u.)	RUL (W.u.)
$0^+;0$	2937	$2^+;1$	E2 IV	41	5
	5933	$3^+;0$	M3 IS	†	‡
		$3^+;1$	M3 IV	†	10
		$3^-;0$	E3 IS	†	50
		$3^-;1$	E3 IV	†	‡
$0^+;1$	5933	$3^+;0$	M3 IV	†	10
		$3^+;1$	M3 IS	†	‡
		$3^-;0$	E3 IV	†	‡
		$3^-;1$	E3 IS	†	50
$0^-;0^{\S}$	2723	$2^+;0$	M2 IS	23	0.2
	2937	$2^+;1$	M2 IV	1280	5
$0^-;1^{\S}$	2723	$2^+;0$	M2 IV	23	5
	2937	$2^+;1$	M2 IS	1280	0.2
$1^+;0$	5933	$3^+;0$	E2 IS	376	100
		$3^+;1$	E2 IV	376	5
		$3^-;0$	M2/E3 IS	11800/†	0.2/50
		$3^-;1$	M2/E3 IV	11800/†	5/‡
$1^+;1$	5933	$3^+;0$	E2 IV	376	5
		$3^+;1$	E2 IS	376	100
		$3^-;0$	M2/E3 IV	11800/†	5/‡
		$3^-;1$	M2/E3 IS	11800/†	0.2/50
$1^-;0$	5933	$3^+;0$	M2/E3 IS	11800/†	0.2/50
		$3^+;1$	M2/E3 IV	11800/†	5/‡
		$3^-;0$	E2 IS	376	100
		$3^-;1$	E2 IV	376	5

Table C.3. B's vs. RUL's for E_x=7383.4 keV (continued)

$J^\pi;T$ Assignment	E_f (keV)	$J^\pi;T$ (Final)	Transition Type	B (W.u.)	RUL (W.u.)
$1^-;1$	5933	$3^+;0$	M2/E3 IV	11800/†	5/‡
		$3^+;1$	M2/E3 IS	11800/†	0.2/50
		$3^-;0$	E2 IV	376	5
		$3^-;1$	E2 IS	376	100
$4^-;0^{\S}$	2723	$2^+;0$	M2/E3 IS	2.6/838	0.2/50
	2937	$2^+;1$	M2/E3 IV	142/50800	5/‡
$4^-;1$	2937	$2^+;1$	M2/E3 IS	142/50800	0.2/50

Table C.4. B's vs. RUL's for E_x=7492.7 keV

$J^\pi;T$ Assignment	E_f (keV)	$J^\pi;T$ (Final)	Transition Type	B (W.u.)	RUL (W.u.)
$1^-;1$	4182	$2^+;1$	E1 IS	0.0042	0.002
$2^+;0$	4468	$0^+;1$	E2 IV	11	5
$2^-;0$	677	$0^+;1$	M2 IV	16	5
	4468	$0^+;1$	M2 IV	345	5
$2^-;1$	677	$0^+;1$	M2 IS	16	0.2
	4468	$0^+;1$	M2 IS	345	0.2
$3^-;0^{\S}$	0	$0^+;1$	M2/E3 IS	0.82/104	0.2/50
	4502	$1^+;1$	M2/E3 IV	418/330000	5/‡
$3^-;1^{\S}$	677	$0^+;1$	E3 IS	1750	50
	4502	$1^+;1$	M2/E3 IS	418/330000	0.2/50

Table C.5. B's vs. RUL's for E_x=7560.5 keV

$J^\pi;T$ Assignment	E_f (keV)	$J^\pi;T$ (Final)	Transition Type	B (W.u.)	RUL (W.u.)
$2^-;0$	4298	$4^+;0$	M2/E3 IS	26/17500	0.2/50
	4343	$5^+;0$	E3 IS	10600	50
$2^-;1^{\S}$	4298	$4^+;0$	M2/E3 IV	26/17500	5/‡
	4343	$5^+;0$	E3 IV	10600	‡
$3^-;0$	3733	$1^+;0$	M2/E3 IS	66/32100	0.2/50
	4343	$5^+;0$	M2/E3 IS	11/7540	0.2/50
$3^-;1$	3733	$1^+;0$	M2/E3 IV	66/32100	5/‡
	4343	$5^+;0$	M2/E3 IV	11/7540	5/‡
$4^-;0^{\S}$	2937	$2^+;1$	M2/E3 IV	26/8650	5/‡
	4182	$2^+;1$	M2/E3 IV	258/160000	5/‡
$4^-;1^{\S}$	2937	$2^+;1$	M2/E3 IS	26/8650	0.2/50
	4182	$2^+;1$	M2/E3 IS	258/160000	0.2/50

Table C.6. B's vs. RUL's for E_x=7562.5 keV

$J^\pi;T$ Assignment	E_f (keV)	$J^\pi;T$ (Final)	Transition Type	B (W.u.)	RUL (W.u.)
$1^+;0^\S$	5506	$1^+;0$	M1/E2 IS	0.68/751	0.05/100
		$1^-;0$	E1 IS	0.023	0.002
	5701	$1^+;0$	M1/E2 IS	0.54/724	0.05/100
$1^+;1$	4736	$3^+;0$	E2 IV	53	5
	6299	$3^+;0$	E2 IV	172	5
$1^-;0^\S$	5701	$1^+;0$	E1 IS	0.018	0.002
	6299	$3^+;0$	M2/E3 IS	5400/†	0.2/50
$1^-;1^\S$	4736	$3^+;0$	M2/E3 IV	1660/†	5/‡
	6299	$3^+;0$	M2/E3 IV	5400/†	5/‡
$2^+;0$	5506	$1^+;0$	M1/E2 IS	0.41/451	0.05/100
		$1^-;0$	E1 IS	0.014	0.002
	5701	$1^+;0$	M1/E2 IS	0.324/434	0.05/100
$2^-;0$	5506	$1^+;0$	E1 IS	0.014	0.002
		$1^-;0$	M1/E2 IS	0.41/451	0.05/100
	5701	$1^+;0$	E1 IS	0.011	0.002
$2^-;1$	677	$0^+;1$	M2 IS	2.7	0.2
$3^-;0^\S$	0	$1^+;0$	M2/E3 IS	8.4/1040	0.2/50
	5701	$1^+;0$	M2/E3 IS	9760/†	0.2/50
$3^-;1^\S$	677	$0^+;1$	E3 IS	287	50
	5701	$1^+;0$	M2/E3 IV	9760/†	5/‡

Table C.7. B's vs. RUL's for E_x=7579.9 keV

$J^\pi;T$ Assignment	E_f (keV)	$J^\pi;T$ (Final)	Transition Type	B (W.u.)	RUL (W.u.)
$1^+;0^\S$	4232	$4^-;0$	E3 IS	17400	50
	4626	$3^-;0$	M2/E3 IS	19/15200	0.2/50
$1^+;1$	4626	$3^-;0$	M2/E3 IV	19/15200	5/‡
	6094	$3^-;1$	M2/E3 IS	52600/†	0.2/50
$2^+;0$	4232	$4^-;0$	M2/E3 IS	17/10500	0.2/50
$2^+;1$	4232	$4^-;0$	M2/E3 IV	17/10500	5/‡
	6094	$3^-;1$	E1 IS	0.016	0.002
$2^-;1$	6094	$3^-;1$	M1/E2 IS	0.48/1000	0.05/100
$3^+;1$	6094	$3^-;1$	E1 IS	0.011	0.002
$3^-;1$	6094	$3^-;1$	M1/E2 IS	0.34/717	0.05/100
$4^-;0^\S$	2723	$2^+;0$	M2/E3 IS	29/8600	0.2/50
	2937	$2^+;1$	M2/E3 IV	29/9650	5/‡
$4^-;1^\S$	2723	$2^+;0$	M2/E3 IV	29/8600	5/‡
	2937	$2^+;1$	M2/E3 IS	29/9650	0.2/50

Table C.8. B's vs. RUL's for E_x=7605.0 keV

$J^\pi;T$ Assignment	E_f (keV)	$J^\pi;T$ (Final)	Transition Type	B (W.u.)	RUL (W.u.)
$1^-;0$	2539	$3^+;0$	M2/E3 IS	27/7490	0.2/50
$1^-;1$	2539	$3^+;0$	M2/E3 IV	27/7490	5/‡
	2937	$2^+;1$	E1 IS	0.015	0.002
$2^-;1$	677	$0^+;1$	M2 IS	0.74	0.2
$3^-;0^\S$	0	$1^+;0$	M2/E3 IS	3.5/422	0.2/50
	709	$1^+;0$	M2/E3 IS	2.6/387	0.2/50
$3^-;1$	2937	$2^+;1$	E1 IS	0.0066	0.002
	4502	$1^+;1$	M2/E3 IS	59/43200	0.2/50

Table C.9. B's vs. RUL's for E_x=7636.0 keV

$J^\pi;T$ Assignment	E_f (keV)	$J^\pi;T$ (Final)	Transition Type	B (W.u.)	RUL (W.u.)
$2^+;0$	4232	$4^-;0$	M2/E3 IS	185/113000	0.2/50
$2^+;1$	4232	$4^-;0$	M2/E3 IV	185/113000	5/‡
$2^-;0$	4298	$4^+;0$	M2/E3 IS	105/66700	0.2/50
$2^-;1$	4298	$4^+;0$	M2/E3 IV	105/66700	5/‡
$4^-;0$§	2723	$2^+;0$	M2/E3 IS	41/12100	0.2/50
	3835	$2^+;0$	M2/E3 IS	212/104000	0.2/50
$4^-;1$§	2723	$2^+;0$	M2/E3 IV	41/12100	5/‡
	2937	$2^+;1$	M2/E3 IS	31/9960	0.2/50

Table C.10. B's vs. RUL's for E_x=7644.3 keV

$J^\pi;T$ Assignment	E_f (keV)	$J^\pi;T$ (Final)	Transition Type	B (W.u.)	RUL (W.u.)
$2^+;0$	4232	$4^-;0$	M2/E3 IS	167/101000	0.2/50
$2^+;1$	4232	$4^-;0$	M2/E3 IV	167/101000	5/‡
$2^-;0$	4298	$4^+;0$	M2/E3 IS	104/65500	0.2/50
	4736	$3^+;0$	E1 IS	0.005	0.002
$2^-;1$	4298	$4^+;0$	M2/E3 IV	104/65500	5/‡
$4^-;0^{\S}$	2723	$2^+;0$	M2/E3 IS	91/26500	0.2/50
	2937	$2^+;1$	M2/E3 IV	112/35900	5/‡
$4^-;1^{\S}$	2723	$2^+;0$	M2/E3 IV	91/26500	5/‡
	2937	$2^+;1$	M2/E3 IS	112/35900	0.2/50

Table C.11. B's vs. RUL's for E_x=7786.4 keV

$J^\pi;T$ Assignment	E_f (keV)	$J^\pi;T$ (Final)	Transition Type	B (W.u.)	RUL (W.u.)
$0^-;0^{\S}$	1973	$3^+;0$	E3 IS	16100	50
	2539	$3^+;0$	E3 IS	34100	50
$0^-;1^{\S}$	1973	$3^+;0$	E3 IV	16100	‡
	2539	$3^+;0$	E3 IV	34100	‡
$1^-;0^{\S}$	1973	$3^+;0$	M2/E3 IS	26/5370	0.2/50
	2539	$3^+;0$	M2/E3 IS	44/11400	0.2/50
$1^-;1^{\S}$	1973	$3^+;0$	M2/E3 IV	26/5370	5/‡
	2539	$3^+;0$	M2/E3 IV	44/11400	5/‡
$4^+;0$	4143	$2^-;0$	M2/E3 IS	7.3/3900	0.2/50
$5^+;0$	4143	$2^-;0$	E3 IS	3190	50
$5^+;1$	4143	$2^-;0$	E3 IV	3190	‡

Table C.12. B's vs. RUL's for E_x=7826.3 keV

$J^\pi;T$ Assignment	E_f (keV)	$J^\pi;T$ (Final)	Transition Type	B (W.u.)	RUL (W.u.)
$0^+;0^\S$	4143	$2^-;0$	M2 IS	426	0.2
	4182	$2^+;1$	E2 IV	386	5
$0^+;1^\S$	4143	$2^-;0$	M2 IV	426	5
	4182	$2^+;1$	E2 IS	386	100
$0^-;0^\S$	1454	$2^+;0$	M2 IS	344	0.2
	4182	$2^+;1$	M2 IV	12100	5
$0^-;1^\S$	1454	$2^+;0$	M2 IV	344	5
	4182	$2^+;1$	M2 IS	12100	0.2
$1^-;1$	4182	$2^+;1$	E1 IS	0.012	0.002
$2^-;1$	4182	$2^+;1$	E1 IS	0.0073	0.002
$3^-;0$	3019	$1^+;0$	M2/E3 IS	14/4430	0.2/50
$3^-;1$	3019	$1^+;0$	M2/E3 IV	14/4430	5/‡
	4182	$2^+;1$	E1 IS	0.005	0.002
$4^-;0^\S$	1454	$2^+;0$	M2/E3 IS	38/6650	0.2/50
	2937	$2^+;1$	M2/E3 IV	98/28900	5/‡
$4^-;1^\S$	1454	$2^+;0$	M2/E3 IV	38/6650	5/‡
	2937	$2^+;1$	M2/E3 IS	98/28900	0.2/50

Table C.13. B's vs. RUL's for E_x=7883.8 keV

$J^\pi;T$ Assignment	E_f (keV)	$J^\pi;T$ (Final)	Transition Type	B (W.u.)	RUL (W.u.)
$2^-;0$	4298	$4^+;0$	M2/E3 IS	57/31400	0.2/50
	4343	$5^+;0$	E3 IS	161000	50
$2^-;1$	4298	$4^+;0$	M2/E3 IV	57/31400	5/‡
	4343	$5^+;0$	E3 IV	161000	‡
$3^-;0$	4343	$5^+;0$	M2/E3 IS	204/115000	0.2/50
$3^-;1$	4343	$5^+;0$	M2/E3 IV	204/115000	5/‡
$4^-;0^\S$	1454	$2^+;0$	M2/E3 IS	2.4/418	0.2/50
	2723	$2^+;0$	M2/E3 IS	1.9/501	0.2/50
$4^-;1$	3835	$2^+;0$	M2/E3 IV	13/5480	5/‡
	4422	$2^+;0$	M2/E3 IV	11/6370	5/‡
$5^-;0^\S$	2723	$2^+;0$	E3 IS	410	50
	3835	$2^+;0$	E3 IS	4480	50
$5^-;1^\S$	2539	$3^+;0$	M2/E3 IV	12/3030	5/‡
	3835	$2^+;0$	E3 IV	4480	‡

Table C.14. B's vs. RUL's for E_x=7920.9 keV

$J^\pi;T$ Assignment	E_f (keV)	$J^\pi;T$ (Final)	Transition Type	B (W.u.)	RUL (W.u.)
$1^+;0$	4626	$3^-;0$	M2/E3 IS	463/301000	0.2/50
$1^+;1^\S$	4626	$3^-;0$	M2/E3 IV	463/301000	5/‡
	4736	$3^+;0$	E2 IV	21	5
$1^-;0^\S$	1973	$3^+;0$	M2/E3 IS	95/18900	0.2/50
	2539	$3^+;0$	M2/E3 IS	218/53300	0.2/50
$1^-;1^\S$	1973	$3^+;0$	M2/E3 IV	95/18900	5/‡
	2539	$3^+;0$	M2/E3 IV	218/53200	5/‡
$3^-;0$	709	$1^+;0$	M2/E3 IS	8.7/1180	0.2/50
$4^-;0^\S$	1454	$2^+;0$	M2/E3 IS	6.6/1120	0.2/50
	2723	$2^+;0$	M2/E3 IS	9.3/2430	0.2/50
$4^-;1^\S$	2937	$2^+;1$	M2/E3 IS	10/2940	0.2/50
	3835	$2^+;0$	M2/E3 IV	58/24500	5/‡

Table C.15. B's vs. RUL's for E_x=7921.8 keV

$J^\pi;T$ Assignment	E_f (keV)	$J^\pi;T$ (Final)	Transition Type	B (W.u.)	RUL (W.u.)
$2^-;0$	4298	$4^+;0$	M2/E3 IS	140/75600	0.2/50
	4343	$5^+;0$	E3 IS	354000	50
$2^-;1$	4298	$4^+;0$	M2/E3 IV	140/75600	5/‡
	4343	$5^+;0$	E3 IV	354000	‡
$3^+;1$	4343	$5^+;0$	E2 IV	15	5
$3^-;0$	4343	$5^+;0$	M2/E3 IS	458/253000	0.2/50
$3^-;1$	4343	$5^+;0$	M2/E3 IV	458/253000	5/‡
$4^-;0$	4182	$2^+;1$	M2/E3 IV	13/6740	5/‡
$4^-;1$	4182	$2^+;1$	M2/E3 IS	13/6740	0.2/‡

Table C.16. B's vs. RUL's for E_x=7996.7 keV

$J^\pi;T$ Assignment	E_f (keV)	$J^\pi;T$ (Final)	Transition Type	B (W.u.)	RUL (W.u.)
$2^-;1$	677	$0^+;1$	M2 IS	3.5	0.2
$3^-;0^\S$	0	$1^+;0$	M2/E3 IS	83/9230	0.2/50
	3733	$1^+;0$	M2/E3 IS	139/54200	0.2/50
$3^-;1^\S$	0	$1^+;0$	M2/E3 IV	83/9230	5/‡
	3733	$1^+;0$	M2/E3 IV	139/54200	5/‡

Table C.17. B's vs. RUL's for E_x=8001.2 keV

$J^\pi;T$ Assignment	E_f (keV)	$J^\pi;T$ (Final)	Transition Type	B (W.u.)	RUL (W.u.)
$2^-;0$	677	$0^+;1$	M2 IV	27	5
$2^-;1$	677	$0^+;1$	M2 IS	27	0.2
$3^-;0^{\S}$	677	$0^+;1$	E3 IV	2580	‡
	709	$1^+;0$	M2/E3 IS	2.5/333	0.2/50
$3^-;1$	677	$0^+;1$	E3 IS	2580	50

Table C.18. B's vs. RUL's for E_x=8007.4 keV

$J^\pi;T$ Assignment	E_f (keV)	$J^\pi;T$ (Final)	Transition Type	B (W.u.)	RUL (W.u.)
$1^-;0$	1973	$3^+;0$	M2/E3 IS	4.4/858	0.2/50
	3928	$3^+;0$	M2/E3 IS	54/22800	0.2/50
$1^-;1^{\S}$	2937	$2^+;1$	E1 IS	0.0057	0.002
	4182	$2^+;1$	E1 IS	0.0041	0.002
$2^-;1$	677	$0^+;1$	M2 IS	0.70	0.2
$3^-;0$	3019	$1^+;0$	M2/E3 IS	1.6/458	0.2/50
	3733	$1^+;0$	M2/E3 IS	10/3940	0.2/50
$3^-;1$	3733	$1^+;0$	M2/E3 IV	10/3940	5/‡

Table C.19. B's vs. RUL's for E_x=8014.3 keV

$J^\pi;T$ Assignment	E_f (keV)	$J^\pi;T$ (Final)	Transition Type	B (W.u.)	RUL (W.u.)
$0^+;0$	4182	$2^+;1$	E2 IV	47	5
$0^-;0$	1454	$2^+;0$	M2 IS	45	0.2
	4182	$2^+;1$	M2 IV	1480	5
$0^-;1$	1454	$2^+;0$	M2 IV	45	5
	4182	$2^+;1$	M2 IS	1480	0.2
$3^-;0$	0	$1^+;0$	M2/E3 IS	2.6/281	0.2/50
	709	$1^+;0$	M2/E3 IS	4.1/538	0.2/50
$4^-;0^{\S}$	0	$1^+;0$	E3 IS	219	50
	709	$1^+;0$	E3 IS	418	50
$4^-;1$	4182	$2^+;1$	M2/E3 IS	165/79400	0.2/50

Bibliography

[Bla91] J. M. Blatt and V. F. Weisskopf, *Theoretical Nuclear Physics*, Dover Publications, Mineola. 1991.

[Ble94] C. Blecken, Y. Chen, and K. A. Muttalib, "Transitions in Spectral Statistics", J. Phys. A **27**, L563 (1994).

[Boh84] O. Bohigas, M. J. Giannoni, and C. Schmit, "Characterization of Chaotic Quantum Spectra and Universality of Level Fluctuation Laws", Phys. Rev. Lett. **52**, 1 (1984).

[Boh88] O. Bohigas and H. A. Weidenmüller, "Aspects of Chaos in Nuclear Physics", Ann. Rev. Nuc. Part. Sci. **38**, 421 (1988).

[Bro73] T. A. Brody, "A Statistical Measure for the Repulsion of Energy Levels", Lett. Nuovo Cimento **7** (1973).

[Bro81] T. A. Brody et al., "Random-Matrix Fluctuations: Spectrum and Strength Fluctuations", Rev. Mod. Phys. **53**, 385 (1981).

[Byb95] C. R. Bybee, *Fourier Transform as Signature for Chaos in Nuclei and Data Acquisition for Compton-Suppressed Spectrometer*, Ph.D. thesis, North Carolina State University, 1995.

[Cam93] J. A. Cameron, "Spins of Proton Capture Resonances in ^{26}Al and ^{30}P from their Gamma-Ray Spectra", Phys. Rev. C **47**, 1498 (1993).

[Dra94] J. M. Drake, *Resonance Tests of Detailed Balance and Design of a Compton Suppression Spectrometer*, Ph.D. thesis, North Carolina State University, 1994.

[Dyk76] W. W. Dykoski and D. Dehnhard, "Single Proton Transfer to ^{29,30}P States", Phys. Rev. C **13**, 80 (1976).

[Dys62] F. J. Dyson, "A Brownian-Motion Model for the Eigenvalues of a Random Matrix", J. Math. Phys. **3**, 1191 (1962).

[End90a] P. M. Endt, "Energy Levels of A = 21 - 44 of Nuclei (VII)", Nucl. Phys. **A521**, 1 (1990).

[End90b] P. M. Endt, "Spectroscopic Information on ^{24}Mg and ^{28}Si from Proton Capture", Nucl. Phys. **A510**, 209 (1990).

[End93] P. M. Endt, "Strengths of Gamma-Ray Transitions in A = 5 - 44 Nuclei. IV", Atomic Data and Nuclear Data Tables **55**, 171 (1993).

[Eva55] R. D. Evans, *The Atomic Nucleus*, McGraw-Hill Book Company, New York, 1955.

[Fra91a] S. C. Frankle, *Nuclear Resonance Spectroscopy in ^{30}P*, Ph.D. thesis, North Carolina State University, 1991.

[Fra91b] S. C. Frankle, E. G. Bilpuch, G. E. Mitchell, J. F. Shriner, Jr., and C. R. Westerfeldt, "Proton Resonances in ^{30}P", Phys. Rev. C **45**, 2746 (1991).

[Fri89] H. Friedrich and D. Wintgen, "The Hydrogen Atom in a Uniform Magnetic Field – An Example of Chaos", Phys. Rep. **183**, 38 (1989).

[Guh90] T. Guhr and H. A. Weidenmüller, "Isospin Mixing and Spectral Fluctuation Properties", Ann. Phys. **199**, 412 (1990).

[Hal83] E. Haller, H. Koppel, and L. S. Cederbaum, Chem. Phys. Lett. **101**, 215 (1983).

[Haq82] R. U. Haq, A. Pandey, and O. Bohigas, "Fluctuation Properties of Nuclear Energy Levels: Do Theory and Experiment Agree?", Phys. Rev. Lett. **48**, 1086 (1982).

[Har69] G. I. Harris et al., "Properties of ^{30}P Levels from the Reaction ^{29}Si(p,γ)^{30}P II", Phys. Rev. **187**, 1413 (1969).

[Hax94] W. C. Haxton, A. Höring, and M. J. Musolf, "Constraints on T-odd and P-even Hadronic Interactions from Nucleon, Nuclear, and Atomic Electric Dipole Moments", Phys. Rev. D **50**, 3422 (1994).

[Hen89] E. M. Henley, "Status of Time Reversal Invariance", in *Weak and Electromagnetic Interactions in Nuclei*, edited by P. Depommier, Editions Frontières, Gif-sur-Yvette Cedex-France, 1989.

[Kno79] G. F. Knoll, *Radiation Detection and Measurement*, John Wiley & Sons, New York, second edition, 1979.

[Kos76] J. V. Kostin et al., "Gamma-ray Decay of Resonant Levels in ^{30}P", Ukr. Fiz. Zh. **21**, 1090 (1976).

[Kra88] K. Krane, *Introductory Nuclear Physics*, John Wiley and Sons, New York, 1988.

[LaB95] M. A. LaBonte, "Angular Distribution Study of the ^{29}Si(p,γ) Reaction", Master's thesis, North Carolina State University, 1995.

[LS78] C. M. Lederer and V. S. Shirley, editors, *Table of Isotopes*, John Wiley and Sons, New York, seventh edition, 1978.

[Meh91] M. L. Mehta, *Random Matrices*, Academic Press, New York, second edition, 1991.

[Nel83] R. O. Nelson, E. G. Bilpuch, G. E. Mitchell, and C. R. Westerfeldt, "Proton Resonances in ^{30}P", Phys. Rev. C **27**, 930 (1983).

[Pan81] A. Pandey, "Statistical Properties of Many-Particle Spectra. IV. New Ensembles by Stieltjes Transform Methods", Ann Phys. (N.Y.) **134**, 110 (1981).

[Poi70] C. P. Poirer et al., "Elastic and Inelastic Proton Scattering on ^{29}Si", Phys. Rev. C **1**, 1982 (1970).

[Por65] C. E. Porter, editor, *Statistical Theories of Spectra: Fluctuations*, Academic, New York, 1965.

[Rad89] D. C. Radford, *GELIFT Reference Manual*, Argonne National Laboratory, 1989.

[Ram81] B. Ramstein, L. H. Rosier, and R. J. DeMeijer, "Investigation of States in ^{30}P via the ^{30}Si(^{3}He,t)^{30}P Reaction at 30 MeV", Nucl. Phys. **A363**, 110 (1981).

[Rei80] L. E. Reichl, *A Modern Course in Statistical Physics*, University of Texas Press, Austin, TX, 1980.

[Rei85] J. P. L. Reinecke et al., "The Energy Levels of ^{30}P", Nucl. Phys. **A435**, 333 (1985).

[Rei92] L. E. Reichl, *The Transition to Chaos in Conservative Classical Systems: Quantum Manifestations*, Springer-Verlag, New York, 1992.

[Rin80] P. Ring and P. Schuck, *The Nuclear Many-Body Problem*, Springer-Verlag, New York, 1980.

[Ros67] H. J. Rose and D. M. Brink, "Angular Distributions of Gamma-Rays in Terms of Phase-Defined Reduced Matrix Elements", Rev. Mod. Phys. **39**, 306 (1967).

[Ros83] H. J. Rose and D. M. Brink, "Statistical Behavior of Atomic Energy Levels: Agreement with Random Matrix Theory", Phys. Rev. Lett. **50**, 492 (1983).

[Sel85] T. H. Seligman, J. J. M. Verbaarschot, and M. R. Zirnbauer, "Fluctuations of Quantum Spectra and Their Semiclassical Limit in the Transition between Order and Chaos", J. Phys. A **18**, 2227 (1985).

[Shr90] J. F. Shriner. Jr., E. G. Bilpuch, P. M. Endt, and G. E. Mitchell, "Fluctuation Properties of States in ^{26}Al", Z. Phys. A **335**, 393 (1990).

[Shr91] J. F. Shriner. Jr., G. E. Mitchell, and T. von Edigy, "Fluctuation Properties of Spacings of Low-Lying Nuclear Levels", Z. Phys. A **338**, 309 (1991).

[Shr92] J. F. Shriner, Jr. and G. E. Mitchell, "Small Sample Size Effects in Statistical Analyses of Eigenvalue Distributions", Z. Phys. A **342**, 53 (1992).

[Sie87] P. J. Siemens and A. S. Jensen, *Elements of Nuclei: Many-Body Physics with the Strong Interaction*, Addison-Wesley, New York, 1987.

[Sod87] J. P. Soderstrum, M. A. Boyd, C. R. Gould, and N. R. Roberson, *XSYS Reference Manual*, Triangle Universities Nuclear Laboratory, Durham, NC, sixth edition, 1987.

[Uzu74] J. Uzureau et al., "Study of the Reaction ^{29}Si(d,n)^{30}P and the Structure of ^{30}P", Nucl. Phys. **A230**, 253 (1974).

[Vav96] G. A. Vavrina, *Resonance Spectroscopy of the $^{29}Si(p,\gamma)^{30}P$ Reaction*, Ph.D. thesis, North Carolina State University, 1996.

[Wes87] C. R. Westerfeldt, R. O. Nelson, E. G. Bilpuch, and G. E. Mitchell, *The TUNL High Resolution Laboratory System and Operating Procedures*, Triangle Universities Nuclear Laboratory, Durham NC, second edition, 1987.

[Wes88] C. R. Westerfeldt, R. O. Nelson, E. G. Bilpuch, and G. E. Mitchell, "A Microcomputer-Based System for Measuring Excitation Functions with Good Energy Resolution", Nucl. Instrum. Methods **A270**, 467 (1988).

[Wig57] E. P. Wigner, "Results and Theory of Resonance Absorption", in *Conference on Neutron Physics by Time-of-Flight*, 1957, Oak Ridge National Laboratory, Gatlinburg, TN, page 59.

[Wil60] D. H. Wilkinson, "Analysis of Gamma Decay Data", in *Nuclear Spectroscopy, Part B*, edited by F. Ajzenberg-Selove, Academic Press, New York, 1960.

[Win88] D. Wintgen and H. Marxer, "Level Statistics of a Quantized Cantori System", Phys. Rev. Lett. **60**, 971 (1988).

[Wun86] G. Wunner et al., "Rydberg Atoms in Uniform Magnetic Fields: Uncovering the Transition from Regularity to Irregularity in a Quantum System", Phys. Rev. Lett. **57**, 3261 (1986).

Biography

Paul Matthew Wallace

Personal:

Born 17 April 1968, Atlanta, GA

Married 22 June 1991 to Elizabeth Sides

Education:

A.S. in Physics, Young Harris College, 1988

B.S. in Physics, Furman University, 1990

M.A. in Physics, Duke University, 1993

Memberships:

Sigma Pi Sigma

American Physical Society

Abstracts:

"A High-Resolution Study of ^{30}P", P. M. Wallace, E. G. Bilpuch, G. E. Mitchell, E. F. Moore, J. F. Shriner, Jr., G. A. Vavrina, and C. R. Westerfeldt, to be published in Bull. Am. Phys. Soc.

"A High-Resolution Study of the ^{29}Si(p,γ) Reaction" P. M. Wallace, E. G. Bilpuch, C. R. Bybee, J. M. Drake, G.E Mitchell, E. F. Moore, J. F. Shriner, Jr., G. A. Vavrina, C. R. Westerfeldt, Bull. Am. Phys. Soc. **39**, 8 (1994)

"A Compton-Suppressed Spectrometer for the Study of ^{29}Si(p,γ)", G. A. Vavrina, E. G. Bilpuch, C. R. Bybee, J. M. Drake, G.E Mitchell, E. F. Moore, J. F. Shriner, Jr., P. M. Wallace, C. R. Westerfeldt, Bull. Am. Phys. Soc. **39**, 8 (1994)